

SOUND WAVE PROPAGATION THROUGH PERIODIC AND NONRECIPROCAL  
STRUCTURES WITH VISCOUS CONSTITUENTS

Dmytro Shymkiv, B.S.

Dissertation Prepared for the Degree of

DOCTOR OF PHILOSOPHY

UNIVERSITY OF NORTH TEXAS

May 2024

APPROVED:

Arkadii Krokhin, Major Professor  
Giordano Tierra Chica, Committee Member  
Yuri Rostovtsev, Committee Member  
Yuzhe Xiao, Committee Member  
Jingbiao Cui, Chair of Department of  
Physics  
John Quintanilla, Dean of the College of  
Science  
Victor Prybutok, Dean of the Toulouse  
Graduate School

Shymkiv, Dmytro. *Sound Wave Propagation through Periodic and Nonreciprocal Structures with Viscous Constituents*. Doctor of Philosophy (Physics), May 2024, 78 pp., 5 tables, 21 figures, 101 numbered references.

Acoustic properties of periodic elastic structures have been a subject of active research for more than a century. Here, I derived and analyzed the dispersion equation for sound waves propagating in a periodic layered heterogeneous structure containing at least one viscous fluid as a constituent. The derivation of the dispersion equation is based on the Navier-Stokes equation for sound wave and the boundary conditions of continuity of fluid displacement and stresses at the interfaces with Bloch periodic boundary condition. The obtained dispersion equation is very general, it is valid for different combinations of elastic layers, any direction of propagation, and frequency of sound. In the case of superlattice consisting of narrow layers with high viscosity fluid and layers of ideal fluid, an acoustic analog of the Borrmann effect is predicted. In the other part of my dissertation, I study the nonreciprocal wave propagation in phononic crystals induced by viscosity. Using Fourier-transformed wave equation, I proved analytically that for an infinite phononic crystal with broken PT-symmetry dispersion relation remains the same switching the direction of the wave propagation, while Fourier components of velocity are nonreciprocal. I optimized shape of the scatterer to reach the highest value of the nonreciprocity in a two-dimensional finite phononic crystal. Sound propagation through crystals with various unit cells is numerically simulated with COMSOL Multiphysics to create a dataset of transmission values. For each introduced parameter the optimized

scatterer's geometries are obtained utilizing machine learning techniques. I found parameters of the crystal, which may serve as a linear non-resonant passive acoustic diode.

Copyright 2024  
by  
Dmytro Shymkiv

## ACKNOWLEDGEMENTS

I wish to express my profound gratitude for the support and guidance I received during the completion of this dissertation. This academic journey has been a significant chapter in my life, and I owe the successful completion of it to the contributions and encouragement of various individuals and entities.

First and foremost, I extend my deepest appreciation to my research advisor, Dr. Arkadii Krokhin, for his exceptional mentorship, unwavering patience, and continuous encouragement. His expertise and insightful feedback have played an instrumental role in shaping the direction of my research. I am truly fortunate to have had such a dedicated and supportive mentor. I acknowledge the support from the Emerging Frontiers in Research and Innovation program of the National Science Foundation (grant no. 1741677).

Heartfelt thanks go to my colleagues and peers who engaged in fruitful discussions and provided a collaborative environment that fostered intellectual growth - Dr. Tae-Youl Choi, Dr. Yurii Zubov, Dr. Hyeonu Heo, Dr. Yuqi Jin, Dr. Ezekiel Walker, Dr. Jyotsna Dhillon, Dr. Andrii Bozhko, Dr. Arup Neogi and all the lab members. The exchange of ideas and perspectives has been an enriching experience that contributed to the depth and breadth of my research.

A special acknowledgment is reserved for my family, whose unwavering support, understanding, and encouragement have been my pillars of strength. Their sacrifices and belief in my abilities have been a driving force behind my academic pursuits.

## TABLE OF CONTENTS

	Page
ACKNOWLEDGEMENTS	iii
LIST OF TABLES	vi
LIST OF FIGURES	vii
CHAPTER 1 INTRODUCTION	1
1.1. Periodic Acoustic Systems	1
1.2. Nonreciprocal Acoustic Structures	2
1.3. Current State of the Problem	3
1.4. Dissertation Description	4
CHAPTER 2 EFFECTS OF VISCOUS DISSIPATION IN PROPAGATION OF SOUND IN PERIODIC LAYERED STRUCTURES	7
2.1. Introduction	7
2.2. Two Eigen Modes in Free Viscous Fluid	11
2.3. Dispersion Equation for Sound Wave in a Superlattice with Viscous Constituents	14
2.3.1. Wave Equation Solutions	14
2.3.2. Refraction at the Interface	16
2.3.3. Boundary Conditions	17
2.3.4. Dispersion Relation	19
2.4. Analysis of Attenuation of Sound in Superlattices with Different Constituents	26
2.4.1. Unit Cell of Viscous and Ideal Fluids	26
2.4.2. Unit Cell of Two Different Viscous Fluids	29
2.4.3. Unit Cell of Viscous Fluid and Dissipationless Solid	34
2.5. Summary	39

CHAPTER 3 NONRECIPROCAL TRANSMISSION AND ITS OPTIMIZATION THROUGH DISSIPATIVE PHONONIC CRYSTALS	41
3.1. Introduction	41
3.1.1. Nonreciprocity	41
3.1.2. Machine Learning in Physics	43
3.2. Acoustic Reciprocity of an Infinite Phononic Crystal	45
3.2.1. Wave Equation in Fourier Representation	45
3.2.2. Eigenvalues and Eigenfunctions of the Wave Equation	48
3.3. The Phononic Crystal and Data Collection	50
3.4. Single Parameter Optimization	52
3.5. Multiple Parameters Optimization	58
3.6. Summary	64
CHAPTER 4 RESULTS AND CONCLUSIONS	66
REFERENCES	69

## LIST OF TABLES

		Page
2.1	Density, elastic moduli and viscosity of the materials used in the numerical calculations.	21
3.1	Material properties of water and aluminum used in the numerical simulations.	52
3.2	The best nonreciprocity $NR$ (maximizing), normalized nonreciprocity $NNR$ (maximizing), and diode efficiency $F$ (minimizing) from the dataset with model predictions and COMSOL validated values for the optimized parameters.	56
3.3	The highest (lowest for $F$ ) nonreciprocity, normalized nonreciprocity and diode efficiency from the dataset.	59
3.4	The highest (lowest for $F$ ) nonreciprocity, normalized nonreciprocity and diode efficiency from the dataset and predictions as well as COMSOL validated values for the optimized parameters. The best values are highlighted and the corresponding radius and rotation angle are provided.	60



## LIST OF FIGURES

		Page
2.1	Unit cell of elastic superlattice with period $d = a + b$ consisting of two layers: viscous fluid $a$ and elastic solid $b$ . Arrows show the incident longitudinal mode in fluid and two (longitudinal and transverse) refracted modes in solid.	15
2.2	Frequency dependence of the attenuation coefficient of the longitudinal sound and normal incidence for water-glycerol superlattice with filling fraction of water $f = 0.8$ . The exact result is calculated from Eq. (2.33) and the linear over viscosity approximation is given by Eq. (2.37). Both results exhibit fast growth near the band edge: the exact value remains finite and the approximate approaches infinity. Note that even for relatively high viscosity of glycerol the decay length is of the order of $10^4$ lattice periods. The opposite case of very strong viscous absorption when the boundary layers overlap within the lattice period is numerically considered in Ref. [80, 95]. Left inset: the band structure of the water-glycerol superlattice. The band gaps are shaded in grey. Right inset: the unit cell with geometrical parameters.	22
2.3	Borrmann effect. Angular dependence of the dimensionless decay coefficient for a superlattice with narrow ( $a = 1$ mm) viscous layer of glycerol and thick layer ( $b \approx d = 100$ mm) of inviscid water. Inset shows the fine structure of deep minima near the frequencies of Bragg scattering.	28
2.4	Graphs showing the transition from $\omega^2$ (dissipation in the bulk) to $\sqrt{\omega}$ (dissipation in the boundary layer) dependence for the decay coefficient with increasing angle of incidence $\theta_a$ in the quasistatic region where the Bloch vector is obtained from Eq. (2.52). At a given frequency the transition occurs within a narrow interval of angles near the angle $\Theta$	

- defined by Eq. (2.53). 31
- 2.5 Nonmonotonic dependence  $\Theta(\eta_b)$  for different  $\eta_a$  at frequency 2 kHz. All the mechanical parameters except shear viscosity correspond to water ( $a = 8$  mm) and glycerol ( $b = 2$  mm). In a superlattice of real water and glycerol the transition from dissipation in the bulk to dissipation in the boundary layer occurs at relatively small angle  $\Theta = 7.8^\circ$  shown by the orange dot. Inset shows the same dependence for a wider range of viscosity  $\eta_b$ . 32
- 2.6 Decay coefficient for water-glycerol superlattice  $\gamma_{ph} = k''_x(f)$  normalized to the decay coefficient of water ( $\gamma_{water}$ ) vs filling fraction  $f$  of glycerol. Strong dependence on the filling fraction is related to the high viscosity contrast between water and glycerol,  $\gamma_{glyc}/\gamma_{water} = 1.6 \cdot 10^3$ . 33
- 2.7 Frequency dependence of the dimensionless decay coefficient for water-PMMA superlattice calculated from Eq. (2.39) for the filling fraction  $f = 0.2$ . The region within the two lowest transmission bands is shown. Shaded regions are the band gaps of the band structure shown in the left top inset. Left bottom inset is the decay coefficient at very low frequencies where  $k''_x \propto \sqrt{\omega}$ . Right top inset is the decay coefficient within the first band gap. Left bottom inset shows the direction of propagation within the unit cell. Note order-of-magnitude difference in the decay coefficient at low frequencies, close to the band edge, and within the band gap. 35
- 2.8 Normalized decay coefficient vs filling fraction for water-PMMA superlattice for different angles of incidence. The frequency of sound is 20 kHz. The right inset shows the case of normal incidence when dissipation occurs in the whole bulk of water. The left inset shows how dissipation in the bulk changes to dissipation within the boundary layer with increasing angle of incidence for different filling fractions. For angles  $\theta_a > 0.03$  the decay coefficient exhibits "abnormal" increasing dependence with

	decreasing amount of viscous water. The curves appear to cross at the same point but on the blowup picture, there are several crossing points within a narrow region near $\theta_a = 0.03$ .	36
2.9	Angular dependence of the normalized decay coefficient of water-PMMA superlattice at filling fraction $f = 0.2$ and frequency 20 kHz. Note the logarithmic scale on the vertical axis. Dashed line shows the position of the critical angle for inviscid fluid Eq. (2.54).	38
3.1	Pressure maps calculated for the crystal with asymmetrical scatterers and ideal fluid for downward (left) and upward (right) wave propagation. The difference in pressure is due only to the asymmetric transmission.	43
3.2	A model of the $5 \times 5$ 2D phononic crystal used in the COMSOL calculations of the transmission spectra. The crystal consists of aluminum scatterers in a water background. Solid Mechanics and Linearized Navier-Stokes moduli were used for calculations of elastic and acoustic fields in the sample. The transmitter and receiver are placed either above or below the structure. The period of the crystal is $a = 15mm$ . The sound hard boundary condition is imposed for the left and right boundaries. All external domains are perfectly matched layers (PML). Sound transmission in the forwards ( $T_F$ ) and backwards ( $T_B$ ) directions are numerically calculated for viscous and inviscid water.	51
3.3	Optimization Pipeline.	53
3.4	Unit cells of the phononic crystal with varying scatterer sector angle. Period is 15 mm; sector radius is 6 mm; sector angle is $10^\circ$ (left), $120^\circ$ (middle), $300^\circ$ (right)	54
3.5	(a) Loss (mean squared error) as a function of the number of epochs for the $NR$ optimization model. (b) Original data points and predictions made with a DNN model for the optimization of $NR$ .	55
3.6	Original data points and predictions made with a DNN model. Left	

	panel: Optimization for $F$ . Right panel: Optimization for $NNR$ .	56
3.7	Transmission spectra for the $5 \times 5$ phononic crystal sample in viscous water with the parameters corresponding to the best $F$ - value. Downward propagation ("Source Top") is shown with red color, while upward propagation ("Source Bot") is depicted with blue color. The top/bottom positions of the source are indicated in Fig. 2.1. The shaded areas are the regions of the band gaps in the infinite phononic crystal with inviscid water. Note that the narrow transmission region between the gaps is not resolved for the finite-size sample.	57
3.8	Ten different asymmetric cross-sections of scatterers.	58
3.9	Original data for the geometry types with the highest $NR$ (left), $NNR$ (center) and the lowest $F$ (right).	59
3.10	Nonreciprocity optimization. Loss (mean squared error) as a function of a number of epoch (top) and predictions of the DNN models of NR (bottom). The model consists of 4 hidden layers with 17 nodes each.	61
3.11	Diode efficiency optimization. Loss (mean squared error) as a function of a number of epoch (top) and predictions of the DNN models of F (bottom). The model consists of 5 hidden layers with 1000 nodes and a 15% dropout rate in each layer.	62
3.12	Transmission spectra through the $5 \times 5$ sample with the parameters providing the highest value of nonreciprocity $NR$ . The parameters of the scatterer are given in Table 3.4. Note that the narrow transmission band lying between two bandgaps (marked as shaded areas) is well-resolved, unlike similar transmission band in Fig.3.8.	63

# CHAPTER 1

## INTRODUCTION

### 1.1. Periodic Acoustic Systems

Humanity has been fascinated by crystals since ancient times due to their perfect periodicity. Crystalline solids are used nowadays in a variety of industries such as semiconductor, optical, electrical. Recently, new types of periodic structures - photonic [91, 39] and phononic [43] crystals have been introduced. They are the artificially created systems which mimic natural crystals. For instance, a typical phononic crystal consists of a periodic array of scatterers (atoms in "usual" crystals) placed in the background material. Due to the periodicity and multiple scattering of sound waves (phononic crystals) or electromagnetic waves (photonic crystal), one can manipulate and tune wave propagation. The most important characteristic of a crystal is a bandstructure, which shows wave frequency  $\omega$  dependence on the wave vector  $\mathbf{k}$  or in other words how wave energy depends on its momentum. This dependence or dispersion might be normal (positive group velocity,  $\partial\omega/\partial k > 0$ ) or anomalous (negative group velocity,  $\partial\omega/\partial k < 0$ ). The latter type of dispersion is widely utilized to achieve negative refraction, perfect lens, cloaking [53, 17, 58, 64]. Flat dispersion, which corresponds to zero group velocity  $\partial\omega/\partial k = 0$ , can be used for acoustic deep-subwavelength imaging [96]. Destructive interference of acoustic waves, propagating inside the crystal, leads to fundamental characteristic of phononic crystal - ability to create band gaps. They are the ranges of frequencies where wave propagation is forbidden. The size, shape, and composition of the unit cell play pivotal roles in determining the properties of these band gaps. Waveguides and filters based on phononic crystals have been designed to selectively allow or block certain frequency ranges, opening avenues for the development of advanced acoustic devices [65]. Periodic acoustic structures may possess a variety of other fascinating properties, including but not limited to topologically protected states [93, 90], exceptional points [23] and nonreciprocal wave propagation [87].

## 1.2. Nonreciprocal Acoustic Structures

Reciprocity is a fundamental principle of the wave propagation. In optics it is known as a Lorentz reciprocity theorem. Rayleigh [73] was the first who formulated a reciprocity theorem for acoustic waves.

$$(1.1) \quad p_A(\mathbf{r}_B) = p_B(\mathbf{r}_A)$$

This equation states the equality of pressure when positions of emitter and receiver are exchanged. It is valid for a point source and emphasizes a symmetry between two points. From 1950s it was known that an external magnetic field can break reciprocity [47, 40]. Nowadays [24] there are various methods of breaking the reciprocity by either introducing a quantity which breaks time-reversal (T) symmetry of the system or using a nonlinear medium [51, 68]. A combination of linear metamaterial with appropriate band gaps and nonlinear medium, which allows second-harmonic generation, is proposed to be used as a sound rectification device [51, 50]. If an acoustic system involves fluid in motion, Doppler effect is a source of nonreciprocity [66]. Time modulation of a periodic in space structure can lead to the nonreciprocity. Dispersion of a simple mass-spring system with time periodic spring constants under specific conditions [59] is different for forward ( $\mathbf{k}$ ) and backward ( $-\mathbf{k}$ ) directions.

Recently, it was shown [86, 31, 79] that viscosity (intrinsic property of fluids) leads to the nonreciprocity of sound waves in systems with broken parity (P) symmetry. Viscosity, which is a source of dissipation, leads to irreversibility of acoustic wave propagation. Despite this, there exists a prevalent opinion that the transmission of sound remains reciprocal even within a dissipative medium [24, 60]. The Navier-Stokes equation, which is a governing equation of fluid dynamics, is non time-reversible due to the terms proportional to the viscosity coefficients. This equation is written for the field of velocities  $\mathbf{v}(\mathbf{r})$ , which does not possess reciprocity in general case. Even in inviscid fluid, where velocity is proportional to the gradient of pressure, velocity is not reciprocal. Pressure reciprocity can not be extended to the reciprocity of its gradients since pressure is not required to be either even or odd

function of coordinates. For a trivial case of homogeneous ideal fluid with a dipole source reciprocity theorem can be written for the component of velocity along the dipole moment [45]. Also, in the case of viscous background with symmetrical scatterers sound propagation is irreversible but reciprocal. If parity (P) symmetry of the scatterers is broken, velocity fields are not symmetric, which makes dissipation different, switching the positions of emitter and receiver. Thus, transmission coefficient related to the sound wave intensity  $I = pv$  becomes nonreciprocal. In contrast to propagation in ideal fluid with broken P symmetry, where transmission is asymmetrical, in viscous media with broken PT symmetry, it acquires a nonreciprocal component.

### 1.3. Current State of the Problem

Fluid viscosity is a fundamental property that governs the resistance of a fluid to deformation or flow. In fluid dynamics, viscosity is central to understanding the behavior of fluids in laminar and turbulent flow regimes. In engineering applications, viscosity is critical for designing lubrication systems, hydraulic systems, and optimizing fluid transport.

Applying to sound wave propagation, viscosity introduces internal friction within a fluid, leading to the damping and attenuation of sound waves. Another reason of energy dissipation for the traveling acoustic wave is thermal losses. In some problems, dissipation is negligible and can be ignored. In homogeneous water sound does not suffer from strong viscous attenuation for frequencies below 1 THz. The impact of viscosity on the scattering pattern generated by an individual scatterer is found to be relatively small [52]. On the other hand, viscothermal effects become important in more complicated systems. In the presence of solid-fluid interfaces, velocity differs significantly within a narrow layer (viscous boundary layer) near the boundary leading to much greater attenuation than in the free fluid [41]. The impact on sound transmission can be notably substantial, even when the thickness of the boundary layer is only about 2% of the width of the slit in the metasurface unit [38]. The combination of multiple scattering and interference significantly amplifies the effects of viscous and thermal losses in sound propagation through a phononic crystal, particularly evident at high filling fractions where the boundary layers of adjacent scatterers begin to

intersect [28, 80, 95]. Calculations of acoustic response of locally resonant metamaterials have to consider viscothermal effects [57]. In the context of acoustic devices, dissipation emerges as a predominant factor that delineates the efficacy of such apparatuses [88, 83, 13]. Sound attenuation can significantly weaken the properties of metamaterials, notably impacting phenomena such as negative refraction and hydrodynamic cloaking [30, 63].

In recent works [35, 36], decay coefficient for acoustic waves, propagating in the 2-dimensional phononic crystal of cylinders immersed in a viscous fluid, is expressed through the infinite sums over reciprocal-lattice vectors. Direct calculations demonstrate that sound attenuation can be enhanced by 2-3 orders of magnitude due to existence of a viscous boundary layer around each solid scatterer. It is shown that in the long-wavelength limit phononic crystal behaves like a homogeneous metamaterial, where effective viscosity as well as elastic moduli, mass density, and speed of sound may exhibit strong anisotropy. However, up until recently [78] there was a lack of complete theory of dissipation in 1-dimensional phononic crystals. In my dissertation I develop such a theory and fulfill this gap.

My research on the sound wave propagation through the structures with viscous constituents is not limited to the study of dissipation itself. Here, I investigate the nonreciprocity in sound wave intensity induced by viscosity as well. I intend to study nonreciprocity in infinite phononic crystals where the concept of transmission can not be applied. The shape of the scatter in Ref.[86] is not optimized and leads to relatively small nonreciprocal contribution to the difference in transmission coefficient for forward and backward sound wave propagation. With machine learning techniques, my goal is to obtain scatterer's geometries providing significant nonreciprocity.

#### 1.4. Dissertation Description

The main goal of my dissertation is to study analytically and numerically the effects on sound propagation through the phononic crystals caused by viscosity.

The second chapter presents the research of viscous dissipation in sound propagation in periodic layered structures (superlattices). If at least one of the constituents of the superlattice is a viscous fluid, solutions of a dispersion relation have non-zero imaginary part due



to dissipation (in a dissipationless system solutions have non-zero imaginary part only within band gaps). I consider the most general case of solid-fluid layered structure and special cases when solid is replaced with either viscous or inviscid (ideal) fluid. Using boundary conditions for velocity and stress I obtain analytically an exact dispersion equation. Simplified versions in the low-viscosity limit for each type of the superlattice are derived for further analysis. I demonstrate and explain differences in decay coefficient for solid-viscous fluid, viscous fluid-viscous fluid and ideal fluid-viscous fluid structures as well as transition from oblique to normal incidence. Also, I examine a limiting case of tiny viscous layers, which leads to dissipationless propagation for specific frequencies.

In the third chapter I study nonreciprocity due to viscosity in phononic crystals and optimize shape of solid scatterers to tune nonreciprocal transmission. Using a Fourier-transformed wave equation derived from a linearized Navier-Stokes equation and a continuity equation I examine reciprocity of an infinite periodic acoustic system. I demonstrate analytically that viscosity leads to nonreciprocity of a velocity field keeping dispersion relation reciprocal. Nonreciprocal transmission is obtained numerically for a finite two-dimensional (2D) crystal for a particular type of unit cell. To exclude a difference in transmission due to asymmetry I calculated transmission for forward/backward wave propagation for viscous/ideal fluid. To compare performance of phononic crystals with different scatterers I introduce three quantities - nonreciprocity (NR), normalized nonreciprocity (NNR) and diode efficiency (F). The latter is used to study unidirectional sound propagation through the crystal. I optimize a shape of a scatterer to achieve the highest values of NR and NNR and the lowest value of the diode efficiency (an ideal diode has  $F = 0$ ). I develop machine learning models trained using numerically calculated data to predict these values for arbitrary values of parameters defining geometry of the scatterer. Finally, the predicted values of NR, NNR and F for the optimized shape are validated using numerical simulations. I demonstrate that nonreciprocity in the studied systems plays a significant role and can not be neglected in a general case. Also, I find parameters of the phononic crystal, which may serve as a linear non-resonant passive acoustic diode.

The final chapter summarizes the dissertation, explains and emphasizes the most crucial findings of my work done.

## CHAPTER 2

# EFFECTS OF VISCOUS DISSIPATION IN PROPAGATION OF SOUND IN PERIODIC LAYERED STRUCTURES <sup>†</sup>

### 2.1. Introduction

Acoustic properties of layered elastic structures have been a subject of active research for more than a century. Combining layers of different widths and of different elastic materials a wide variety of elastic properties can be tailored, which makes these structures applicable in many areas of modern technology [94]. Quite a full collection of acoustic and elastic properties of layered structures can be found in two fundamental books [89, 6].

A special case of layered media is a medium with spatial periodicity, i.e., elastic superlattice or one-dimensional (1D) phononic crystal. Due to additional symmetry related to periodicity, mathematical theory of wave propagation in superlattices has been strongly advanced. In particular, the dispersion relation between the Bloch vector  $\mathbf{k}$  and frequency  $\omega$  has been derived in analytical form [76]. If the constituents are dissipative, the dispersion relation  $\omega = \omega(\mathbf{k})$  becomes complex and the oscillations of acoustic pressure decays exponentially with distance, even for the frequency lying within a propagating band. A phenomenological method to introduce dissipation is to add imaginary parts to the elastic constants [14, 77]. Since dissipation vanishes in static limit, the imaginary additions are linear over  $\omega$  (viscous friction), which enhances the effect of dissipation on dispersion of sound [33, 56, 1].

If at least one of the constituents of phononic crystal is a viscous fluid, a microscopic description of fluid dynamics in acoustic field becomes possible through the Navier-Stokes equation. As compared to bulk losses, viscous friction is much stronger near a fluid-solid interface due to formation of a narrow boundary layer  $\delta$ , where the tangential component of velocity of oscillating fluid,  $\mathbf{v}(x, t)$  decays exponentially towards the interface with distance

---

<sup>†</sup>Reproduced in part or in full from Dmitrii Shymkiv, Arkadii Krokhin; Effects of viscous dissipation in propagation of sound in periodic layered structures. *J. Acoust. Soc. Am.* 1 February 2024; 155 (2): 990-1004. <https://doi.org/10.1121/10.0024719>, with the permission of AIP Publishing.

$x, v(x, t) \sim (1 - e^{-x/\delta}) e^{-i\omega t}$ . Dissipated power depends on velocity gradients  $(\partial v_i / \partial x_j)^2$ . Since the width of the boundary layer is usually much less than the wavelength  $\lambda$  the viscous losses in the bulk can be neglected as compared to the losses within the layer  $\delta$ . The bulk losses grow as  $\eta\omega^2$  and the boundary layer losses grow as  $\sqrt{\omega\eta}$ , where  $\eta$  is the shear viscosity coefficient. At low frequencies this essential difference gives rise to so-called Konstantinov's effect, which predicts enhanced absorption at reflection of sound from a fluid-solid interface [41].

Due to Konstantinov's effect acoustic absorption in a fluid-solid phononic crystal is strongly inhomogeneous and its calculation requires solution of the linearized Navier-Stokes equation and continuity equation. Mathematical analysis made on the basis of linearized Navier-Stokes equation show that some effects originated from fluid viscosity and lack of inverse symmetry in periodic 2D and 3D elastic structures cannot be fully described by the wave equation for inviscid fluid where elastic modulus and fluid density acquire phenomenological imaginary additions [31]. The phenomenological Rayleigh damping model [72, 1], widely used in seismology and architecture [12], is also unable to correctly account for enhanced viscous dissipation within the boundary layer. Strongly inhomogeneous distribution of fluid velocities gives rise to spatial dispersion of the dissipative terms in the wave equation, which depend not only on  $\omega$ , but also on  $\mathbf{k}$ . Moreover, formation of the viscous boundary layer and dissipated power depend on the shape of solid inclusions. In particular, presence of sharp corners, where velocity gradients and local dissipated power become very high, is ignored in the phenomenological approach. The phenomenological approach can be improved [28] by adopting some results from the acoustics of porous medium, in particular, by accounting for the effects of the viscous boundary layer in the imaginary parts of effective mass density and effective elastic moduli.

The microscopic approach based on the Navier-Stokes dynamical equation accounts for formation of a highly dissipative boundary layer around each scatterer as well as for viscous dissipation in the bulk. The wave equation for sound in a viscous environment with shear and bulk viscosity coefficients can be formally reduced to the wave equation in

a dissipationless isotropic solid with complex frequency-dependent Lamé coefficients, which are microscopically justified [21].

Scattering of sound by solid inclusions of different shape embedded in a viscous fluid has a long history, starting from the pioneering works by Sewell [81] and Lamb [44]. I refer here to a relatively modern study [52] where the Navier-Stokes equation is used for analytical calculations of the scattering cross section, acoustic-radiation force, and attenuation coefficient for an elastic sphere and cylinder in a viscous background. The field of fluid velocities was represented as a superposition of two components: acoustic potential wave and vortex shear wave [66]. The influence of viscosity on the scattering pattern produced by a single scatterer turns out to be quite low [52]. However, multiple scattering and interference strongly enhance viscous and thermal losses for sound propagating in a phononic crystal, especially at high filling fractions when the boundary layers of the neighbouring scatterers start to overlap [28, 80, 95, 75, 35, 36]. In the long-wavelength limit phononic crystal behaves like a homogeneous metamaterial where effective viscosity may exhibit strong anisotropy [35, 36] together with elastic moduli, mass density, and speed of sound.

This chapter addresses sound propagation through a periodic layered structure containing viscous fluid constituents. A microscopic theory based on Navier-Stokes equation is developed. While the analytical calculations are cumbersome, it is possible to reduce the dispersion equation to the form similar to that derived by Rytov[76]. The obtained dispersion equation gives in implicit form the relation  $f(\omega, \mathbf{k}) = 0$  for any frequency and direction of propagation. At finite viscosity the solutions  $\mathbf{k} = \mathbf{k}(\omega)$  of the dispersion equation are complex,  $\mathbf{k} = \mathbf{k}'(\omega) + i\mathbf{k}''(\omega)$  at any frequency  $\omega$ . Analyzing the dispersion relation in the long-wavelength limit I obtain analytical expression for the attenuation coefficient  $k''(\omega)$ , which exhibits very strong uniaxial anisotropy. Namely, the frequency dependence  $k''(\omega)$  turns out to be different for oblique and normal incidence of sound. I explain a transition from  $\omega^2$  dependence of dissipated power to  $\sqrt{\omega}$  law when direction of propagation slightly deviates from propagation parallel to the superlattice axis. The effective viscosity as a frequency-independent parameter can be introduced in the long-wavelength limit for

normal incidence only. Viscous losses are analyzed in the vicinity of the band gaps, where group velocity vanishes, which leads to strong increase of dissipation. If one of the fluids is viscous and another is inviscid, the low-frequency expansion of  $k''(\omega)$  starts from the terms higher than  $\sqrt{\omega}$ , i.e. the Konstantinov's effect is suppressed since there is no viscous friction at the interface. There is an interesting opposite case of very viscous but narrow layer in contact with a layer of ideal (inviscid) fluid. For this combination of materials an acoustic analog of so-called Borrmann effect, is predicted when for certain frequencies the transmission becomes anomalously high. At these frequencies, the nodes of fluid velocity lie inside the viscous layers, which strongly reduces viscous losses.

While the proposed theory is based on the microscopic, not a phenomenological approach, it remains a classical macroscopic hydrodynamic theory in the sense that the thickness of the fluid layers contains many atomic spacings. The atomic structure becomes important in consideration of hydrodynamics of nanofluids (lubricants), when the direct interactions between atomically flat solid surface and atomically thin liquid layer contribute to the friction forces. The classical no-slip boundary condition is violated in this case due to arrangement of the molecules of liquid into layers parallel to solid surfaces [16] and the effective viscosity strongly exceeds its classical macroscopic value [100]. Inter-molecular interactions not only enhance classical friction forces but also make the dependence on the discrete thickness of the stacked sheets of atoms a discontinuous function [2]. A similar situation occurred in 1947 with the theory of anomalous skin-effect in metals. The "noneffectiveness concept" proposed by Pippard [67], being phenomenological explained the physical nature of the effect and most of the experimental results for surface impedance. One year later a microscopic theory based on the kinetic equation for conduction electrons was developed by Reuter and Sondheimer [74]. Both theories are classical, but the microscopic theory is more complete, explaining some fine details related to electron scattering at rough metal surface.

## 2.2. Two Eigen Modes in Free Viscous Fluid

The main equation of fluid dynamics is a Navier-Stokes equation, which is the equation of motion for a viscous fluid [45]. A linearized form of this equation reads

$$(2.1) \quad \rho \frac{\partial v_i}{\partial t} = -\frac{\partial p}{\partial x_i} + \frac{\partial}{\partial x_i} (\xi \nabla \cdot \mathbf{v}) + \frac{\partial}{\partial x_k} \left[ \eta \left( \frac{\partial v_i}{\partial x_k} + \frac{\partial v_k}{\partial x_i} - \frac{2}{3} \delta_{ik} \nabla \cdot \mathbf{v} \right) \right],$$

where  $\mathbf{v}$ ,  $p$  are velocity and pressure fields;  $\rho$ ,  $\eta$ ,  $\xi$  are density, shear viscosity and bulk viscosity coefficients of the fluid respectively. Another important relation in fluid mechanics is a continuity equation, which is a conservation of mass law:

$$(2.2) \quad \frac{\partial \rho}{\partial t} + \nabla \cdot (\rho \mathbf{v}) = 0.$$

To derive a wave equation for a sound wave propagating in the fluid an equation of state has to be introduced:

$$(2.3) \quad \left( \frac{\partial p}{\partial \rho} \right)_{s=const} = c,$$

where  $s$  is entropy and  $c$  is a speed of sound. Speed of sound is related to density and elastic bulk modulus ( $\lambda$ ) via  $c = \sqrt{\lambda/\rho}$ . Excluding pressure from Eq.(2.1) using Eqs.(2.2) and (2.3) an acoustic wave equation can be written as

$$(2.4) \quad \rho \frac{\partial^2 v_i}{\partial t^2} - \frac{\partial}{\partial x_i} (\lambda \nabla \cdot \mathbf{v}) = \frac{\partial}{\partial x_k} \left[ \eta \left( \frac{\partial \dot{v}_i}{\partial x_k} + \frac{\partial \dot{v}_k}{\partial x_i} - \frac{2}{3} \delta_{ik} \nabla \cdot \dot{\mathbf{v}} \right) \right] + \frac{\partial}{\partial x_i} (\xi \nabla \cdot \dot{\mathbf{v}}).$$

If a monochromatic plane wave oscillates at frequency  $\omega$ , then a general form of the solutions of Eq.(2.4) is

$$(2.5) \quad \mathbf{v}(\mathbf{r}, t) = \mathbf{V} e^{i\mathbf{k} \cdot \mathbf{r}} e^{-i\omega t}.$$

Substitution of this solution into the wave equation (2.4) leads to a linear equation for velocity amplitude  $\mathbf{V}$ :

$$(2.6) \quad (\omega^2 + i\omega \frac{\eta}{\rho} k^2) \mathbf{V} = (c^2 - \frac{1}{3\rho} i\omega \eta - i\omega \frac{\xi}{\rho}) (\mathbf{k} \cdot \mathbf{V}) \mathbf{k}.$$

It has solutions if either  $\mathbf{V} \parallel \mathbf{k}$  or both sides of Eq.(2.6) equal to zero. The first mode corresponds to the eigenmode with longitudinal polarization and dispersion:

$$(2.7) \quad k_l^2 = \frac{\omega^2/c^2}{1 - \frac{i\omega}{\rho c^2}(\frac{4}{3}\eta + \xi)}.$$

The other mode has transverse polarization  $\mathbf{V} \perp \mathbf{k}$  and dispersion:

$$(2.8) \quad k_t^2 = \frac{i\omega\rho}{\eta} = \frac{2i}{\delta^2}, \quad \delta = \sqrt{\frac{2\eta}{\omega\rho}}.$$

In a general case a plane wave might be inhomogenous:

$$(2.9) \quad \mathbf{k} = k' \mathbf{n} + ik'' \mathbf{a},$$

where  $\mathbf{n}$  and  $\mathbf{a}$  are the propagation and attenuation unit vectors respectively. They have different direction and an angle  $\gamma$  between these vectors is the degree of inhomogeneity [37]. For any complex inhomogenous wave vector  $\mathbf{k}$  its real ( $k'$ ) and imaginary ( $k''$ ) part can be represented with  $R = \text{Re}(k^2)$  and  $I = \text{Im}(k^2)$ :

$$(2.10) \quad k^2 = k'^2 - k''^2 + 2ik'k'' \cos \gamma = R + iI,$$

$$(2.11) \quad k'^2 = \frac{1}{2} \left( R + \sqrt{R^2 + \frac{I^2}{\cos^2 \gamma}} \right),$$

$$(2.12) \quad k''^2 = \frac{1}{2} \left( -R + \sqrt{R^2 + \frac{I^2}{\cos^2 \gamma}} \right).$$

Only longitudinal mode is responsible for propagating sound wave. Propagation over a long distance is possible if the decay factor  $e^{-k''x}$  does not change significantly at the wavelength distance  $2\pi/k'_l = 2\pi c/\omega$ , which implies  $I \ll R$  i.e.,

$$(2.13) \quad \frac{I}{R} = \frac{\omega}{\rho c^2} \left( \frac{4}{3}\eta + \xi \right) \approx \frac{\omega\eta}{\rho c^2} \ll 1.$$

Taking into account this inequality,  $k''_l$  in Eq. (2.12) can be expanded as

$$(2.14) \quad k''_l \approx \frac{I}{2\sqrt{R} \cos \gamma_l} = k'_l \frac{\omega}{2\rho c^2 \cos \gamma_l} \left( \frac{4}{3}\eta + \xi \right) \ll k'_l.$$



$k_l''$  is the bulk decay coefficient of sound wave, which leads to the exponential attenuation  $\sim e^{-k_l'' x}$  of the wave amplitude over distance due to viscous dissipation in bulk. Equation (2.14) describes a wide range of frequencies

$$(2.15) \quad \omega \ll \omega^* = \rho c^2 / \eta$$

where sound attenuation due to the presence of viscosity of a fluid is small. For instance, sound waves do not experience strong decay due to viscosity in water for frequencies below 1 THz.

The transverse mode (2.8) is a "deaf" mode and is not related to a propagating wave since  $R = 0$ . If this mode is excited, it decays over a length  $\delta = \sqrt{2\eta/\rho\omega}$ , which is the thickness of the viscous boundary layer

$$(2.16) \quad k_t' = k_t'' = 1/\delta\sqrt{\cos\gamma_t}.$$

The acoustic transverse wave in fluids is similar to electromagnetic wave in metals. Reaching the metal surface from the dielectric background, the latter decays within the skin layer of the metal due to its high conductivity. The fields decay exponentially in both acoustic and electromagnetic (normal skin-effect) cases and the thicknesses of both boundary and skin layer decrease with frequency in the same way as  $\omega^{-1/2}$ . Longitudinal and transverse modes are decoupled in an infinite fluid without obstacles. Moreover, if the fluid is isotropic,  $\gamma = 0$  since all directions have the same properties. The modes become coupled at any interface via the velocity non-slip boundary condition. This coupling leads to an orders of magnitude increase in the viscous dissipation experienced by an acoustic wave in comparison to the decay in free fluid [41].

The inequality for wave attenuation coefficients and phase velocities [61] has to remain valid for the longitudinal (2.14) and transverse (2.16) modes.

$$(2.17) \quad \frac{k_l''}{k_l'(1 + k_l''^2/k_l'^2)^2} \geq \frac{4c_t^2}{3c_l^2} \frac{k_t''}{k_t'(1 + k_t''^2/k_t'^2)^2}.$$

For the longitudinal mode:

$$(2.18) \quad \frac{k_l''}{k_l'} = \frac{\omega}{2\rho c^2} \left( \frac{4}{3}\eta + \xi \right) \ll 1; \quad c_l = c = \omega/k_l'.$$

For the transverse mode:

$$(2.19) \quad k_t'' = k_t'; \quad c_t = \omega/k_t' = \omega\delta; \quad \delta = \sqrt{2\eta/\rho\omega}.$$

Using the above mentioned expressions in (2.17) the final inequality reads

$$(2.20) \quad \frac{\xi}{\rho} \geq 0,$$

which is definitely correct.

### 2.3. Dispersion Equation for Sound Wave in a Superlattice with Viscous Constituents

I consider a binary periodic structure consisting of parallel layers. The unit cell of length  $d = a + b$  is shown in Fig. 2.1. The layer  $a$  is a viscous fluid. In general case, the layer  $b$  is an elastic solid. Manipulating with its elastic moduli, the particular cases of ideal or viscous fluid can be analyzed as well.

#### 2.3.1. Wave Equation Solutions

In presence of boundaries the solution of the wave equation (2.4) is written as a sum of longitudinal (potential) and transverse (solenoidal) mode

$$(2.21) \quad \mathbf{v}(\mathbf{r}) = \mathbf{v}_l(\mathbf{r}) + \mathbf{v}_t(\mathbf{r}).$$

It follows from the structure of the solutions of Eq. (2.6) that the longitudinal mode is potential,  $\mathbf{v}_l = \nabla\phi$  and the transverse mode is solenoidal,  $\mathbf{v}_t = \nabla \times \mathbf{A}$ , where  $\mathbf{A} = (0, 0, A_z)$ . Each potential satisfies wave equation with the corresponding speed of sound,  $\omega/k_l$  and  $\omega/k_t$ . In the solid layer the speeds are real. In the fluid layer both speeds are complex according to Eqs. (2.7) and (2.8). The solutions of the wave equations for the potentials are represented by superpositions of plane waves travelling along and against axis  $x$ . Scattering at the vertical boundary does not change the  $y$ -component of the complex wave vector of each mode,  $k_{(l,t)y}^{(a)} = k_{(l,t)y}^{(b)}$ . Within each layer the velocities  $\mathbf{v}_l$  and  $\mathbf{v}_t$  are obtained by differentiating the corresponding potentials. For the longitudinal mode the

terms representing plane waves travelling along and against axis  $x$  enter with the same sign to the  $y$  component of velocity,  $v_{yl} = \partial\phi/\partial y$ , and with the opposite signs to the  $x$  component,  $v_{xl} = \partial\phi/\partial x$ , since  $\phi = [A_0 e^{ik_x x} + B_0 e^{-ik_x x}] e^{ik_y y}$ .

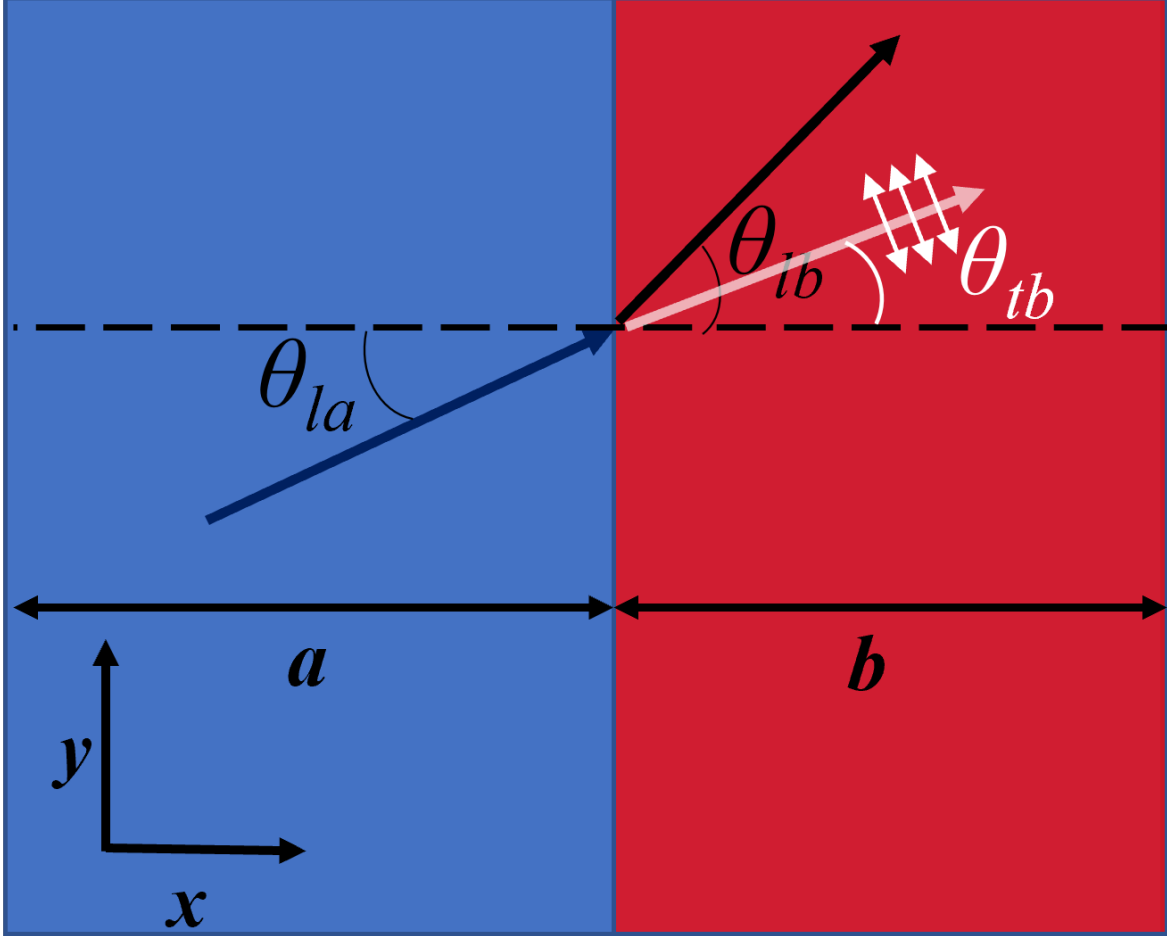


FIGURE 2.1. Unit cell of elastic superlattice with period  $d = a + b$  consisting of two layers: viscous fluid  $a$  and elastic solid  $b$ . Arrows show the incident longitudinal mode in fluid and two (longitudinal and transverse) refracted modes in solid.

The general solution for the velocity in the longitudinal mode can be written as follows:

$$(2.22) \quad \mathbf{v}_l(\mathbf{r}) = (\mathbf{n}_l + i\epsilon\mathbf{a}_l) \left[ A e^{k'_l x (i \cos \theta_l - \epsilon \cos(\theta_l - \gamma_l))} \mp B e^{-k'_l x (i \cos \theta_l - \epsilon \cos(\theta_l - \gamma_l))} \right] e^{k'_l y (i \sin \theta_l - \epsilon \sin(\theta_l - \gamma_l))},$$

where the minus (plus) sign is selected for the  $x$  ( $y$ ) component. The small parameter  $\epsilon = k_l''/k_l' = (\frac{4}{3}\eta + \xi)\omega/(2\rho c^2 \cos \gamma_l) \sim \omega^*/\omega \ll 1$  defines the attenuation rate. Angles  $\theta_l$  and  $\gamma_l$  give the directions of the unit vectors  $\mathbf{n}_l = (\cos \theta_l, \sin \theta_l)$  and  $\mathbf{a}_l = (\cos(\theta_l - \gamma_l), \sin(\theta_l - \gamma_l))$ .

The transverse mode has two polarizations in the "plane" perpendicular to the wave vector  $\mathbf{k}_t$ , i.e. to  $\mathbf{n}_t + i\mathbf{a}_t$ , where  $\mathbf{n}_t = (\cos \theta_t, \sin \theta_t)$  and  $\mathbf{a}_t = (\cos(\theta_t - \gamma_t), \sin(\theta_t - \gamma_t))$ . Any two non-collinear vectors lying in this "plane" may serve as polarization vectors, for example, the vectors  $\hat{\mathbf{z}} \times (\mathbf{n}_t + i\mathbf{a}_t) = (-n_{ty} - ia_{ty}, n_{tx} + ia_{tx})$  and  $\hat{\mathbf{z}} \times (-\mathbf{a}_t + i\mathbf{n}_t) = (a_{ty} - in_{ty}, -a_{tx} + in_{tx})$ . Using the former vector, the solution for the transverse mode is written as follows:

$$(2.23) \quad \mathbf{v}_t = \hat{\mathbf{z}} \times (\mathbf{n}_t + i\mathbf{a}_t) \left[ C e^{\frac{x}{\delta \sqrt{\cos \gamma_t}} (i \cos \theta_t - \cos(\theta_t - \gamma_t))} \pm D e^{-\frac{x}{\delta \sqrt{\cos \gamma_t}} (i \cos \theta_t - \cos(\theta_t - \gamma_t))} \right] e^{\frac{y}{\delta \sqrt{\cos \gamma_t}} (i \sin \theta_t - \sin(\theta_t - \gamma_t))},$$

where plus (minus) sign is selected for  $v_{xt} = \partial A_z / \partial y$  ( $v_{yt} = -\partial A_z / \partial x$ ).

### 2.3.2. Refraction at the Interface

Refraction at the boundary between the layer  $a$  of viscous fluid and the layer  $b$  of elastic solid (Fig. 2.1) leads to the coupling among the longitudinal and transverse modes in the fluid and solid. All four modes propagate with equal  $y$ -component of the wave vector,  $k_{ly} = k_{ty}$ . Since these  $y$ -components conserve at refraction/reflection, the Snell's law generalized for an inhomogeneous wave is written as follows:

$$(2.24) \quad \frac{\omega}{c_a} [\sin \theta_{la} + i\epsilon_a \sin(\theta_{la} - \gamma_{la})] = \frac{\sin \theta_{ta} + i \sin(\theta_{ta} - \gamma_{ta})}{\delta_a \sqrt{\cos \gamma_{ta}}} = \frac{\omega}{c_{lb}} \sin \theta_{lb} = \frac{\omega}{c_{tb}} \sin \theta_{tb}.$$

Here  $c_{lb(tb)}$  is speed of longitudinal (transverse) mode in solid. The set of equations in Eq. (2.24) describes several interesting effects related to mutual transformations from longitudinal to transverse sound and the Fano resonances associated with multiple reflections and refractions. These effects were studied in details in Refs. [6, 22, 71]. Here I am interested in calculation of acoustic energy dissipated in the fluid  $a$ .

The real part of Eq. (2.24) yields

$$(2.25) \quad \frac{\omega}{c_a} \sin \theta_{la} = \frac{\omega}{c_{lb}} \sin \theta_{lb} = \frac{\omega}{c_{tb}} \sin \theta_{tb} = \frac{\sin \theta_{ta}}{\delta_a \sqrt{\cos \gamma_{ta}}}.$$

The first and second equality are the Snell's law for the longitudinal-to-longitudinal refraction,  $\sin \theta_{la} / \sin \theta_{lb} = c_a / c_b$ , and for the longitudinal-to-transverse refraction,  $\sin \theta_{la} / \sin \theta_{tb} = c_a / c_{tb}$ . The equality  $\frac{\omega}{c_a} \sin \theta_{la} = \frac{\sin \theta_{ta}}{\delta_a \sqrt{\cos \gamma_{ta}}}$  means that  $\sin \theta_{ta} \sim \delta_a \frac{\omega}{c_a} = k'_{la} \delta_a \ll 1$ . Thus, due to low viscosity (see Eq. (2.13)) the transverse mode "propagates" almost perpendicular to the boundary and does not suffer from refraction. Note that this property is additional evidence that this mode is similar to the electromagnetic wave, which for any angle of incidence "propagates" perpendicular to metal surface at a distance of the order of skin layer. .

Separating the imaginary part of Eq. (2.24), one obtains the following relation for the angles  $\theta_{ta}$  and  $\gamma_{ta}$ :

$$(2.26) \quad \frac{\epsilon_a \omega}{c_a} \sin(\theta_{la} - \gamma_{ta}) = \frac{\sin(\theta_{ta} - \gamma_{ta})}{\delta_a \sqrt{\cos \gamma_{ta}}},$$

which assumes that the difference  $\theta_{ta} - \gamma_{ta}$  is cubic over a small parameter  $\epsilon_a \delta_a \omega / c_a \sim (k'_{la} \delta_a)^3$ .

Finally, the set of equations 2.24 can be written in a compact form

$$(2.27) \quad \frac{\sin \theta_{la}}{\sin \theta_{lb}} = \frac{c_a}{c_{lb}}, \quad \frac{\sin \theta_{la}}{\sin \theta_{tb}} = \frac{c_a}{c_{tb}}, \quad \theta_{ta} = \gamma_{ta} = \frac{\omega \delta_a}{c_a} \sin \theta_{l(a)} \ll 1.$$

The relation between the angles  $\theta_{la}$  and  $\gamma_{la}$  depends on the initial conditions of excitation of sound and remains indefinite. This, however, does not affect further calculations since dissipation of the longitudinal mode gives negligible contribution to the attenuation of sound. The principal contribution comes from the transverse mode, which excites oscillations of fluid parallel to the interface at any direction of propagation of sound wave in the layered structure but the direction exactly parallel to the axis when  $\theta_{ta} = \gamma_{ta} = 0$ .

### 2.3.3. Boundary Conditions

Within each layer the velocities of the longitudinal and transverse mode are given by Eqs. (2.22) and (2.23) respectively. These equations contain four indefinite coefficients for each layer, i.e., in total there are eight unknowns. They are obtained from the boundary conditions at the interface  $x = a$ , see Fig. 2.1). When sound wave passes through the interface (the oscillating total velocity in Eq. (2.21) satisfies the no-slip boundary condition, which means that  $\mathbf{v} = \mathbf{v}_l + \mathbf{v}_t$  is continuous at  $x = a$ . Also, the normal,  $F_x = \sigma_{xx} n_x$ , and the

tangential,  $F_y = \sigma_{yx}n_x$ , components of the force are continuous that leads to continuity of the components  $\sigma_{xx}$ ,  $\sigma_{xy}$  of the stress tensor. Each continuity condition is supplemented by Floquet periodicity condition that relates the value at  $x = 0$  with the corresponding value at  $x = a + b = d$ . Eight boundary conditions can be written as follows:

$$\begin{aligned}
(2.28) \quad & v_{xa}(x = a) = v_{xb}(x = a), \\
& v_{ya}(x = a) = v_{yb}(x = a), \\
& e^{ik_x d} v_{xa}(x = 0) = v_{xb}(x = a + b), \\
& e^{ik_x d} v_{ya}(x = 0) = v_{yb}(x = a + b), \\
& \sigma_{xx}^{(a)}(x = a) = \sigma_{xx}^{(b)}(x = a), \\
& e^{ik_x d} \sigma_{xx}^{(a)}(x = 0) = \sigma_{xx}^{(b)}(x = a + b), \\
& \sigma_{xy}^{(a)}(x = a) = \sigma_{xy}^{(b)}(x = a), \\
& e^{ik_x d} \sigma_{xy}^{(a)}(x = 0) = \sigma_{xy}^{(b)}(x = a + b).
\end{aligned}$$

Here  $k_x$  is the  $x$ -component of the Bloch vector. In a linear medium the components of the stress tensor are calculated through the total velocity Eq. (2.21). For viscous fluid

$$(2.29) \quad \sigma_{ik} = \frac{i}{\omega} (\lambda_f + \frac{2}{3} i\omega\eta - i\omega\xi) \delta_{ik} \nabla \cdot \mathbf{v} + \eta \left( \frac{\partial v_i}{\partial x_k} + \frac{\partial v_k}{\partial x_i} \right).$$

If one of the layers is elastic solid, the stress tensor is obtained from Eq. (2.29) by substitution

$$(2.30) \quad \lambda_f + \frac{2}{3} i\omega\eta - i\omega\xi \rightarrow \lambda_s, \quad \eta \rightarrow \frac{i\mu_s}{\omega},$$

where  $\lambda_s$  and  $\mu_s$  are the Lamé coefficients of the solid layer. Note that the stress tensor (2.29) and the relations (2.30) allow formal treatment of viscous fluid as elastic solid with complex Lamé coefficients. This analogy was explored in Ref. [21] for calculation of the contribution of surface degrees of freedom to the specific heat of a finite-size fluid sample and for band structure calculations of solid-viscous fluid phononic crystal [80, 95].

### 2.3.4. Dispersion Relation

Boundary conditions Eq. (2.28) form a set of homogeneous equations for eight unknown coefficients defining the velocity of the longitudinal (2.22) and transverse (2.23) mode over the unit cell. The dispersion relation  $\omega = \omega(\mathbf{k})$  is obtained from the condition of vanishing of the determinant of this homogeneous set. The explicit form of the  $8 \times 8$  determinant is given below:

$$(2.31) \quad \det \begin{pmatrix} -e^{iak_a} k_a & e^{-iak_a} k_a & e^{iak_a} k_y & e^{-iak_a} k_y & e^{iak_b} k_b & -e^{-iak_b} k_b & -e^{iak_b} k_y & -e^{-iak_b} k_y \\ -e^{idk_x} k_a & e^{idk_x} k_a & e^{idk_x} k_y & e^{idk_x} k_y & e^{idk_b} k_b & -e^{-idk_b} k_b & -e^{idk_b} k_y & -e^{-idk_b} k_y \\ -e^{iak_a} k_y & -e^{-iak_a} k_y & -e^{iak_a} \kappa_a & e^{-iak_a} \kappa_a & e^{iak_b} k_y & e^{-iak_b} k_y & e^{iak_b} \kappa_b & -e^{-iak_b} \kappa_b \\ -e^{idk_x} k_y & -e^{idk_x} k_y & -e^{idk_x} \kappa_a & e^{idk_x} \kappa_a & e^{idk_b} k_y & e^{-idk_b} k_y & e^{idk_b} \kappa_b & -e^{-idk_b} \kappa_b \\ e^{iak_a} f_a & e^{-iak_a} f_a & -e^{iak_a} m_a & e^{-iak_a} m_a & -e^{iak_b} f_b & -e^{-iak_b} f_b & e^{iak_b} m_b & -e^{-iak_b} m_b \\ e^{idk_x} f_a & e^{idk_x} f_a & -e^{idk_x} m_a & e^{idk_x} m_a & -e^{idk_b} f_b & -e^{-idk_b} f_b & e^{idk_b} m_b & -e^{-idk_b} m_b \\ e^{iak_a} n_a & -e^{-iak_a} n_a & e^{iak_a} h_a & e^{-iak_a} h_a & -e^{iak_b} n_b & e^{-iak_b} n_b & -e^{iak_b} h_b & -e^{-iak_b} h_b \\ e^{idk_x} n_a & -e^{idk_x} n_a & e^{idk_x} h_a & e^{idk_x} h_a & -e^{idk_b} n_b & e^{-idk_b} n_b & -e^{idk_b} h_b & -e^{-idk_b} h_b \end{pmatrix} = 0.$$

Here  $k_{a,b} = \sqrt{k_{l(a,b)}^2 - k_y^2}$ ,  $\kappa_{a,b} = \sqrt{k_{t(a,b)}^2 - k_y^2}$  are the  $x$ -components of the wave vector of the longitudinal and transverse mode in the layers and  $k_y$  is common for the both modes  $y$ -component of the wave vector. The dispersion relations for the modes in the media  $a$  and  $b$  are given by Eqs. (2.7) and (2.8). Other notations are defined as follows:

$$(2.32) \quad f_{a,b} = \frac{i}{\omega} (\rho_{a,b} \omega^2 + 2i\omega \eta_{a,b} k_y^2),$$

$$m_{a,b} = 2\eta_{a,b} k_y \kappa_{a,b}, \quad n_{a,b} = 2\eta_{a,b} k_{a,b} k_y, \quad h_{a,b} = \eta_{a,b} (-k_y^2 + \kappa_{a,b}^2).$$

Explicit calculation of the determinant leads to  $8! = 40,320$  terms in the dispersion equation. However, it can be essentially simplified in some particular cases and/or in the approximation of low viscosity. If sound wave propagates along the superlattice axis (normal incidence), the determinant factorises in two terms corresponding to the longitudinal and transverse mode. Only for this geometry these two modes are decoupled, giving rise to the

following two independent dispersion relations:

$$(2.33) \quad \cos(k_x d) = \cos(ak_a) \cos(bk_b) - \frac{1}{2} \left[ \frac{k_a \rho_b}{k_b \rho_a} + \frac{k_b \rho_a}{k_a \rho_b} \right] \sin(ak_a) \sin(bk_b),$$

$$(2.34) \quad \cos(k_x d) = \cos(a\kappa_a) \cos(b\kappa_b) - \frac{1}{2} \left[ \frac{\kappa_a \rho_b}{\kappa_b \rho_a} + \frac{\kappa_b \rho_a}{\kappa_a \rho_b} \right] \sin(a\kappa_a) \sin(b\kappa_b).$$

Here  $k_{a,b}(\kappa_{a,b})$  is the  $x$ -component of the longitudinal (transverse) mode in each layer.

$$(2.35) \quad k_{a,b} = \frac{\omega/c_{a,b}}{\sqrt{1 - i \frac{\omega}{\rho_{a,b} c_{a,b}^2} (\frac{4}{3} \eta_{a,b} + \xi_{a,b})}},$$

$$(2.36) \quad \kappa_{a,b} = \sqrt{\frac{2i}{\delta_{a,b}}}.$$

If layer  $b$  is an elastic dissipationless solid, then  $k_b = \omega/c_l$ ,  $\eta_b = \xi_b = 0$  and  $\kappa_b = \omega/c_t$ . Note that in the limit of weak attenuation, the imaginary part of  $k_{a,b} \propto \omega^2$ , which is a signature of pure bulk dissipation. The boundary layer is not formed at normal incidence.

Equations (2.33) and (2.34) have "standard" Rytov's form. Equation (2.34) provides dispersion for the transverse wave. It turns out to be almost a deaf mode since it cannot be excited at normal incidence if the wave source is in the far zone or if the environment outside the superlattice is an ideal fluid. The dispersion equations are exact over viscosity coefficients  $\eta$  and  $\xi$ . In the most interesting case of low viscosity the linear expansion of Eq. (2.33) gives the following result for the attenuation coefficient of the longitudinal wave:

$$(2.37) \quad k_x''(\omega)d = \frac{\omega^2}{2 \sin(k'_x d)} \left\{ \frac{(\frac{4}{3} \eta_a + \xi_a)a}{\rho_a c_a^3} \sin\left(\frac{\omega a}{c_a}\right) \cos\left(\frac{\omega b}{c_b}\right) + \frac{(\frac{4}{3} \eta_b + \xi_b)b}{\rho_b c_b^3} \sin\left(\frac{\omega b}{c_b}\right) \cos\left(\frac{\omega a}{c_a}\right) \right. \\ \left. + \frac{1}{2\omega} \left( \frac{\frac{4}{3} \eta_a + \xi_a}{\rho_a c_a^2} - \frac{\frac{4}{3} \eta_b + \xi_b}{\rho_b c_b^2} \right) \left( \frac{\rho_b c_b}{\rho_a c_a} - \frac{\rho_a c_a}{\rho_b c_b} \right) \sin\left(\frac{\omega a}{c_a}\right) \sin\left(\frac{\omega b}{c_b}\right) \right. \\ \left. + \frac{1}{2} \left( \frac{\rho_a c_a}{\rho_b c_b} + \frac{\rho_b c_b}{\rho_a c_a} \right) \left[ \frac{(\frac{4}{3} \eta_a + \xi_a)a}{\rho_a c_a^3} \cos\left(\frac{\omega a}{c_a}\right) \sin\left(\frac{\omega b}{c_b}\right) + \frac{(\frac{4}{3} \eta_b + \xi_b)b}{\rho_b c_b^3} \sin\left(\frac{\omega a}{c_a}\right) \cos\left(\frac{\omega b}{c_b}\right) \right] \right\}.$$

Close to the edges of the Brillouin zone, where  $k_x d \rightarrow \pm\pi$  the dissipation infinitively grows due to the factor  $\sin(k_x d)$  in the denominator. Here propagating wave becomes a standing wave and even very low viscosity leads to high dissipated power. Of course, the



linear approximation fails in this region. Away from the band edges the linear approximation is very close to the exact values of  $k_x''$  calculated from Eq. (2.33). Frequency dependence of the attenuation coefficient for water-glycerol superlattice is given in Fig. 2.2. Material properties can be found in Table 2.1. Near the edges of the band gaps the attenuation coefficient exhibits sharply non-monotonic behavior. Here the difference between the exact and approximate values becomes essential.

Material	$\rho, \frac{kg}{m^3}$	$\lambda, GPa$	$\eta, Pa \cdot s$	$\mu, GPa$
Water	1000	1.96	0.001	-
Glycerol	1200	3.072	0.9	-
Polymethyl methacrylate (PMMA)	1200	3	-	1.7

TABLE 2.1. Density, elastic moduli and viscosity of the materials used in the numerical calculations.

At low frequencies the graph  $k_x''(\omega)$  in Fig. 2.2 is close to a parabola. The parabolic dependence is a signature of a homogeneous medium. In the low-frequency limit  $\omega a/c_a, \omega b/c_b \ll 1$  a periodic structure homogenizes with effective elastic modulus  $\lambda_{eff} = \left(\frac{f}{\lambda_a} + \frac{1-f}{\lambda_b}\right)^{-1}$ , effective mass density  $\rho_{eff} = f\rho_a + (1-f)\rho_b$ , and effective speed of sound  $c_{eff} = \sqrt{\lambda_{eff}/\rho_{eff}}$ . Here  $f = a/d$  is the filling fraction of material  $a$ . In the long-wavelength limit Eq. (2.37) can be further simplified replacing sine functions by their arguments. After simple algebra Eq. (2.37) yields  $k_x'' \sim \omega^2$ . Due to this quadratic scaling the effective viscosity of a periodic structure

$$(2.38) \quad \frac{4}{3}\eta_{eff} + \xi_{eff} = \lambda_{eff}^2 \left( f \frac{\frac{4}{3}\eta_a + \xi_a}{\lambda_a^2} + (1-f) \frac{\frac{4}{3}\eta_b + \xi_b}{\lambda_b^2} \right).$$

can be introduced through the attenuation coefficient (2.14) of the corresponding homogeneous effective medium,  $k_x'' = \frac{\omega^2}{2\rho_{eff}c_{eff}^3}(\frac{4}{3}\eta_{eff} + \xi_{eff})$ . Each layer of the viscous fluid gives an additive contribution to the effective viscosity with the weighting factors  $\lambda_{eff}^2/\lambda_{a,b}^2$ . Note that because of relatively low acoustic contrast between water and glycerol, the region of linear dispersion of sound extends practically to the first band gap.

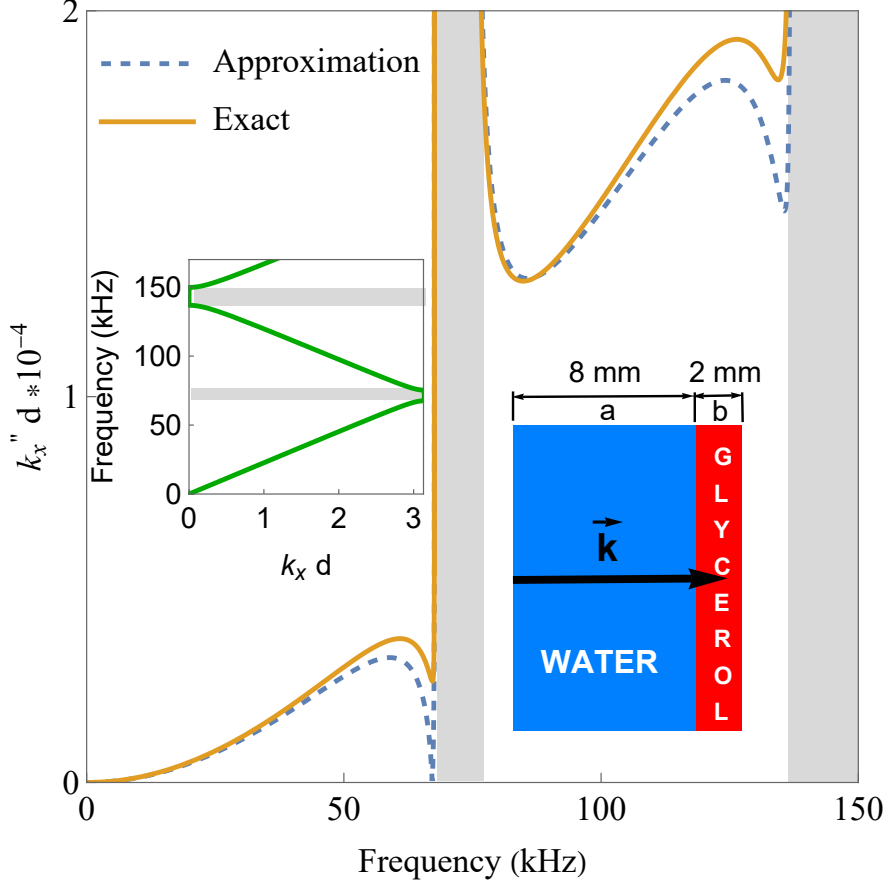


FIGURE 2.2. Frequency dependence of the attenuation coefficient of the longitudinal sound and normal incidence for water-glycerol superlattice with filling fraction of water  $f = 0.8$ . The exact result is calculated from Eq. (2.33) and the linear over viscosity approximation is given by Eq. (2.37). Both results exhibit fast growth near the band edge: the exact value remains finite and the approximate approaches infinity. Note that even for relatively high viscosity of glycerol the decay length is of the order of  $10^4$  lattice periods. The opposite case of very strong viscous absorption when the boundary layers overlap within the lattice period is numerically considered in Ref. [80, 95]. Left inset: the band structure of the water-glycerol superlattice. The band gaps are shaded in grey. Right inset: the unit cell with geometrical parameters.

The superlattice behaves as a homogeneous medium up to the frequency 50 kHz. The decay coefficient exhibits here the parabolic dependence on frequency and the effective viscosity can be evaluated from Eq. (2.38).

In the case of oblique incidence the longitudinal and transverse modes are strongly coupled at the interface between two viscous fluids (or between viscous fluid and a solid). The exact dispersion equation obtained from the determinant Eq. (2.31) becomes too cumbersome. It, however, can be essentially simplified assuming weak viscous losses. Due to formation of the viscous boundary layer  $\delta$  the dissipated power scales as  $\sqrt{\omega\eta}$ . At frequencies,  $\omega \ll \omega^*$  power dissipated in the bulk gives much less contribution since it scales as  $\omega^2\eta$ . While dissipation at oblique incidence exceeds greatly dissipation at normal incidence, the assumption of weak sound attenuation remains, i.e. the wave propagates through the lattice without essential decay for many periods. The viscous boundary layer  $\delta$  and the power dissipated within this layer originate from the last two equations of the set (2.28) containing off-diagonal elements  $\sigma_{xy}$ . The corresponding terms in the determinant Eq. (2.31) lead (at oblique incidence) to the terms proportional to different powers of  $\delta$  in the dispersion relation. Assuming weak dissipation, only the linear over  $\delta \propto \sqrt{\eta}$  terms are left. The contribution of bulk dissipation proportional to different powers of  $\eta$  and  $\xi$  can usually be neglected except for a narrow interval of angles of propagation almost parallel to the superlattice axis. Within this narrow interval a transition from dissipation in the boundary layer to dissipation in the bulk of the fluid occurs. This transition is analyzed in Section 2.4.2, using the dispersion equation, where all the bulk dissipation terms are calculated exactly. Note that the terms of order  $\delta^2 \propto \eta$  can be easily discriminated from the linear over  $\eta$  bulk terms, since the  $\delta^2$ -contribution, being related to the boundary layer, vanishes at normal incidence. One more approximation that simplifies the dispersion relation is due to the limit  $\tan((1+i)\frac{a}{\delta}) \rightarrow i$  valid if  $\delta \ll a$ . The latter condition is usually satisfied for a very wide range of frequencies. Taking into account the aforementioned approximations, the dispersion equation for the most practical case of fluid-solid superlattice is obtained in the following form:

(2.39)

$$\begin{aligned}
& 8[\alpha_1\alpha_2 \sin(b\kappa_b) + \alpha_2 k_y^2 \sin(bk_b) + (1+i)\delta_a(\beta_0 \cos(bk_b) + \beta_1 \cos(b\kappa_b))] \cos(k_x d) = -8\alpha_1 k_y^2 \sin(ak_a) \\
& - [\alpha_1 - \alpha_2 - k_y^2]^2 \sin(x_1) - [\alpha_1 + \alpha_2 - k_y^2]^2 \sin(x_2) + [\alpha_1 - \alpha_2 + k_y^2]^2 \sin(x_3) + [\alpha_1 + \alpha_2 + k_y^2]^2 \sin(x_4) \\
& + (1+i)\delta_a [-(\alpha_1 - \alpha_2 - k_y^2)(\beta_2 - \beta_3 + \beta_4) \cos(x_1) + (\alpha_1 + \alpha_2 - k_y^2)(\beta_2 + \beta_3 - \beta_4) \cos(x_2) \\
& - (\alpha_1 - \alpha_2 + k_y^2)(\beta_2 - \beta_3 - \beta_4) \cos(x_3) + (\alpha_1 + \alpha_2 + k_y^2)(\beta_2 + \beta_3 + \beta_4) \cos(x_4) + \beta_5 \cos(ak_a)].
\end{aligned}$$

Here

$$\begin{aligned}
(2.40) \quad \alpha_1 &= \frac{(\omega^2 - 2c_t^2 k_y^2)^2 c_b}{4c_t^3 \sqrt{(\omega^2 - c_b^2 k_y^2)(\omega^2 - c_t^2 k_y^2)}}, \quad \alpha_2 = \frac{\rho_a \omega^4 c_a}{4\rho_b c_t^3 \sqrt{(\omega^2 - c_a^2 k_y^2)(\omega^2 - c_t^2 k_y^2)}}, \\
\beta_0 &= \frac{k_y^2 \rho_a \omega^4 (\omega^2 (\rho_a / \rho_b - 1) + 2c_t^2 k_y^2) c_a c_b}{8\rho_b c_t^5 \sqrt{(\omega^2 - c_a^2 k_y^2)(\omega^2 - c_b^2 k_y^2)(\omega^2 - c_t^2 k_y^2)}}, \quad \beta_1 = \frac{\rho_a \omega^4 (\omega^2 \rho_a / \rho_b + 2c_t^2 k_y^2) (\omega^2 - 2c_t^2 k_y^2) c_a c_b}{16\rho_b c_t^7 \sqrt{(\omega^2 - c_a^2 k_y^2)(\omega^2 - c_b^2 k_y^2)(\omega^2 - c_t^2 k_y^2)}}, \\
\beta_2 &= \frac{\rho_a \omega^4 c_b}{4\rho_b c_t^4 \sqrt{\omega^2 - c_b^2 k_y^2}}, \quad \beta_3 = \frac{(\omega^2 \rho_a / \rho_b + 2c_t^2 k_y^2)^2 c_a}{4c_t^4 \sqrt{\omega^2 - c_a^2 k_y^2}}, \quad \beta_4 = \frac{k_y^2 (\omega^2 (\rho_a / \rho_b - 1) + 2c_t^2 k_y^2)^2 c_a c_b}{4c_t^3 \sqrt{(\omega^2 - c_a^2 k_y^2)(\omega^2 - c_b^2 k_y^2)(\omega^2 - c_t^2 k_y^2)}}, \\
\beta_5 &= \frac{k_y^2 (\omega^2 - 2c_t^2 k_y^2) (\omega^2 \rho_a / \rho_b + 2c_t^2 k_y^2) (\omega^2 (\rho_a / \rho_b - 1) + 2c_t^2 k_y^2) c_a c_b}{c_t^5 \sqrt{(\omega^2 - c_a^2 k_y^2)(\omega^2 - c_b^2 k_y^2)(\omega^2 - c_t^2 k_y^2)}}.
\end{aligned}$$

The subindex  $a(b)$  is related to viscous fluid (elastic solid). The direction of propagation is fixed by the transverse wave vector component  $k_y$ , which is given by the angle of incidence of the external excitation and it is conserved during wave refraction at the superlattice interfaces. Together with frequency  $\omega$  these two parameters completely define the Bloch wave in the layered structure. The longitudinal components of the wave vectors in the fluid and solid layers are obtained from the local dispersion relations

$$\begin{aligned}
(2.41) \quad k_a^2 + k_y^2 &= \frac{\omega^2 / c_a^2}{1 - i \frac{\omega}{\rho_a c_a^2} (\frac{4}{3} \eta_a + \xi_a)}, \quad c_a^2 = \frac{\lambda_a}{\rho_a}, \\
k_b^2 + k_y^2 &= \frac{\omega^2}{c_b^2}, \quad c_b^2 = \frac{\lambda_b + 2\mu_b}{\rho_b}, \\
\kappa_b^2 + k_y^2 &= \frac{\omega^2}{c_t^2}, \quad c_t^2 = \frac{\mu_b}{\rho_b}.
\end{aligned}$$

Other notations in Eq. (2.39) are defined as

$$(2.42) \quad \begin{aligned} x_1 &= ak_a - b(k_b - \kappa_b), & x_2 &= ak_a + b(k_b - \kappa_b), \\ x_3 &= ak_a - b(k_b + \kappa_b), & x_4 &= ak_a + b(k_b + \kappa_b). \end{aligned}$$

The limiting case when  $\delta_a, \eta_a, \xi_a = 0$  corresponds to completely the dissipationless structure of elastic solid and ideal fluid. In this case the dispersion equation becomes real

$$(2.43) \quad \begin{aligned} &8[\alpha_1\alpha_2 \sin(b\kappa_b) + \alpha_2k_y^2 \sin(bk_b)] \cos(k_xd) = -8\alpha_1k_y^2 \sin(ak_a) - [\alpha_1 - \alpha_2 - k_y^2]^2 \sin(x_1) \\ &-[\alpha_1 + \alpha_2 - k_y^2]^2 \sin(x_2) + [\alpha_1 - \alpha_2 + k_y^2]^2 \sin(x_3) + [\alpha_1 + \alpha_2 + k_y^2]^2 \sin(x_4) \end{aligned}$$

Equation (2.43) coincides with the result reported in Ref. [101].

In the special case of normal incidence of longitudinal sound wave, the boundary layer is not formed and dissipation occurs in the bulk of viscous fluid. The dispersion relation accounting for the dissipative losses in the bulk and oblique propagation can be written in the same form as Eq. (2.39) but the parameters  $\alpha$  and  $\beta$  are redefined. General formulas for these parameters are given below:

$$(2.44) \quad \begin{aligned} \alpha_1 &= \frac{(\rho_b\omega^2 - 2\mu_bk_y^2)^2}{4k_b\kappa_b\mu_b^2}, & \alpha_2 &= \frac{(\rho_a\omega^2 + 2i\omega\eta_ak_y^2)\rho_b\omega^2}{4k_a\kappa_b\mu_b^2}, \\ \beta_0 &= \frac{k_y^2((\rho_a\omega^2 + i\omega\eta_ak_y^2)(\omega^2(\rho_a - \rho_b) + 2\mu_bk_y^2) + i\omega\eta_ak_y^2\rho_a\omega^2)\rho_b\omega^2}{8k_ak_b\kappa_b\mu_b^3}, \\ \beta_1 &= \frac{[(\rho_a\omega^2 + 2i\omega\eta_ak_y^2)(\rho_a\omega^2 + \mu_bk_y^2) + \mu_bk_y^2\rho_a\omega^2](\rho_b\omega^2 - 2\mu_bk_y^2)\rho_b\omega^2}{16k_ak_b\kappa_b\mu_b^4}, \\ \beta_2 &= \frac{\rho_a\rho_b\omega^4}{4k_b\mu_b^2}, & \beta_3 &= \frac{(\rho_a\omega^2 + 2(\mu_b + i\omega\eta_a)k_y^2)(\rho_a\omega^2 + 2\mu_bk_y^2)}{4k_a\mu_b^2}, \\ \beta_4 &= \frac{k_y^2(\omega^2(\rho_a - \rho_b) + 2(\mu_b + i\omega\eta_a)k_y^2)(\omega^2(\rho_a - \rho_b) + 2\mu_bk_y^2)}{4k_ak_b\kappa_b\mu_b^2}, \\ \beta_5 &= \frac{k_y^2(\rho_b\omega^2 - 2\mu_bk_y^2)[(\rho_a\omega^2 + 2(\mu_b + i\omega\eta_a)k_y^2)(\omega^2(\rho_a - \rho_b) + 2\mu_bk_y^2) + i\omega\eta_ak_y^2\rho_b\omega^2]}{k_ak_b\kappa_b\mu_b^3}. \end{aligned}$$

Note that the local dispersion relations Eq. (2.41) include bulk dissipation. In the case of normal incidence the dispersion relation (2.39) with parameters given by Eq. (2.44)

is simplified to the following form:

$$(2.45) \quad \cos(k_x d) = \cos(ak_a) \cos(bk_b) + \frac{1}{2} \left( \frac{k_a(\lambda_a - \frac{4}{3}i\omega\eta_a - i\omega\xi_a)}{k_b(\lambda_b + 2\mu_b)} + \frac{k_b(\lambda_b + 2\mu_b)}{k_a(\lambda_a - \frac{4}{3}i\omega\eta_a - i\omega\xi_a)} \right) \sin(ak_a) \sin(bk_b).$$

Equation (2.45) coincides with Eq. (2.33) providing the local dispersion relations (2.41) are satisfied.

## 2.4. Analysis of Attenuation of Sound in Superlattices with Different Constituents

### 2.4.1. Unit Cell of Viscous and Ideal Fluids

In a superlattice where the layer  $a$  is a viscous fluid and the layer  $b$  is an ideal fluid ( $\eta_b = 0$ ) the dispersion relation (2.39) can be simplified to the following form

$$(2.46) \quad \begin{aligned} \cos(k_x d) &= \cos(ak_a) \cos(bk_b) \\ &- \frac{1}{2} \left[ \frac{\omega\rho_b k_a}{(\omega\rho_a + 2i\eta_a k_y^2)k_b} + \frac{(\omega\rho_a + 2i\eta_a k_y^2)k_b}{\omega\rho_b k_a} \right] \sin(ak_a) \sin(bk_b) \\ &- 2ik_y^2 \eta_a \delta_a \left[ \frac{k_a}{\omega\rho_a + 2i\eta_a k_y^2} \sin(ak_a) \cos(bk_b) + \frac{k_b}{\omega\rho_b} \sin(bk_b) \cos(ak_a) \right]. \end{aligned}$$

In the quasistatic limit  $\omega, k_x \rightarrow 0$  the complex Bloch vector  $k_x = k'_x + ik''_x$  can be calculated explicitly

$$(2.47) \quad \begin{aligned} \frac{k_x^2 d^2}{2} &\approx \left( \frac{k'_x{}^2}{2} + ik'_x k''_x \right) d^2 = \omega^2 \frac{(a\rho_a + b\rho_b)}{2\lambda_a \lambda_b} \left[ a\lambda_b + b\lambda_a - (b\lambda_a c_b^2 + a\lambda_b c_a^2) \frac{\sin^2(\theta_a)}{c_a^2} \right] \\ &+ i \frac{2\sqrt{2}\eta_a^{3/2} \omega^{5/2} [a\lambda_b + b\lambda_a - (b\lambda_a c_b^2 + a\lambda_b c_a^2)(\sin(\theta_a)/c_a)^2]}{\sqrt{\rho_a} \lambda_a \lambda_b} \left( \frac{\sin(\theta_a)}{c_a} \right)^2. \end{aligned}$$

The imaginary part of the right-hand side of Eq.(2.47) is proportional to  $\sin^2(\theta_a)$ , i.e., it contributes to dissipation only at oblique incidence. The decay coefficient scales as  $k''_x \propto (\omega\eta)^{3/2}$ , which is different from the scaling of dissipation at solid-viscous or viscous-viscous interface. This qualitative difference is due to lack of shear modulus in an ideal fluid. At normal incidence dissipation is due solely to the losses in the bulk of viscous fluid. These losses are omitted in Eq. (2.47).

In a special case when the viscous layer is sufficiently thin the dissipative losses vanish at the frequency of Bragg reflection. In X-ray diffraction, the effect of anomalous

transmission through a crystal was observed by Borrmann in 1941 [5]. Optical analog of the Borrmann effect in 1D photonic crystals with absorbing layers was observed in Ref. [4, 62]. Anomalous transmission of sound through a periodic set of absorbing porous sheets in air was reported in Ref. [10]. The peaks of transmission are close to the positions of the band gaps, where transmission is usually suppressed. Theoretical treatment of this acoustic analog of the Borrmann effect was reported in Ref. [15] where porous sheets are considered as  $\delta$ -like resistive scatterers. Acoustic resistance of a narrow porous layer gives rise to a jump discontinuity of acoustic pressure at each sheet.

Borrmann effect in acoustics may be realized in a superlattice of narrow layers of high-viscosity fluid and thick layers of ideal fluid. Let the thickness  $a$  of the viscous layer is much less than the wavelength. At the same time, the thickness  $a$  exceeds much the thickness of the boundary layer, *viz.*

$$(2.48) \quad \delta_a \omega / c_a \ll a \omega / c_a \ll 1.$$

Expanding trigonometric functions in Eq. (2.46) and keeping linear over  $a\eta_a$  terms the following dispersion equation is obtained:

$$(2.49) \quad \cos(k_x d) = \cos(k_b d) - iU \sin(k_b d), \quad k_{a,b} = \sqrt{\left(\frac{\omega}{c_{a,b}}\right)^2 - k_y^2},$$

where

$$(2.50) \quad U = (ak_a'') \frac{\omega \rho_b}{k_b c_a \rho_a} + \frac{a \delta_a^2 k_y^2}{2k_b} \left( k_b^2 \frac{\rho_a}{\rho_b} - k_a^2 \frac{\rho_b}{\rho_a} \right).$$

It is clear that dissipation vanishes at the frequencies of Bragg's diffraction where  $\sin(k_b d) = 0$ . Figure 2.3 shows the angular dependence of the decay coefficient for two frequencies of 35 and 60 kHz. Very narrow deep minima appear exactly at the Bragg's frequencies. The same dispersion equation was obtained for the superlattice with resistive scatterers [15]. The strength of the parameter  $U$  is proportional to the amplitude of jump discontinuity of pressure. Here the nature of the parameter  $U$  is related to viscosity of the layer  $a$ . The first term in Eq. (2.50) is due to dissipation in the bulk. It is proportional to the decay coefficient of the longitudinal mode (2.14) in free fluid,  $k_a'' = \omega^2 (\frac{4}{3}\eta_a + \xi_a) / (2\rho_a c_a^3)$ . While

the second term contains the thickness  $\delta_a^2$  and it vanishes at normal incidence,  $k_y = 0$ , it cannot be associated with dissipation in the boundary layer since the layer is not formed at the interface with ideal fluid. Also, dissipation in the boundary layer is proportional to  $\delta_a$ . This term, as well as the first term is the contribution of the bulk dissipation modified by multiple scattering at oblique incidence.

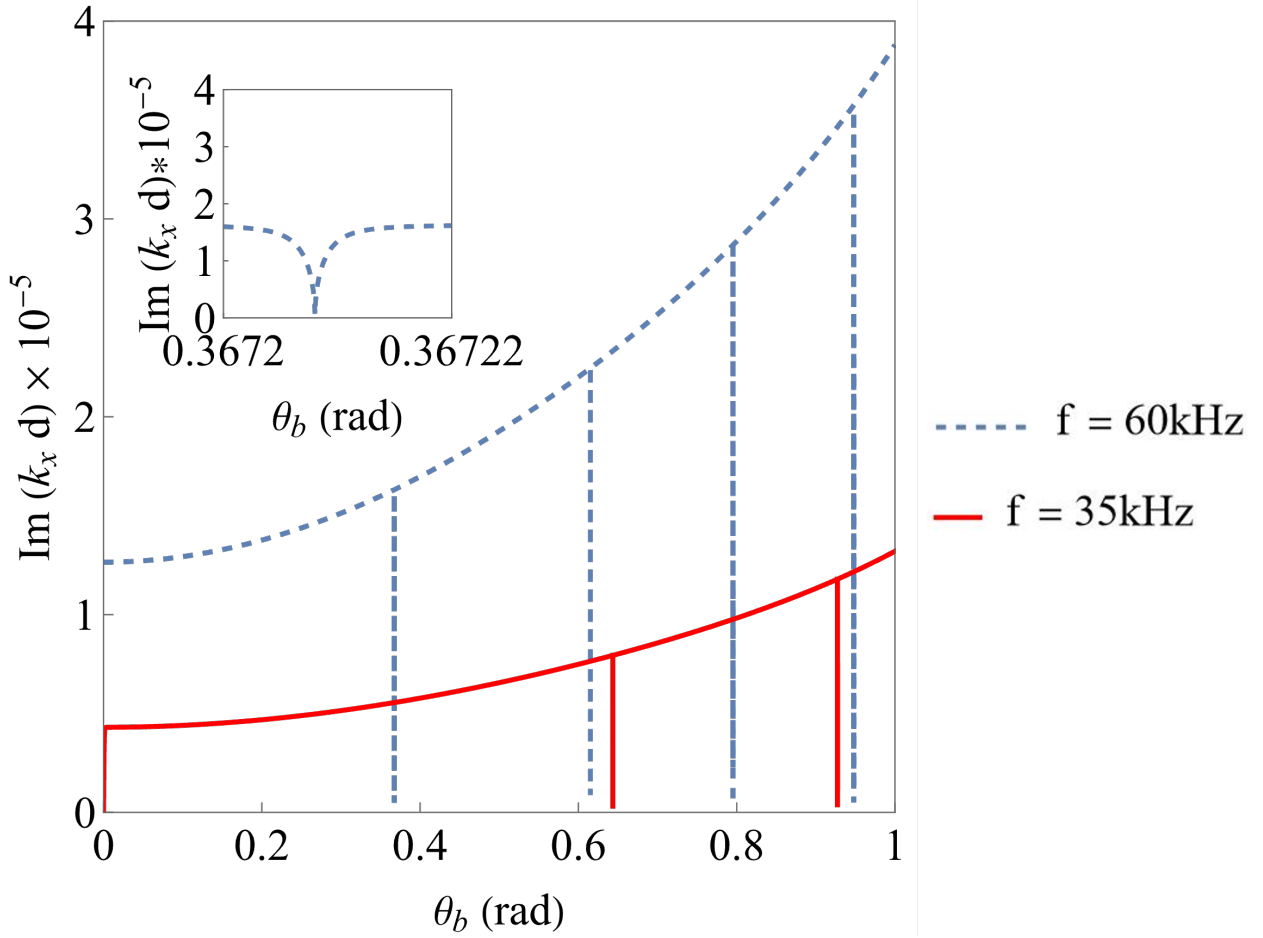


FIGURE 2.3. Borrmann effect. Angular dependence of the dimensionless decay coefficient for a superlattice with narrow ( $a = 1$  mm) viscous layer of glycerol and thick layer ( $b \approx d = 100\text{mm}$ ) of inviscid water. Inset shows the fine structure of deep minima near the frequencies of Bragg scattering.

Assuming that the speeds of sound in the viscous and ideal fluid do not differ much, it is easy to see that both terms contributing to  $U$  are small parameters. The first term  $\sim ak_i'' \ll 1$  since the decay length of sound  $1/k_i''$  is much longer than the period of the



lattice. The second term  $\sim a\delta_a^2/\lambda^3 \ll 1$  since  $a$  and  $\delta_a$  are small in comparison with the wavelength  $\lambda$ . If the angle of incidence is not small, i.e.,  $k_y \sim k_x$ , both terms are of the same order of magnitude. This can be seen by expressing each term through, density, viscosity and frequency. Thus, the Borrmann effect may be observed in transmission of sound through a superlattice with narrow viscous layers. The structure of the resonant peaks in the transmission coefficient was analyzed in details in Ref. [15].

#### 2.4.2. Unit Cell of Two Different Viscous Fluids

If both layers in the unit cell are different viscous fluids, for example water and glycerol, the dispersion equation becomes more complicated due to existence of two boundary layers,  $\delta_a$  and  $\delta_b$ . The dispersion equation is obtained from the determinant Eq. (2.31) assuming weak dissipation. Keeping the linear over  $\delta_a$  and  $\delta_b$  terms and all the terms related to bulk dissipation the dispersion equation can be reduced to the following form:

$$(2.51) \quad \begin{aligned} \cos(k_x d) &= \cos(ak_a) \cos(bk_b) \\ &- \frac{1}{2} \left[ \frac{k_b(\rho_a \omega + 2i\eta_a k_y^2)}{k_a(\rho_b \omega + 2i\eta_b k_y^2)} + \frac{k_a(\rho_b \omega + 2i\eta_b k_y^2)}{k_b(\rho_a \omega + 2i\eta_a k_y^2)} \right] \sin(ak_a) \sin(bk_b) \\ &- \frac{ik_y^2 \delta_a \delta_b (\rho_a - \rho_b) [(\rho_a - \rho_b)\omega + 2i(\eta_a - \eta_b)k_y^2]}{2(\delta_a \rho_a + \delta_b \rho_b)} \times \\ &\left[ \frac{\cos(ak_a) \sin(bk_b)}{k_b(\rho_a \omega + 2i\eta_a k_y^2)} + \frac{\sin(ak_a) \cos(bk_b)}{k_a(\rho_b \omega + 2i\eta_b k_y^2)} \right]. \end{aligned}$$

This dispersion relation is symmetric over indices  $a$  and  $b$ . Note that while the last term contains quadratic over  $\delta_a$  and  $\delta_b$  contribution in the numerator, it is kept due to presence of a linear combination of deltas in the denominator. In the quasistatic limit the decay coefficient can be explicitly obtained from Eq. (2.51):

$$(2.52) \quad \begin{aligned} \frac{k_x^2 d^2}{2} &\approx \left( \frac{k_x'^2}{2} + ik_x' k_x'' \right) d^2 = \omega^2 \frac{(a\rho_a + b\rho_b)}{2\lambda_a \lambda_b} \left[ a\lambda_b + b\lambda_a - (b\lambda_a c_b^2 + a\lambda_b c_a^2) \frac{\sin^2(\theta_a)}{c_a^2} \right] \\ &+ \frac{i\omega^{3/2} (\rho_a - \rho_b)^2 (a\rho_a + b\rho_b) \sqrt{\eta_a \eta_b}}{\sqrt{2} (\rho_a \rho_b)^{3/2} (\sqrt{\eta_a \rho_a} + \sqrt{\eta_b \rho_b})} \left( \frac{\sin(\theta_a)}{c_a} \right)^2 + i\omega^3 \frac{a\rho_a + b\rho_b}{2} \left[ \frac{a(\frac{4}{3}\eta_a + \xi_a)}{\lambda_a^2} + \frac{b(\frac{4}{3}\eta_b + \xi_b)}{\lambda_b^2} \right] \\ &+ i\omega^3 ab \left[ \left( \frac{\eta_b}{\lambda_a} + \frac{\eta_a}{\lambda_b} - \frac{\eta_b \rho_a}{\lambda_b \rho_b} - \frac{\eta_a \rho_b}{\lambda_a \rho_a} \right) \left( \frac{\sin(\theta_a)}{c_a} \right)^2 + \left[ \frac{\eta_b \rho_a}{\rho_b^2} + \frac{\eta_a \rho_b}{\rho_a^2} - \frac{\eta_a}{\rho_b} - \frac{\eta_b}{\rho_a} \right] \left( \frac{\sin(\theta_a)}{c_a} \right)^4 \right]. \end{aligned}$$

The real parts of Eqs. (2.47) and (2.52) are the same since both of them give linear dispersion relation  $\omega = c_{eff}k$  in the corresponding homogenized medium with  $c_{eff} = \sqrt{\lambda_{eff}/\rho_{eff}}$ . The symmetry over indices  $a$  and  $b$  remains true since  $\sin \theta_a/c_a = \sin \theta_b/c_b$ .

The imaginary part of the Bloch vector  $k_x''$  calculated from Eq. (2.52) contains contributions of order  $\sqrt{\omega}$  and  $\omega^2$ , which are due to dissipation in the boundary layers and in the bulk of the fluids respectively. The boundary-layer contribution vanishes for small angles of incidence when  $\theta_a \rightarrow 0$ . It also vanishes if  $\rho_a \rightarrow \rho_b$ . This effect is a manifestation of the Third Newton's Law when two surfaces interacting only through friction forces are equally accelerated if their densities are the same. Due to equal acceleration, viscous friction between two very viscous fluids with close densities is strongly suppressed. If the angle  $\theta_a$  is not small the sound decay is due to dissipation in the boundary layers and  $k_x'' \propto \sqrt{\omega}$ . This term scales with viscosities as  $\frac{\sqrt{\omega}\sqrt{\eta_a\eta_b}}{\sqrt{\eta_a\rho_a+\sqrt{\eta_b\rho_b}}}$ , which is a generalization of  $\sqrt{\omega\eta}$  scaling for solid-fluid interface.

The boundary-layer term  $\propto \omega^{3/2} \sin^2 \theta_a$  in Eq.(2.52) contributes to dissipation only at oblique incidence. A smooth transition from dissipation in the boundary layer to dissipation in the bulk occurs within a narrow interval of angles near  $\theta_a = \Theta$ . Frequency dependence of the attenuation coefficient  $k_x''$  changes from  $\omega^2$  at  $\theta_a < \Theta$  to  $\sqrt{\omega}$  at  $\theta_a > \Theta$ . This transition is shown in Fig. 2.4. It is clear that the decay coefficient grows fast with angle  $\theta_a$  due to change of the dissipation mechanism from the bulk one to dissipation in the boundary layer. Equation (2.52) was used to plot Fig. 2.4. From the same equation the estimate for the transition angle  $\theta_a = \Theta$  can be obtained by equating the imaginary term  $\propto \omega^{3/2} \sin^2 \theta_a$ , which is responsible for attenuation in the boundary layer, to the  $\theta_a$ -independent imaginary term  $\propto \omega^3$  contributing to the bulk attenuation

$$(2.53) \quad \left(\frac{\sin(\Theta)}{c_a}\right)^2 = \frac{\omega^{3/2} (\rho_a\rho_b)^{3/2}}{\sqrt{2} (\rho_a - \rho_b)^2} \left(\sqrt{\frac{\rho_a}{\eta_b}} + \sqrt{\frac{\rho_b}{\eta_a}}\right) \left(a\frac{4}{3}\frac{\eta_a + \xi_a}{\lambda_a^2} + b\frac{4}{3}\frac{\eta_b + \xi_b}{\lambda_b^2}\right).$$

The angle  $\Theta$  increases with frequency ( $\Theta \propto \omega^{3/4}$ ) that can be seen in Fig. 2.4 where the transition from the concave to convex part is shifted to higher frequencies with  $\theta_a$ . Dependence on viscosity is nonmonotonic due to presence of two competing terms in the

numerator and denominator. If the viscosity  $\eta_a$  is fixed, the transition angle grows  $\sim \eta_b^{-1/4}$  for  $\eta_b \rightarrow 0$ . In the region  $\eta_b > \eta_a$  it increases as  $\eta_b^{1/2}$ . Of course, these asymptotics are valid as long as  $\Theta < 1$ . The graphs in Fig. 2.5 show the dependance  $\Theta(\eta_b)$  for different values of  $\eta_a$  at frequency 2 kHz which lies in the region of linear dispersion.

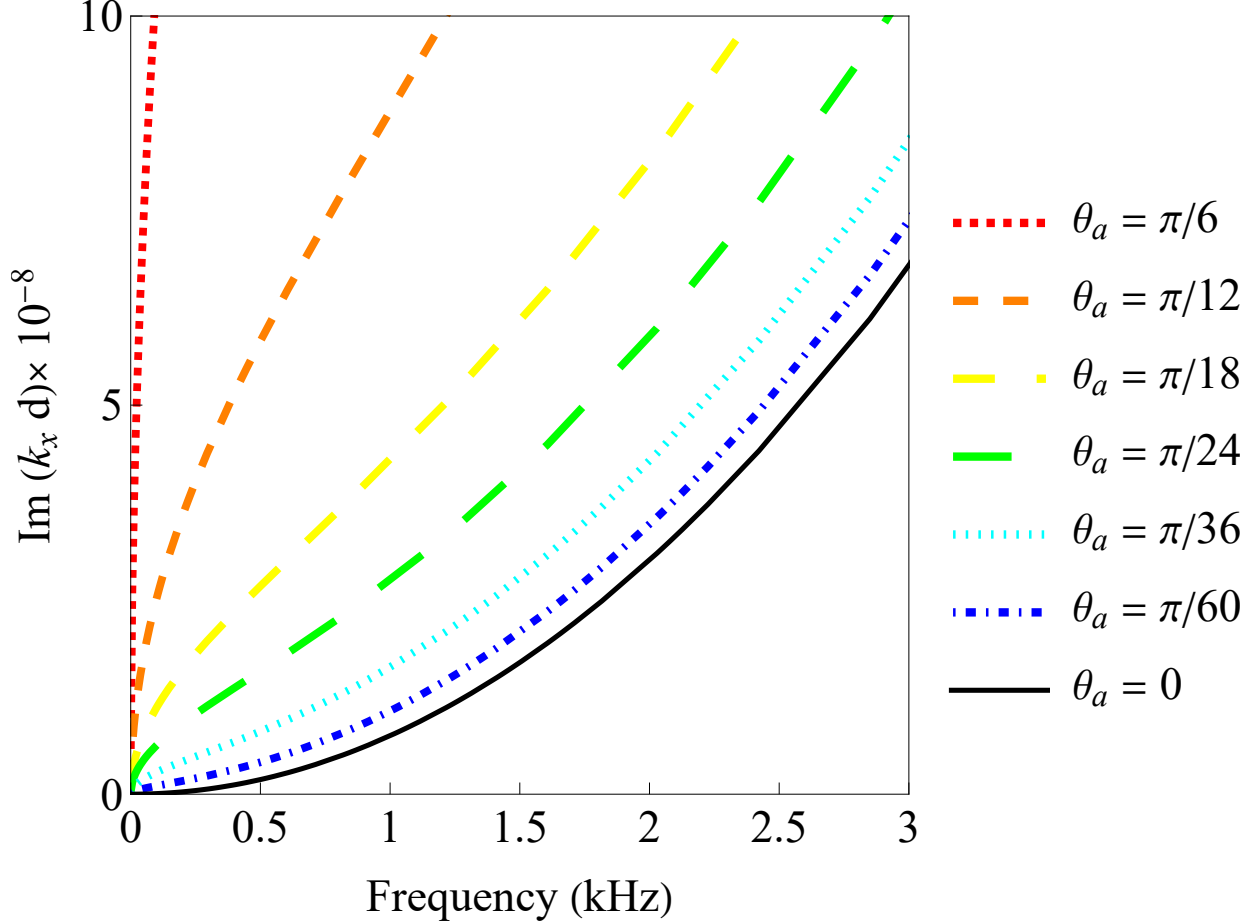


FIGURE 2.4. Graphs showing the transition from  $\omega^2$  (dissipation in the bulk) to  $\sqrt{\omega}$  (dissipation in the boundary layer) dependence for the decay coefficient with increasing angle of incidence  $\theta_a$  in the quasistatic region where the Bloch vector is obtained from Eq. (2.52). At a given frequency the transition occurs within a narrow interval of angles near the angle  $\Theta$  defined by Eq. (2.53).

At normal incidence the effective viscosities Eq. (2.38) can be introduced. They do not depend on frequency and linearly depend on the filling fraction  $f$ . At oblique incidence, the effective viscosity  $\eta$  becomes frequency dependent; therefore, it is more convenient to

work with the decay coefficient  $k_x''$ , for which dependence on the filling fraction is obtained from Eq. (2.52).

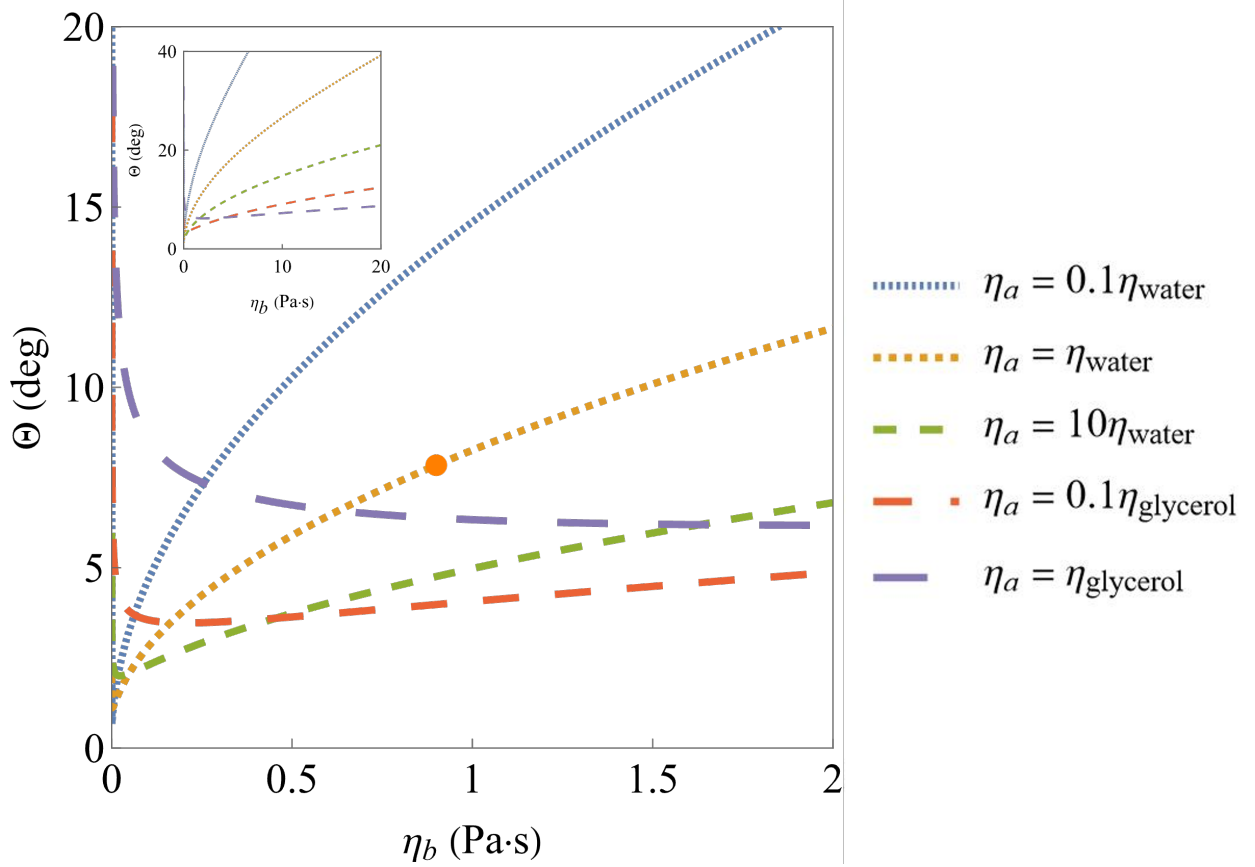


FIGURE 2.5. Nonmonotonic dependence  $\Theta(\eta_b)$  for different  $\eta_a$  at frequency 2 kHz. All the mechanical parameters except shear viscosity correspond to water ( $a = 8$  mm) and glycerol ( $b = 2$  mm). In a superlattice of real water and glycerol the transition from dissipation in the bulk to dissipation in the boundary layer occurs at relatively small angle  $\Theta = 7.8^\circ$  shown by the orange dot. Inset shows the same dependence for a wider range of viscosity  $\eta_b$ .

This dependence is shown in Fig. 2.6 for frequency 20 kHz which lies well below the first bandgap. Since the thickness of each layer must be much longer than the boundary layer thickness,  $\delta_a, \delta_b \ll a, (d - a)$ , the filling fraction of glycerol in Fig. 2.6 lies within  $0.1 < f < 0.9$ . The decay coefficient increases fast with the thickness of the more viscous

fluid (glycerol). Similar behavior was predicted for 2D phononic crystal [35, 36] where the circumference of the solid rods (and then the length of the boundary layer) increases with the filling fraction as  $\sqrt{f}$ . For 1D phononic crystal the area covered by both boundary layers does not change with the filling fraction. The dependence  $k_x''(f)$  appears because for larger filling fractions the less viscous fluid (water) is gradually replaced by glycerol with viscosity almost  $10^3$  of the viscosity of water. Thus, the physical reason of strong  $f$ -dependence in Fig. 2.6 is not related to the dissipation in the boundary layers. It is due to high viscosity contrast and to the contribution of bulk dissipation in glycerol which cannot be neglected.

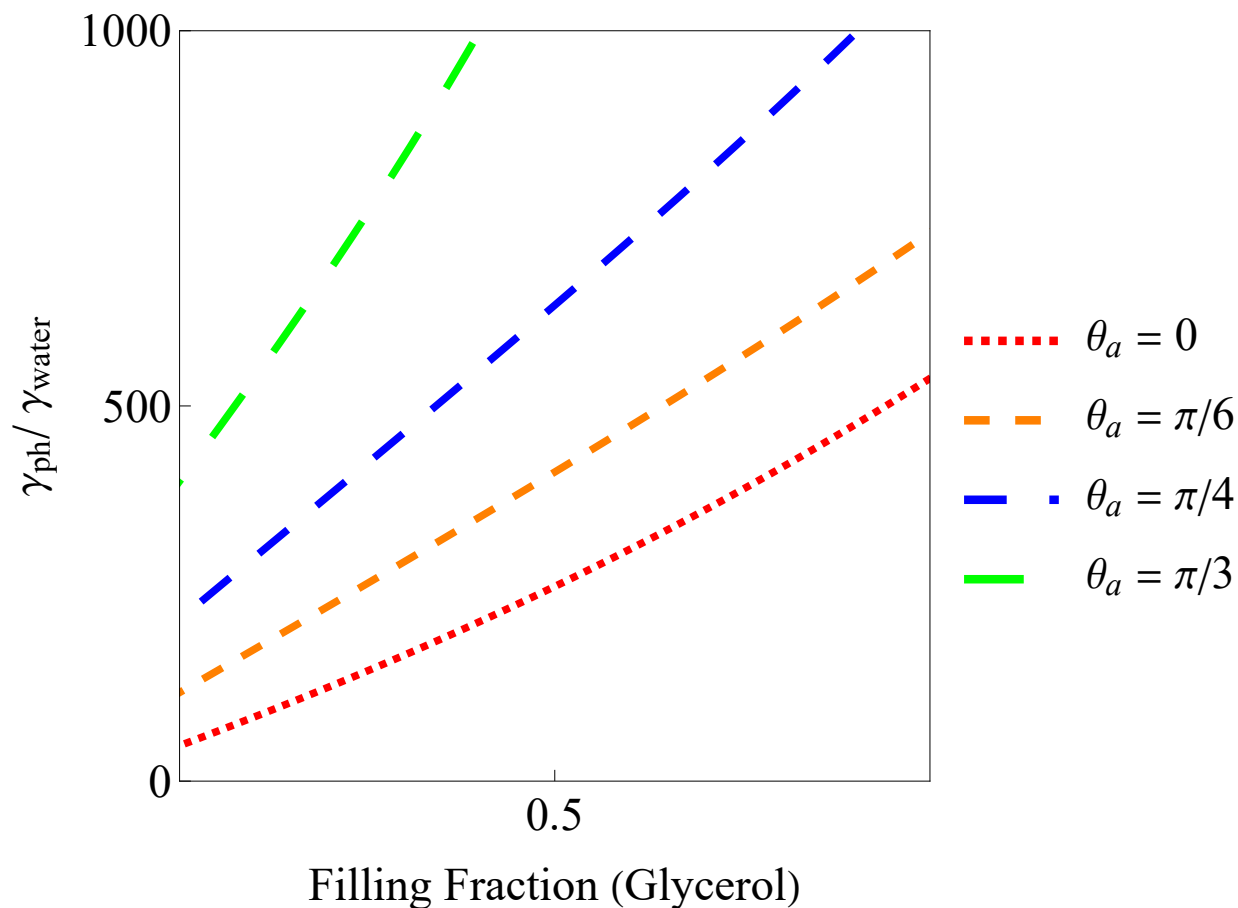


FIGURE 2.6. Decay coefficient for water-glycerol superlattice  $\gamma_{ph} = k_x''(f)$  normalized to the decay coefficient of water ( $\gamma_{water}$ ) vs filling fraction  $f$  of glycerol. Strong dependence on the filling fraction is related to the high viscosity contrast between water and glycerol,  $\gamma_{glyc}/\gamma_{water} = 1.6 \cdot 10^3$ .

### 2.4.3. Unit Cell of Viscous Fluid and Dissipationless Solid

Solid-fluid layered structure is feasible for experimental realization. I assume that sound wave decays much less in the solid layer, therefore its elastic coefficients  $\lambda_b$  and  $\mu_b$  are real. Although the dispersion equation for solid-fluid superlattice (2.39) looks more complicated than that for fluid - fluid structure (2.51), the frequency and angular dependencies of the decay coefficient  $k_x''$  remain qualitatively the same. For normal incidence only the bulk mechanism of dissipation with the decay coefficient  $\propto \eta_a \omega^2$  contributes to the decay of sound wave. In the case of an oblique incidence viscous dissipation prevails and scales as  $\sqrt{\eta_a \omega}$ .

Behavior of the decay coefficient within a wide band of frequencies for water-PMMA structure is plotted in Fig. 2.7. At very low frequencies where superlattice homogenizes the decay coefficient exhibits  $\sqrt{\omega}$  dependence due to Konstantinov's effect at oblique incidence. At higher frequencies, the dispersion of sound becomes nonlinear and frequency dependence of the Bloch vector is obtained from the quite complicated Eq. (2.39). Near the band edges the Bloch wave becomes a standing wave that leads to very fast growth of viscous losses. At the band edge, the viscous losses are an order of magnitude higher than within the transmission zone. However, the Bloch wave remains a propagating mode since still  $k_x'' d \ll 1$ . Only within the band gap the wave essentially decays at a distance of the lattice period, but this decay is due to Bragg scattering. Viscous losses remain relatively low because of low viscosity of water. For a finite-length lattice even low viscosity losses play an important role within the band gap frequencies increasing the tunneling time of a pulse through the sample [92].

The dependence of the decay coefficient  $\gamma_{ph} = k_x''$  on the filling fraction of solid PMMA is obtained from Eq. (2.39). This dependence is plotted in Fig. 2.8 for different angles of incidence and frequency 20 kHz. This frequency is well below the band gap as shown in Fig. 2.7. For normal incidence (blue curve) the dissipation is very low. The right inset shows how the decay coefficient decreases from its value in water ( $f = 0.1$ ) to practically zero value in a superlattice with very small content of water ( $f = 0.9$ ).

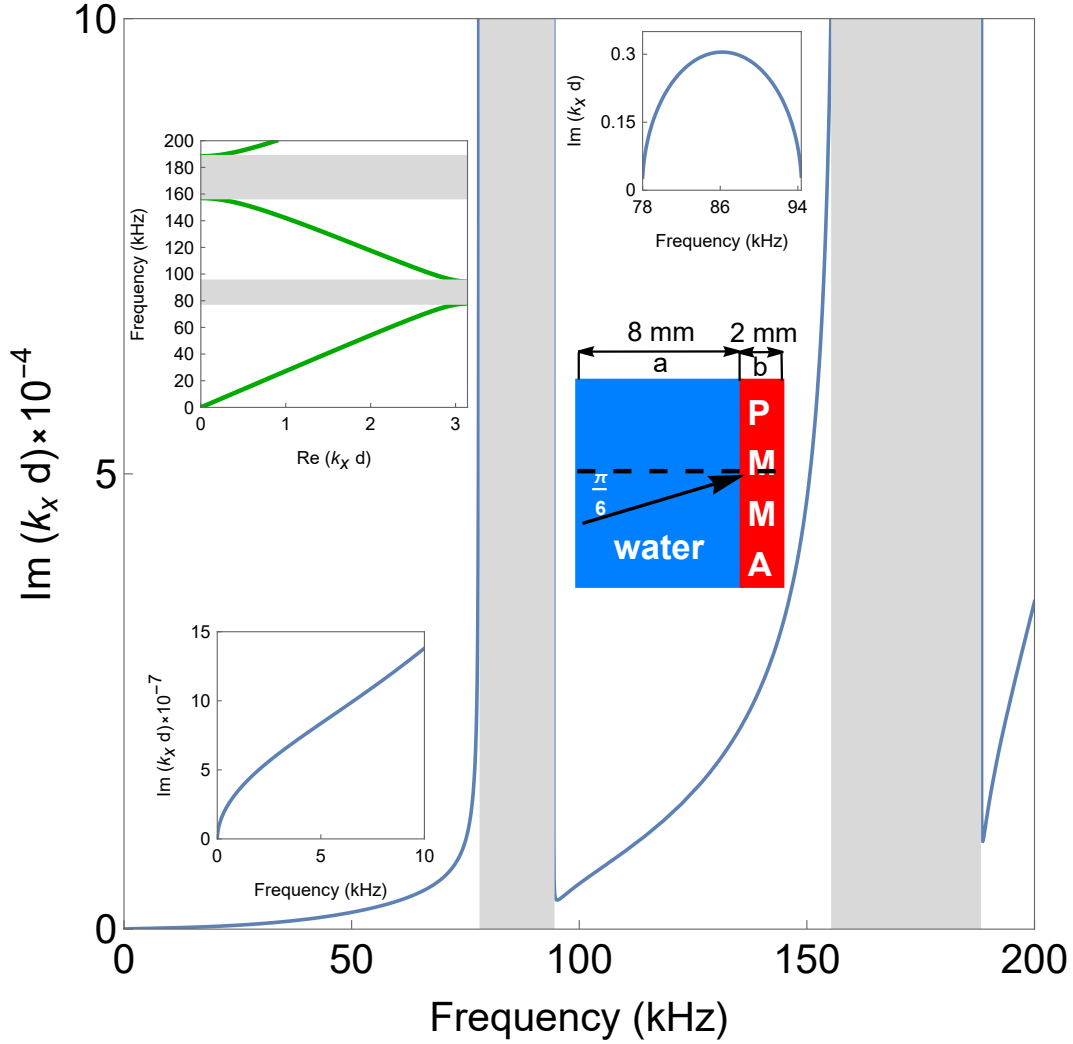


FIGURE 2.7. Frequency dependence of the dimensionless decay coefficient for water-PMMA superlattice calculated from Eq. (2.39) for the filling fraction  $f = 0.2$ . The region within the two lowest transmission bands is shown. Shaded regions are the band gaps of the band structure shown in the left top inset. Left bottom inset is the decay coefficient at very low frequencies where  $k_x'' \propto \sqrt{\omega}$ . Right top inset is the decay coefficient within the first band gap. Left bottom inset shows the direction of propagation within the unit cell. Note order-of-magnitude difference in the decay coefficient at low frequencies, close to the band edge, and within the band gap.

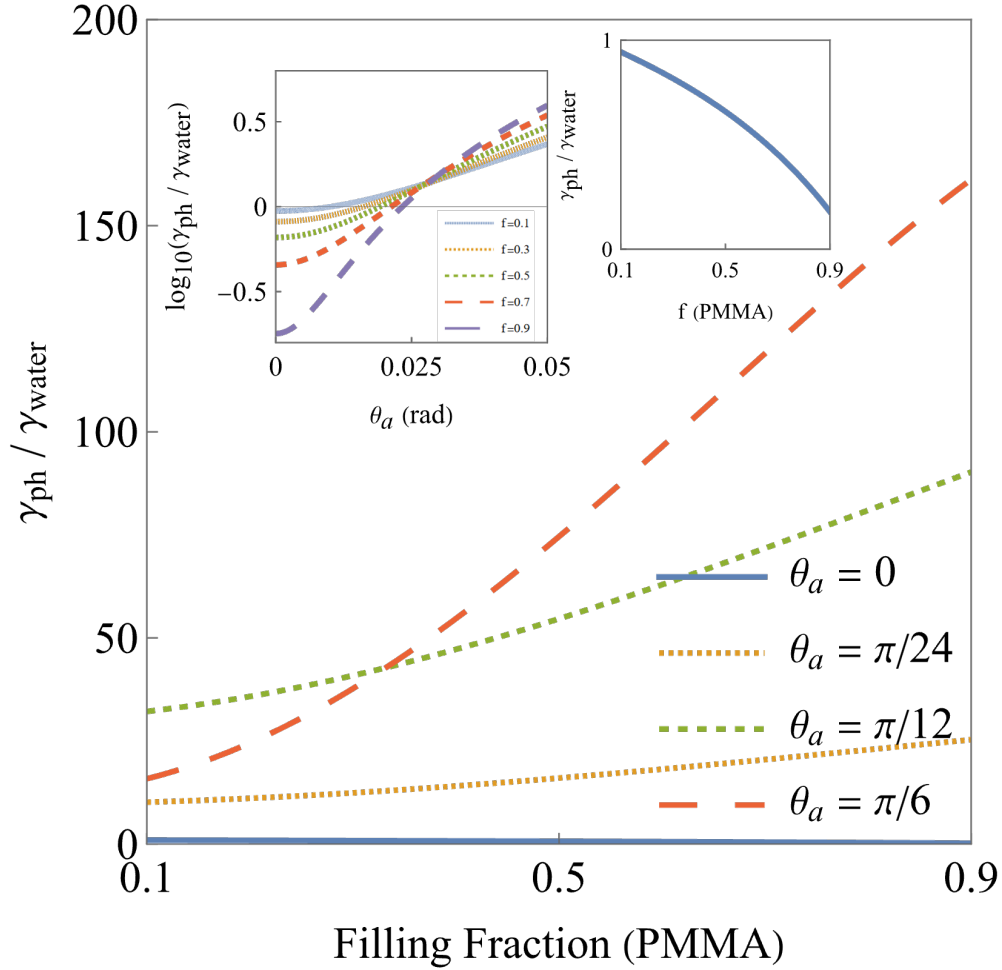


FIGURE 2.8. Normalized decay coefficient vs filling fraction for water-PMMA superlattice for different angles of incidence. The frequency of sound is 20 kHz. The right inset shows the case of normal incidence when dissipation occurs in the whole bulk of water. The left inset shows how dissipation in the bulk changes to dissipation within the boundary layer with increasing angle of incidence for different filling fractions. For angles  $\theta_a > 0.03$  the decay coefficient exhibits "abnormal" increasing dependence with decreasing amount of viscous water. The curves appear to cross at the same point but on the blowup picture, there are several crossing points within a narrow region near  $\theta_a = 0.03$ .



For very small angles of incidence,  $\theta_a < 0.03$ , when attenuation is due to dissipation in the bulk, the decay coefficient still decreases with the filling fraction of solid. This can be seen in the left inset to Fig. 2.8. Also, for larger angles,  $\theta_a > 0.03$ , this tendency is changed to the opposite one due to the increasing contribution of the dissipation within the boundary layer  $\delta$ . Once the boundary-layer contribution becomes dominant, the decay coefficient becomes larger by orders of magnitude. Dissipation occurs within the boundary layer  $\delta$  and the rest amount of viscous fluid does not contribute to attenuation of sound. While  $\delta$  does not change with  $f$  (for  $a \gg \delta$ ), the decay coefficient in Fig. 2.8 smoothly grows with decreasing of the fraction of the viscous constituent, as it is seen in Fig. 2.8. Such "abnormal" dependence is due to variation of the effective mechanical parameters,  $c_{eff}$  and  $\rho_{eff}$ , with the filling fraction.

The angular dependence of the decay coefficient at fixed filling fraction exhibits a strong anomaly related to a specific nature of wave conversion at a boundary between solid and fluid. Due to presence of transverse and longitudinal modes in the solid layer and only a single longitudinal mode in the fluid layer, so-called transmission zeros appears in the spectrum of a solid plate immersed in ideal fluid if the angle of incidence does not exceed the critical value [22, 71]

$$(2.54) \quad \theta_c = \arcsin \frac{V_f/V_t}{2\sqrt{1 - V_t^2/V_l^2}},$$

where  $V_f$ , and  $V_t$ ,  $V_l$  are the phase velocities of sound in fluid and solid respectively. For water-PMMA boundary the critical angle is 0.756 rad. In a series of curves in Fig. 2.9 giving the angular dependence of the decay coefficient for different viscosities anomalously high decay appears close to  $\theta_c = 0.756$ . The position of the peak depends slightly on the viscosity of fluid due to the imaginary terms in the dispersion relation. A dissipationless solid-fluid bilayer structure becomes nontransparent when the factor for  $\cos(k_x d)$  in the left-hand-side of Eq. (2.43) vanishes [22, 71],

$$(2.55) \quad \alpha_1 \alpha_2 \sin(b\kappa_b) + \alpha_2 k_y^2 \sin(bk_b) = 0.$$

Therefore, in Fig. 2.9 the decay coefficient tends to infinity at  $\theta_c = 0.756$  for inviscid fluid.

Note that in the low-frequency limit the solution of Eq. (2.55) gives the result for the critical angle (2.54). In the case of a viscous fluid the corresponding term in Eq. (2.39) acquires imaginary part. This term remains very small but finite at the critical angle, giving rise to a large but finite attenuation coefficient in Fig. 2.9.

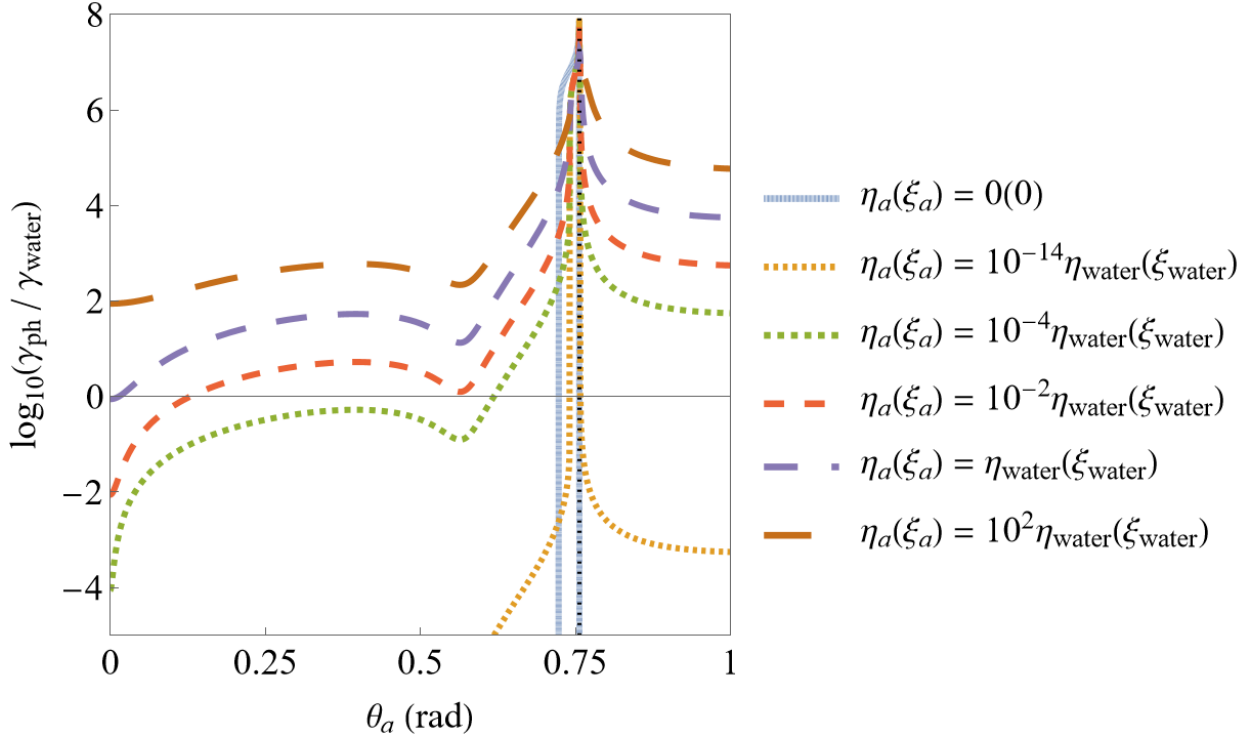


FIGURE 2.9. Angular dependence of the normalized decay coefficient of water-PMMA superlattice at filling fraction  $f = 0.2$  and frequency 20 kHz. Note the logarithmic scale on the vertical axis. Dashed line shows the position of the critical angle for inviscid fluid Eq. (2.54).

Dissipation for  $\theta_a > \theta_c$  exceeds that by two-three orders of magnitude at smaller angles of incidence. Here the level of dissipation does not change much with the angle but it strongly depends on viscosity. It is obvious that the sound absorption at  $\theta_a > \theta_c$  is pure dissipative but the reason for anomalously high decay remains unclear. This requires more detailed study.

## 2.5. Summary

I derived and analyzed the dispersion equation for sound waves propagating in a periodic layered heterogeneous structure containing at least one viscous fluid as a constituent. The derivation of the dispersion equation is based on the Navier-Stokes equation for sound wave and the boundary conditions of continuity of fluid displacement and stresses at the interfaces plus Bloch periodic boundary condition. The boundary conditions result in vanishing  $8 \times 8$  determinant. The obtained dispersion equation is very general, it is valid for different combinations of elastic layers, any direction of propagation, and frequency of sound. It was analyzed for normal and oblique incidence. In the region of low frequencies where a superlattice behaves as a homogeneous medium with effective speed of sound the decay coefficient of sound wave is proportional to  $\omega^2\eta$  at normal incidence, where  $\eta$  plays a role of corresponding effective viscosity. This behavior is a signature of viscous dissipation in the bulk of the fluid. For oblique incidence the decay coefficient scales as  $\sqrt{\omega\eta}$  that corresponds to much stronger decay within a narrow boundary layer. The transition from dissipation in the bulk to dissipation in the boundary layer occurs within a narrow range of frequencies. At frequencies close to a band edge dissipation strongly increases because a propagating Bloch wave becomes a standing wave. In a special case of viscous and ideal fluid constituents the boundary layer is not formed, leading to unusual scaling of the decay coefficient,  $k_x'' \propto (\omega\eta)^{3/2}$ . In the case of superlattice consisting of narrow layers with high viscosity fluid and layers of ideal fluid an acoustic analog of the Borrmann effect is predicted. Unlike previous studies of the acoustic Borrmann effect [10, 15], the result obtained in Ref. [78] for anomalous transmission does not require presence of jump discontinuity of pressure at narrow layers. It can be observed in a periodic structure of layers with high contrast of viscosities.

The results of this chapter serve as a supplement to the theory of phononic crystals with viscoelastic constituents. Since in the case of 1D periodicity the dispersion equation is known in an explicit form, many results obtained in the limit of weak viscosity can be presented analytically and within a wide range of parameters [6, 76, 33, 66], unlike the

cases of 2D and 3D periodicity [56, 46, 27, 69], where analytical results for the decay length are available only in the long-wavelength limit [75, 35, 36]. Analytical results are more valuable since in many cases the numerical methods of calculation of transmission through a long, multi-layered system with low-viscosity constituents (air or water), turn out to be unsuccessful. Finite-difference methods require high machine precision incompatible with memory capabilities of standard computers. Obtained results are quite universal being available for design of acoustic devices which require low or high absorption. In particular, multi-wall and multi-layered structures are widely used in road construction [94] and in architecture for soundproofing [49, 70].

## CHAPTER 3

### NONRECIPROCAL TRANSMISSION AND ITS OPTIMIZATION THROUGH DISSIPATIVE PHONONIC CRYSTALS <sup>†</sup>

#### 3.1. Introduction

##### 3.1.1. Nonreciprocity

Reciprocity in the propagation of a monochromatic acoustic wave through a set of solid scatterers is traditionally formulated for pressure  $p_B(\mathbf{r}_A)$  measured at a point  $\mathbf{r}_A$  when the source of sound is at point  $\mathbf{r}_B$ . According to the Rayleigh theorem [73], switching the positions of the emitter and receiver conserves pressure,

$$(3.1) \quad p_B(\mathbf{r}_A) = p_A(\mathbf{r}_B).$$

Originally, the reciprocity theorem was demonstrated for an inviscid fluid, where the field of acoustic velocities is potential,  $\nabla \times \mathbf{v}_{ac} = 0$ . However, it remains true even in viscous media, where velocity acquires a solenoidal part,  $\mathbf{v} = \mathbf{v}_{ac} + \mathbf{v}_{vor}$ . The distribution of velocities  $\mathbf{v}(\mathbf{r})$  is a solution of the wave equation obtained from the Navier-Stokes equation where pressure is excluded using the continuity equation. The distribution of pressure is obtained from the linearized continuity equation, which yields

$$(3.2) \quad p(\mathbf{r}) = -\frac{ic^2\rho}{\omega}\nabla \cdot \mathbf{v},$$

where  $c$  is the speed of sound,  $\rho$  in the fluid density, and  $\omega/2\pi$  is the wave frequency. Since  $\nabla \cdot \mathbf{v}_{vor} = 0$ , pressure is defined only by the potential part of velocity, and the reciprocity relation (3.1) is also satisfied in a viscous fluid.

Reciprocity in fluid dynamics originates from time-reversal symmetry ( $T$  symmetry) of the Euler equation. While viscous dissipation breaks  $T$  symmetry, making fluid dynamics irreversible, dissipation is not considered as a factor of nonreciprocity in modern literature

---

<sup>†</sup>©2024 IEEE Reprinted in part or in full, with permission, from Shymkiv, Dmitrii & Mazumder, Arnav & Arriaga, Jesús & Krokhin, Arkadii. (2023). Optimization of Nonreciprocal Transmission Through Dissipative Phononic Crystals With Machine Learning Techniques. IEEE Open Journal of Ultrasonics, Ferroelectrics, and Frequency Control. PP. 1-1. 10.1109/OJUFFC.2023.3334234.

[24, 60] since relation (3.1) remains true. So, is there a measurable quantity which becomes nonreciprocal due to viscous losses? The answer is yes: sound intensity,  $I = pv$ .

In an ideal (inviscid) fluid pressure serves as potential for acoustic velocity,  $\mathbf{v}(\mathbf{r}) \propto \nabla p(\mathbf{r})$ . The reciprocity of pressure does not mean the same symmetry for its gradient, i.e.,  $\mathbf{v}_A(\mathbf{r}_B) \neq \mathbf{v}_B(\mathbf{r}_A)$ , since this kind of reciprocity does not mean that pressure as a function of coordinates is either even or odd. This asymmetry of velocity is consistent with time-reversal symmetry of fluid dynamics. However, this asymmetry in a viscous fluid leads to different dissipated power upon switching positions of the emitter and receiver. The local dissipation is defined by the binary combinations of velocity gradients  $(\partial v_i / \partial x_k)^2$  [45]. Asymmetry in a distribution of local velocities and their gradients leads to a difference in the total dissipated power [86, 31]. The difference in attenuation of the signal on the way from the emitter to receiver is a source of dissipation-induced nonreciprocity. Indeed, the replacement  $t \rightarrow -t$  and  $\eta, \xi \rightarrow -\eta, -\xi$  does not restore the initial state of the signal, where  $\eta$  and  $\xi$  are the viscosity coefficients. Of course, a case of mirror symmetry in a distribution of scatterers can be excluded. In this special case, the transmission is irreversible and reciprocal. In what follows, I consider scatterers without mirror symmetry, when the  $P$  symmetry (parity symmetry) of the system is broken. The difference in sound intensities,  $I_{AB} = I_A(\mathbf{r}_B) - I_B(\mathbf{r}_A) = \Delta I_{AB}^{ac} + \Delta I_{AB}^{nr}$  has two different contributions. The asymmetric part,  $\Delta I_{AB}^{ac}$ , exists even in an inviscid fluid if  $P$  symmetry is broken. For the reference, Figure 3.1 shows asymmetrical pressure distributions for the forward and backward wave propagation in the case of inviscid fluid. The truly nonreciprocal part,  $\Delta I_{AB}^{nr}$ , is due to broken  $PT$  symmetry. The relation between these contributions depends on viscosity, which is a measure of the violation of  $T$  symmetry.

Difference between forwards and backwards transmission may be explored for the rectification of acoustic signals and noise control [98, 99, 97]. While in a linear system the asymmetry may be a useful property that allows for the aforementioned applications. The presence of unbroken  $T$  symmetry and reciprocal transmission means that they are not true acoustic diodes [55]. Here, I propose a phononic crystal with highly asymmetric aluminum

rods in viscous water, which serves as a passive acoustic diode. The design of the phononic crystal was optimized using machine learning methods to reach the best performance.

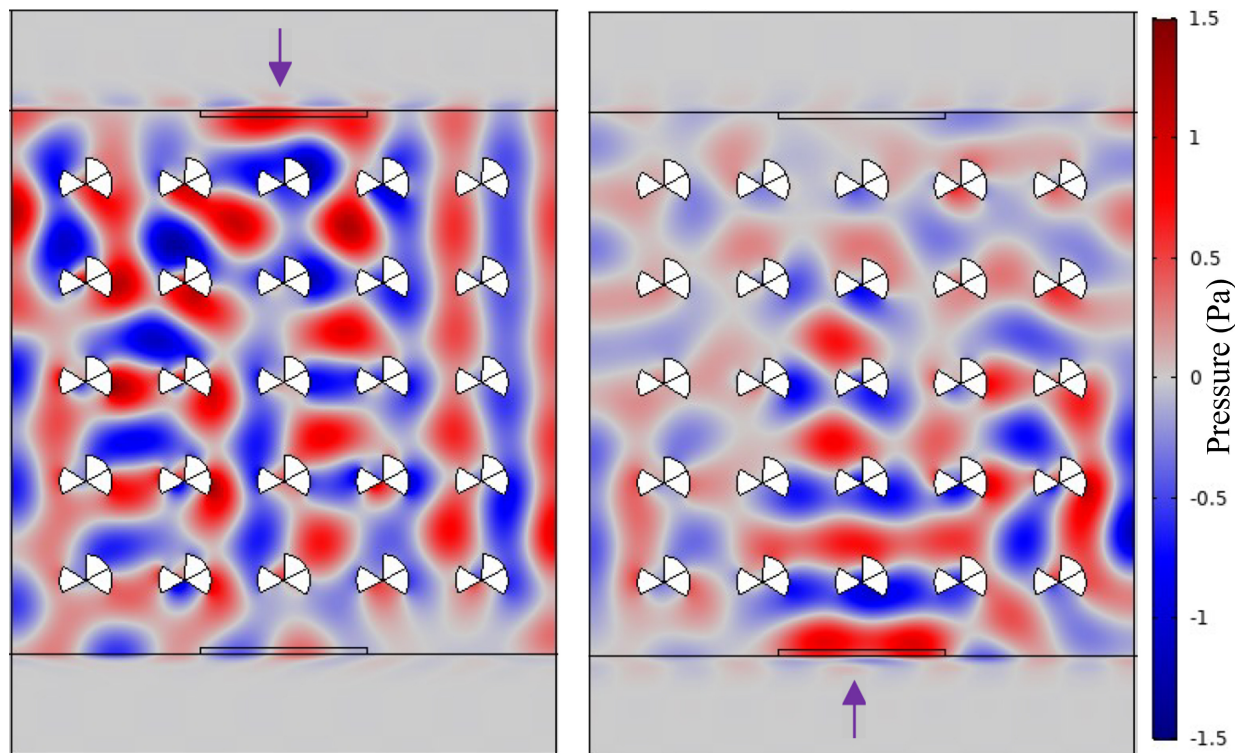


FIGURE 3.1. Pressure maps calculated for the crystal with asymmetrical scatterers and ideal fluid for downward (left) and upward (right) wave propagation. The difference in pressure is due only to the asymmetric transmission.

Since the rectification ability of an acoustic diode with respect to intensity is partially due to asymmetry and partially to dissipation-induced nonreciprocity, it belongs neither to the class of reciprocal sound rectification devices [98, 99, 97], nor to completely nonreciprocal acoustic diodes [68, 25, 29, 20]. Note that the dissipation-induced mechanism of nonreciprocity was already explored in the rectification of elastic waves [82].

### 3.1.2. Machine Learning in Physics

In recent years, the incorporation of machine learning (ML) techniques into physics research has attracted significant attention [7, 8]. This emerging intersection between physics and the innovative field of machine learning has paved the way for novel avenues in scientific

exploration and discovery.

Supervised learning, a fundamental paradigm in machine learning, has found practical applications in the domain of quantum mechanics [9]. The capacity of supervised learning algorithms to discern intricate patterns and correlations is particularly valuable in predicting quantum states and comprehending quantum phenomena. Researchers have applied supervised learning to optimize quantum circuit designs, predict material properties, and enhance simulations of quantum systems [3].

Unsupervised learning techniques have made substantial progress in astrophysics research [19]. Clustering algorithms, including k-means and hierarchical clustering, have been employed to categorize astronomical objects based on their observed properties. Unsupervised learning methods facilitate the identification of concealed patterns in extensive datasets, contributing to the discovery of celestial objects, classification of galaxies, and detection of anomalies in astronomical phenomena [11]. The collaboration between unsupervised learning and astrophysics has streamlined data analysis processes, augmenting our understanding of the expansive cosmos.

In photonics/phononics, machine learning has emerged as a tool for the design and optimization of optical/acoustical devices and systems. Photonics research often involves complicated mixture of light-matter interactions and complex optical phenomena. Machine learning techniques, such as neural networks, have been applied to predict the performance of photonic devices, optimize design parameters, and expedite the discovery of innovative optical materials [32]. ML techniques have proven valuable in predicting and optimizing phononic properties of materials, aiding in the design of novel phononic devices and metamaterials [48]. The ability of machine learning to distinguish patterns in extensive datasets allows researchers to navigate the complex design space of photonic/phononic structures with efficiency.

In this chapter, I optimize design of the phononic crystal to reach the highest absolute and relative nonreciprocity value as well as the best diode efficiency. In order to perform optimization, Deep Learning, a class of machine learning models, is used due to its



unparalleled efficiency in modelling highly nonlinear data. Although these models primarily focus on generating accurate predictions from data, they can also be used to obtain extreme or optimal values that are not present in the original dataset. Other popular methods of optimization involve genetic or evolutionary algorithms. However, these methods require a large number of time-consuming numerical calculations at each generational step. On the other hand, in the Deep Learning approach, once a dataset is calculated, a model can be trained and optimized to find the best parameters, which potentially reduces computational time. Deep Learning is widely used in similar problems in optimization of the properties of metasurfaces [42] and nanostructures [54].

## 3.2. Acoustic Reciprocity of an Infinite Phononic Crystal

### 3.2.1. Wave Equation in Fourier Representation

The concept of transmission can not be applied for an infinite structures. Distance between a sound source and a receiver is infinite, therefore they do share any information with each other. In this case, reciprocal/nonreciprocal properties of the phononic crystal can be described in terms of dispersion relation or in other words if the dispersion relation remains constant switching the wave propagation direction  $\omega(\mathbf{k}) = \omega(-\mathbf{k})$ . Since wave vectors belong to reciprocal (not direct) space, it is convenient to rewrite a wave equation in this space to analyze reciprocal/nonreciprocal nature of sound propagation in an infinite crystal.

For a harmonic perturbation  $\mathbf{v}(\mathbf{r}, t) = \mathbf{v}(\mathbf{r})e^{i\omega t}$  wave equation (2.4) reads

$$(3.3) \quad \rho\omega^2 v_i + \frac{\partial}{\partial x_i}(\lambda \nabla \cdot \mathbf{v}) = i\omega \frac{\partial}{\partial x_k} \left[ \eta \left( \frac{\partial v_i}{\partial x_k} + \frac{\partial v_k}{\partial x_i} - \frac{2}{3} \delta_{ik} \nabla \cdot \mathbf{v} \right) \right] + i\omega \frac{\partial}{\partial x_i} (\xi \nabla \cdot \mathbf{v}).$$

Using the Bloch theorem velocity can be expressed through the infinite set of reciprocal-lattice vectors  $\mathbf{G}$ :

$$(3.4) \quad \mathbf{v}(\mathbf{r}) = \sum_{\mathbf{G}} \mathbf{v}(\mathbf{G}) e^{i(\mathbf{k}+\mathbf{G})\cdot\mathbf{r}}.$$

The other periodic functions  $(\rho, \lambda, \eta, \xi)$  can be represented via the corresponding

Fourier series:

$$(3.5) \quad \rho(\mathbf{r}) = \sum_{\mathbf{G}} \rho(\mathbf{G}) e^{i\mathbf{G}\cdot\mathbf{r}}.$$

The components  $\rho(\mathbf{G})$  are defined as

$$(3.6) \quad \rho(\mathbf{G}) = \frac{1}{V_c} \int_{\text{cell}} \rho(\mathbf{r}) e^{-i\mathbf{G}\cdot\mathbf{r}} d\mathbf{r},$$

where integration should be done over the volume (or area in 2-dimensional case)  $V_c$  of the 3-dimensional unit cell. Note, that

$$(3.7) \quad \frac{1}{V_c} \int_{\text{cell}} e^{i(\mathbf{G}_n - \mathbf{G}_m)\cdot\mathbf{r}} d\mathbf{r} = \delta_{nm},$$

which states the orthonormality of the basis  $e^{i\mathbf{G}\cdot\mathbf{r}}$ .

All the terms in the wave equation (3.3) have a product of two periodic functions, for instance,

$$(3.8) \quad \rho\mathbf{v} = \sum_{\mathbf{G}} \rho(\mathbf{G}) e^{i\mathbf{G}\cdot\mathbf{r}} \sum_{\mathbf{G}'} \mathbf{v}(\mathbf{G}') e^{i(\mathbf{k}+\mathbf{G}')\cdot\mathbf{r}}.$$

To apply the condition of orthonormality in the form of Eq.(3.7) the following transformations can be performed

$$(3.9) \quad \sum_{\mathbf{G}} \rho(\mathbf{G}) e^{i\mathbf{G}\cdot\mathbf{r}} = \sum_{\mathbf{G}-\mathbf{G}'} \rho(\mathbf{G}-\mathbf{G}') e^{i\mathbf{G}-\mathbf{G}'\cdot\mathbf{r}} = \sum_{\mathbf{G}} \rho(\mathbf{G}-\mathbf{G}') e^{i\mathbf{G}-\mathbf{G}'\cdot\mathbf{r}}.$$

They lead to the desired structure, where only  $\mathbf{G}$  but not  $\mathbf{G}-\mathbf{G}'$  appears in the exponent.

$$(3.10) \quad \rho\mathbf{v} = -\omega^2 e^{-i\omega t} \sum_{\mathbf{G}} \sum_{\mathbf{G}'} \rho(\mathbf{G}-\mathbf{G}') \mathbf{v}(\mathbf{G}') e^{i(\mathbf{k}+\mathbf{G})\cdot\mathbf{r}}.$$

A wave equation in the Fourier representation can be obtained by performing transformations similar to Eqs. (3.8-3.10) to all the terms in Eq. (3.3) and applying orthonormality condition:

$$\begin{aligned}
(3.11) \quad & \sum_{\mathbf{G}'} \left\{ \omega^2 \rho(\mathbf{G} - \mathbf{G}') \delta_{ik} - \lambda(\mathbf{G} - \mathbf{G}') [\mathbf{k} + \mathbf{G}]_i [\mathbf{k} + \mathbf{G}']_k \right\} v_k(\mathbf{G}') = \\
& - i\omega \sum_{\mathbf{G}'} \xi(\mathbf{G} - \mathbf{G}') [\mathbf{k} + \mathbf{G}]_i [\mathbf{k} + \mathbf{G}']_k v_k(\mathbf{G}') - \\
& - i\omega \sum_{\mathbf{G}'} \eta(\mathbf{G} - \mathbf{G}') \left\{ [\mathbf{k} + \mathbf{G}] \cdot [\mathbf{k} + \mathbf{G}'] \delta_{ik} + [\mathbf{k} + \mathbf{G}']_i [\mathbf{k} + \mathbf{G}]_k - \frac{2}{3} [\mathbf{k} + \mathbf{G}]_i [\mathbf{k} + \mathbf{G}']_k \right\} v_k(\mathbf{G}'),
\end{aligned}$$

where parentheses mean the argument of the function. In fact, it is not a single equation but an infinite set of linear equations for an infinite number of unknown Fourier amplitudes  $v_k(\mathbf{G}')$ .

Eq. 3.11 can be rewritten in a vector form:

$$\begin{aligned}
(3.12) \quad & \omega^2(\mathbf{k}) \sum_{\mathbf{G}'} \rho(\mathbf{G} - \mathbf{G}') \mathbf{v}_{\mathbf{k}}(\mathbf{G}') = \\
& = [\mathbf{k} + \mathbf{G}] \sum_{\mathbf{G}'} \left\{ \lambda(\mathbf{G} - \mathbf{G}') - i\omega(\mathbf{k}) \xi(\mathbf{G} - \mathbf{G}') + i\omega(\mathbf{k}) \frac{2}{3} \eta(\mathbf{G} - \mathbf{G}') \right\} [\mathbf{k} + \mathbf{G}'] \cdot \mathbf{v}_{\mathbf{k}}(\mathbf{G}') - \\
& - i\omega(\mathbf{k}) \sum_{\mathbf{G}'} \eta(\mathbf{G} - \mathbf{G}') \{ [\mathbf{k} + \mathbf{G}] \cdot [\mathbf{k} + \mathbf{G}'] \mathbf{v}_{\mathbf{k}}(\mathbf{G}') + [\mathbf{k} + \mathbf{G}'] [\mathbf{k} + \mathbf{G}] \cdot \mathbf{v}_{\mathbf{k}}(\mathbf{G}') \},
\end{aligned}$$

where subscript  $\mathbf{k}$  means that  $\mathbf{v}_{\mathbf{k}}(\mathbf{G}')$  correspond to the wave propagation in the direction of  $\mathbf{k}$ .

One important conclusion can be made using the following form of the wave equation:

$$\begin{aligned}
(3.13) \quad & \sum_{\mathbf{G}'} \left\{ \omega^2 \rho(\mathbf{G} - \mathbf{G}') + i\omega \eta(\mathbf{G} - \mathbf{G}') [\mathbf{k} + \mathbf{G}] \cdot [\mathbf{k} + \mathbf{G}'] \right\} \mathbf{v}(\mathbf{G}') = \\
& = [\mathbf{k} + \mathbf{G}] \sum_{\mathbf{G}'} \left[ \lambda(\mathbf{G} - \mathbf{G}') - i\omega \xi(\mathbf{G} - \mathbf{G}') + i\omega \frac{2}{3} \eta(\mathbf{G} - \mathbf{G}') \right] [\mathbf{k} + \mathbf{G}'] \cdot \mathbf{v}(\mathbf{G}') - \\
& - i\omega \sum_{\mathbf{G}'} \eta[\mathbf{G} - \mathbf{G}'] [\mathbf{k} + \mathbf{G}'] (\mathbf{k} + \mathbf{G}) \cdot \mathbf{v}(\mathbf{G}').
\end{aligned}$$

Phenomenologically dissipation can be included in an elastic medium by considering elastic modulus being complex [85]. That approach is extensively employed to investigate how dispersion relation is affected by viscous or viscoelastic damping [26, 34].

It follows from Eq. (3.13) that the effects of viscosity in a phononic crystal can not be described accurately by this method. Although, elastic modulus and density matrices

become complex and frequency-dependent:

$$(3.14) \quad \lambda(\mathbf{G} - \mathbf{G}') = \lambda(\mathbf{G} - \mathbf{G}') - i\omega\xi(\mathbf{G} - \mathbf{G}') + i\omega\frac{2}{3}\eta(\mathbf{G} - \mathbf{G}'),$$

$$(3.15) \quad \rho(\mathbf{G} - \mathbf{G}') = \rho(\mathbf{G} - \mathbf{G}') + \frac{i}{\omega}\eta(\mathbf{G} - \mathbf{G}')[\mathbf{k} + \mathbf{G}] \cdot [\mathbf{k} + \mathbf{G}'],$$

there is one additional term in the right hand side of the equation (3.13), which can not be attributed to neither of these material parameters.

### 3.2.2. Eigenvalues and Eigenfunctions of the Wave Equation

In the dissipationless phononic crystal ( $\eta = \xi = 0$ ), equation (3.12) reduces to

$$(3.16) \quad \omega^2(\mathbf{k}) \sum_{\mathbf{G}'} \rho(\mathbf{G} - \mathbf{G}') \mathbf{v}_{\mathbf{k}}(\mathbf{G}') = [\mathbf{k} + \mathbf{G}] \sum_{\mathbf{G}'} \lambda(\mathbf{G} - \mathbf{G}') [\mathbf{k} + \mathbf{G}'] \cdot \mathbf{v}_{\mathbf{k}}(\mathbf{G}').$$

Dispersion relation  $\omega(\mathbf{k})$  is the set of eigenvalues of the generalized eigenvalue problem  $Av = \omega^2 Bv$ . The process of obtaining dispersion relation for the waves propagating in a dissipative media becomes more complicated, since  $\omega(\mathbf{k})$  enters both linearly and quadratically in the wave equation (3.12). It is a so-called quadratic eigenvalue problem, which can be solved with generalized eigenvalue problem methods after a series of transformations [84]. Also, dispersion equation can be obtained by equating the determinant of the corresponding matrix (3.12) to zero.

To analyze reciprocity/nonreciprocity of the dispersion relation and Fourier components of velocity wave equations for forward  $\mathbf{k}$  and backward  $-\mathbf{k}$  should be compared.

Replacements

$$(3.17) \quad \begin{aligned} \mathbf{k} &\rightarrow -\mathbf{k} \\ \mathbf{G} &\rightarrow -\mathbf{G} \\ \mathbf{G}' &\rightarrow -\mathbf{G}' \end{aligned}$$

in Eq. (3.12) lead to the wave equation for backward propagation:

$$\begin{aligned}
(3.18) \quad & \omega^2(-\mathbf{k}) \sum_{\mathbf{G}'} \rho(\mathbf{G}' - \mathbf{G}) \mathbf{v}_{-\mathbf{k}}(-\mathbf{G}') = \\
& = [\mathbf{k} + \mathbf{G}] \sum_{\mathbf{G}'} \left\{ \lambda(\mathbf{G}' - \mathbf{G}) - i\omega(-\mathbf{k})\xi(\mathbf{G}' - \mathbf{G}) + i\omega(-\mathbf{k})\frac{2}{3}\eta(\mathbf{G}' - \mathbf{G}) \right\} [\mathbf{k} + \mathbf{G}'] \cdot \mathbf{v}_{-\mathbf{k}}(-\mathbf{G}') - \\
& \quad - i\omega(-\mathbf{k}) \sum_{\mathbf{G}'} \eta(\mathbf{G}' - \mathbf{G}) \{ [\mathbf{k} + \mathbf{G}] \cdot [\mathbf{k} + \mathbf{G}'] \mathbf{v}_{-\mathbf{k}}(-\mathbf{G}') + [\mathbf{k} + \mathbf{G}'] [\mathbf{k} + \mathbf{G}] \cdot \mathbf{v}_{-\mathbf{k}}(-\mathbf{G}') \},
\end{aligned}$$

From the definition of Fourier components (3.6) it follows that

$$(3.19) \quad \rho(-\mathbf{G}) = \frac{1}{V_c} \int_{cell} \rho(\mathbf{r}) e^{i\mathbf{G} \cdot \mathbf{r}} d\mathbf{r} = \rho^*(\mathbf{G}),$$

If P-symmetry is not broken, namely, the scatterers are symmetric, then all the Fourier components are real and  $\rho(\mathbf{G}) = \rho(\mathbf{G})^* = \rho(-\mathbf{G})$ . It leads to the reciprocity of the dispersion relation, namely,  $\omega(\mathbf{k}) = \omega(-\mathbf{k})$ , since the corresponding matrices in Eqs. (3.12) and (3.18) are identical. In the case of asymmetric inclusions  $\rho(\mathbf{G}) \neq \rho^*(\mathbf{G}) = \rho(-\mathbf{G})$  matrices become different but mutually transposed. Since determinants of the original and transposed matrices are the same  $\det(A) = \det(A^T)$ , dispersion relations remain identical and therefore reciprocal.

Similar analysis can be performed for Fourier components  $\mathbf{v}_{\mathbf{k}}(\mathbf{G})$ . If the media is dissipationless, equation (3.16) with transformations (3.17) for the wave propagating in  $-\mathbf{k}$  direction reads:

$$(3.20) \quad \omega^2(-\mathbf{k}) \sum_{\mathbf{G}'} \rho(\mathbf{G}' - \mathbf{G}) \mathbf{v}_{-\mathbf{k}}(-\mathbf{G}') = [\mathbf{k} + \mathbf{G}] \sum_{\mathbf{G}'} \lambda(\mathbf{G}' - \mathbf{G}) [\mathbf{k} + \mathbf{G}'] \cdot \mathbf{v}_{-\mathbf{k}}(-\mathbf{G}').$$

If inclusions are symmetric, corresponding matrix elements in (3.20) and (3.16) are identical since  $\rho(\mathbf{G}) = \rho(-\mathbf{G})$ . The reciprocity condition can be written in the form  $\mathbf{v}_{-\mathbf{k}}(-\mathbf{G}) = \mathbf{v}_{\mathbf{k}}(\mathbf{G})$ . More general case of asymmetric scatterers leads to

$$(3.21) \quad \mathbf{v}_{-\mathbf{k}}^*(-\mathbf{G}) = \mathbf{v}_{\mathbf{k}}(\mathbf{G}),$$

since  $\rho^*(\mathbf{G}) = \rho(-\mathbf{G})$ .

For a phononic crystal with viscous constituents equation (3.21) becomes invalid due to the linear over frequency terms in the wave equation (3.18).

In conclusion, it is proved that the eigenvalues of the wave equation for sound propagating through the viscous media is reciprocal, but eigenfunctions are nonreciprocal due to viscous losses. Since the wave equations for sound propagating in viscous fluid and solid have the same form (2.30), these results can be applied not only for fluid-fluid but also for solid-fluid structures.

### 3.3. The Phononic Crystal and Data Collection

In this and next sections of the chapter I intend to optimize the shape of the scatterer to reach as high as possible nonreciprocal part of the intensity difference for forward and backward sound wave propagation. The transmission spectra of a phononic crystal of aluminum rods with an asymmetric cross-section submerged in water are numerically calculated with COMSOL Multiphysics. A typical  $5 \times 5$  sample of a phononic crystal is shown in Fig. 3.2. All the relevant material parameters are provided in Table 3.1.

Acoustical nonreciprocity in a phononic crystal is quantified using the forwards  $T_F$  and backwards  $T_B$  sound transmission through the crystal. The following physical quantities: nonreciprocity  $NR$

$$(3.22) \quad NR = (T_F - T_B)_{vis} - (T_F - T_B)_{id}$$

normalized nonreciprocity ( $NNR$ )

$$(3.23) \quad NNR = \left( \frac{T_F - T_B}{\max(T_F, T_B)} \right)_{vis} - \left( \frac{T_F - T_B}{\max(T_F, T_B)} \right)_{id}$$

and diode efficiency

$$(3.24) \quad F = \left( \frac{\min(T_F, T_B)}{\max(T_F, T_B)} \right)_{vis}$$

have been optimized. Here subscript *vis* refers to the transmission calculated for the viscous water, while *id* transmissions is calculated for the inviscid water, where  $\xi = \eta = 0$ .

In Eq. (3.22),  $(T_F - T_B)_{vis}$  is the total difference in the transmission, which includes asymmetric and nonreciprocal parts, while  $(T_F - T_B)_{id}$  is the reciprocal part caused only by asymmetry. I would like to maximize the magnitude of both  $NR$  and  $NNR$ .

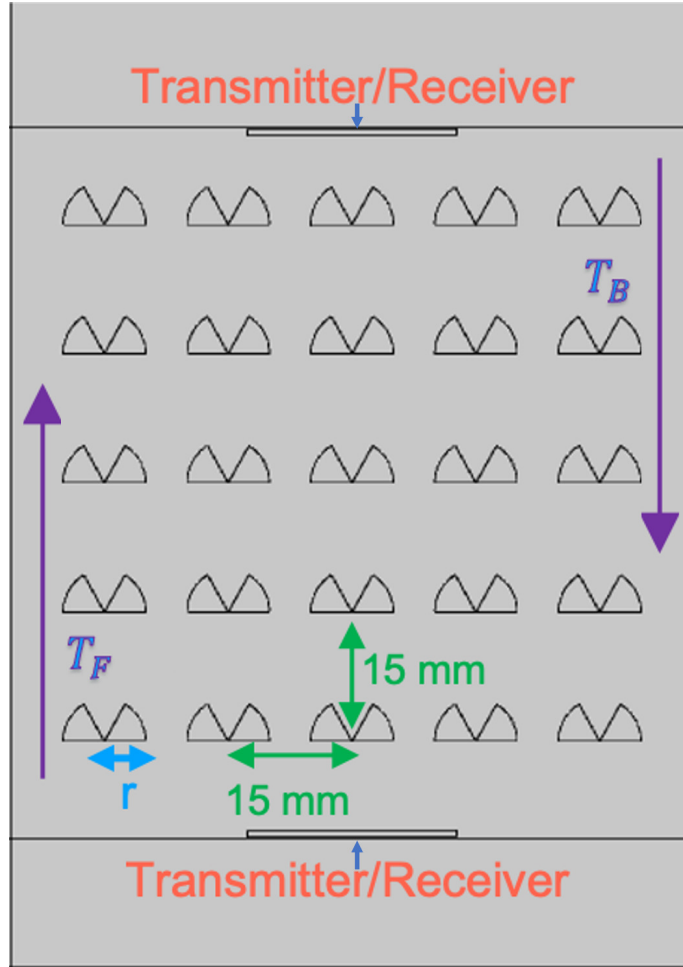


FIGURE 3.2. A model of the  $5 \times 5$  2D phononic crystal used in the COMSOL calculations of the transmission spectra. The crystal consists of aluminum scatterers in a water background. Solid Mechanics and Linearized Navier-Stokes moduli were used for calculations of elastic and acoustic fields in the sample. The transmitter and receiver are placed either above or below the structure. The period of the crystal is  $a = 15\text{mm}$ . The sound hard boundary condition is imposed for the left and right boundaries. All external domains are perfectly matched layers (PML). Sound transmission in the forwards ( $T_F$ ) and backwards ( $T_B$ ) directions are numerically calculated for viscous and inviscid water.

Material	Density, kg/m <sup>3</sup>	Young's Modulus, GPa	Poisson's Ratio	$\eta$ , mPa·s	$\xi$ , mPa·s	Compressibility, 10 <sup>-10</sup> /Pa
Water	1000	-	-	1.04	3.38	4.6
Aluminum	2700	69.14	0.33	-	-	-

TABLE 3.1. Material properties of water and aluminum used in the numerical simulations.

In Eq.(3.24),  $F$  is in the range between 0 and 1. In an ideal acoustic diode,  $F = 0$ , which means that it allows for the propagation of sound only in one direction. Therefore, the closer  $F$  is to 0 the better the corresponding crystal performs as a diode.

Any machine learning model requires some set of data to train on and then evaluate its performance with. For these purposes, the transmission values at frequency 100 kHz are calculated for a number of phononic crystals with different cross-sections of the scatterers using COMSOL Muliphysics. Various geometrical parameters of the scatterers of the crystal are parametrically swept in COMSOL, and the corresponding sound transmission values, in the forwards and backwards directions, are recorded. These simulations are run both with the phononic crystal submerged in viscous and inviscid water. Once all desired transmission spectra are calculated, a standard optimization pipeline (see Fig. 3.3) is applied.

### 3.4. Single Parameter Optimization

As a prototype for a scatterer geometry, a rod with a sector angle of 120° [86] was chosen. A reasonable generalization valid for optimization is a sector with variable angle. As the first step of optimization the transmissions are calculated for 171 different sector angles in the range between 5° and 345° with a step of 2° (Fig. 3.4). Angles less than 5° and exceeding 345° are not considered since they are near-symmetrical in shape and because of high resolution requirements in mesh creation in COMSOL.

From the dataset, it was found that the configuration with the the highest nonreciprocity value,  $NR$ , corresponds to an angle of 243°. However, a Deep Neural Network (DNN) model is believed to provide an angle with a higher nonreciprocity value.



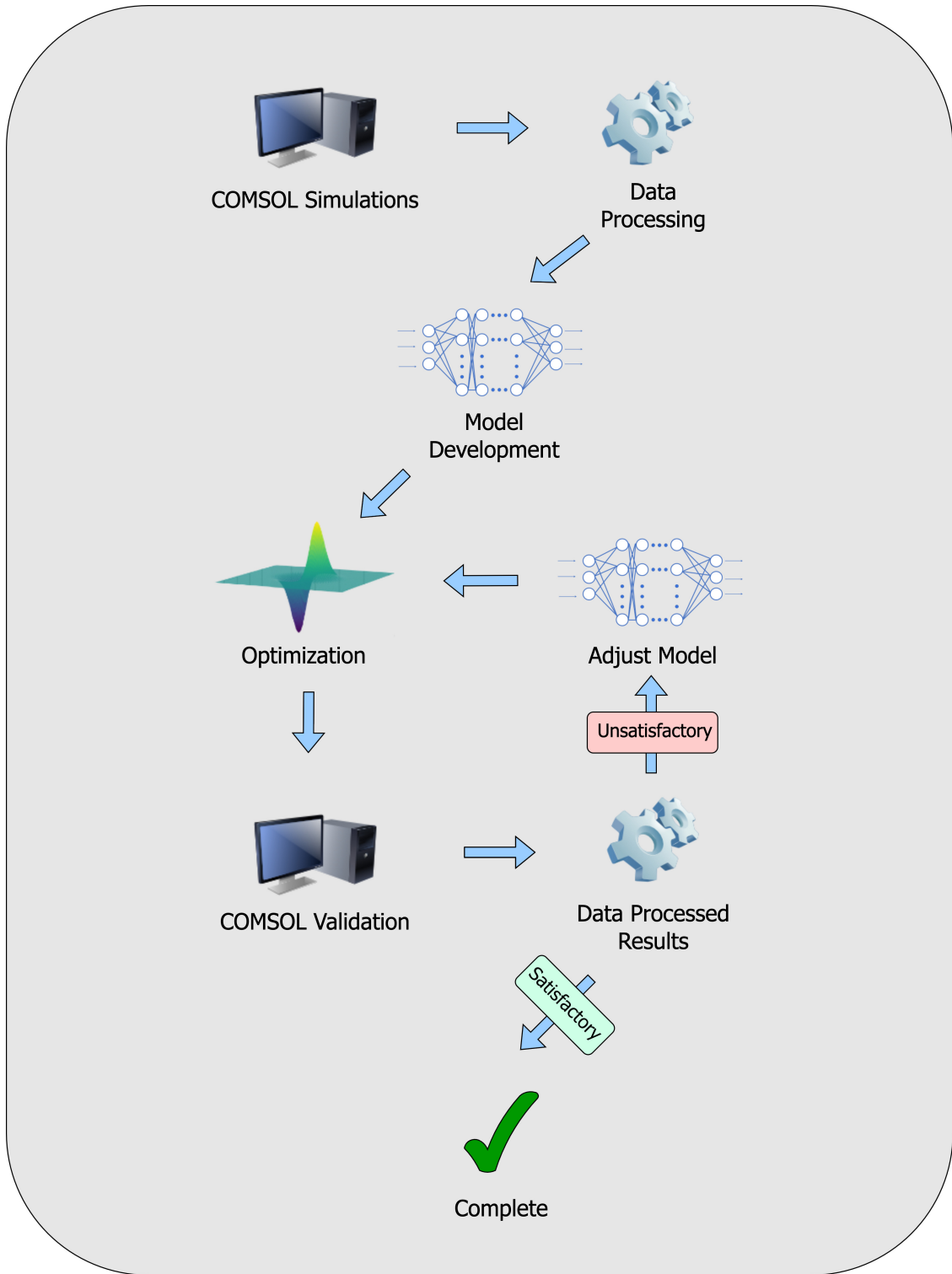


FIGURE 3.3. Optimization Pipeline.

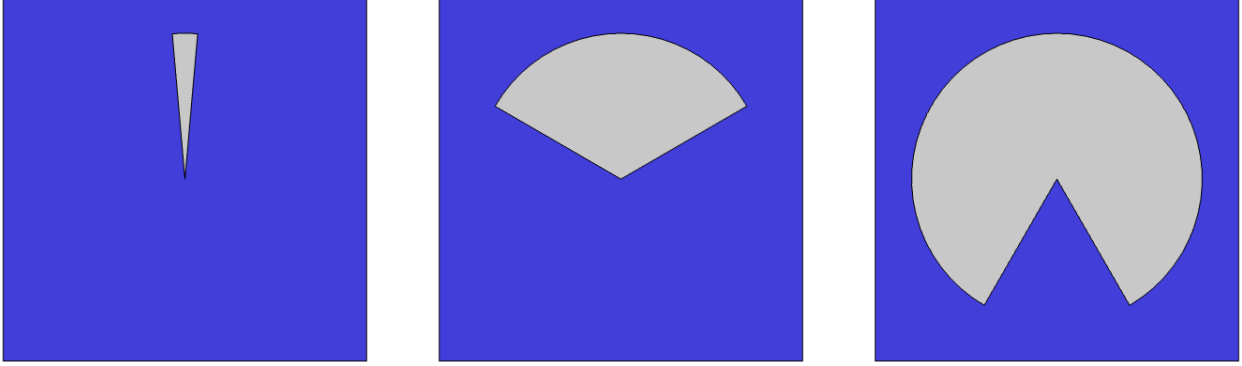


FIGURE 3.4. Unit cells of the phononic crystal with varying scatterer sector angle. Period is 15 mm; sector radius is 6 mm; sector angle is  $10^\circ$ (left),  $120^\circ$ (middle),  $300^\circ$ (right)

Firstly, normalization and division of the initial dataset into training (60%), testing (20%), and validation (20%) sets was performed. Then a simple neural network with 2 hidden layers and 35 nodes each was trained with features as angles and labels as nonreciprocity values. Training and validation losses as functions of the number of epochs (learning curves) show no overfitting. The sector angle with the highest nonreciprocity from model predictions is  $243.7165^\circ$ , which is a 3.4% (0.279 a.u.) increase in nonreciprocity compared to the highest value from the original dataset (Fig. 3.5). Direct transmission calculations with this sector angle using COMSOL confirm that nonreciprocity is higher (0.382 a.u.) than that obtained in the original dataset. Although the calculated nonreciprocity is not identical to the predicted one, the predicted sector angle provides a higher nonreciprocity value. Finally, using this optimization method, a nonreciprocity value is obtained that is more than 40% higher than the highest value from the initial dataset.

Similarly, by adjusting the model parameters to reach a lower loss (mean squared error) and avoid overfitting, the optimized sector angles are found for normalized nonreciprocity and diode efficiency. Predictions in Figs. 3.5 and 3.6 do not have a one-to-one correspondence with points from the datasets, especially when fluctuations are small and rapid.

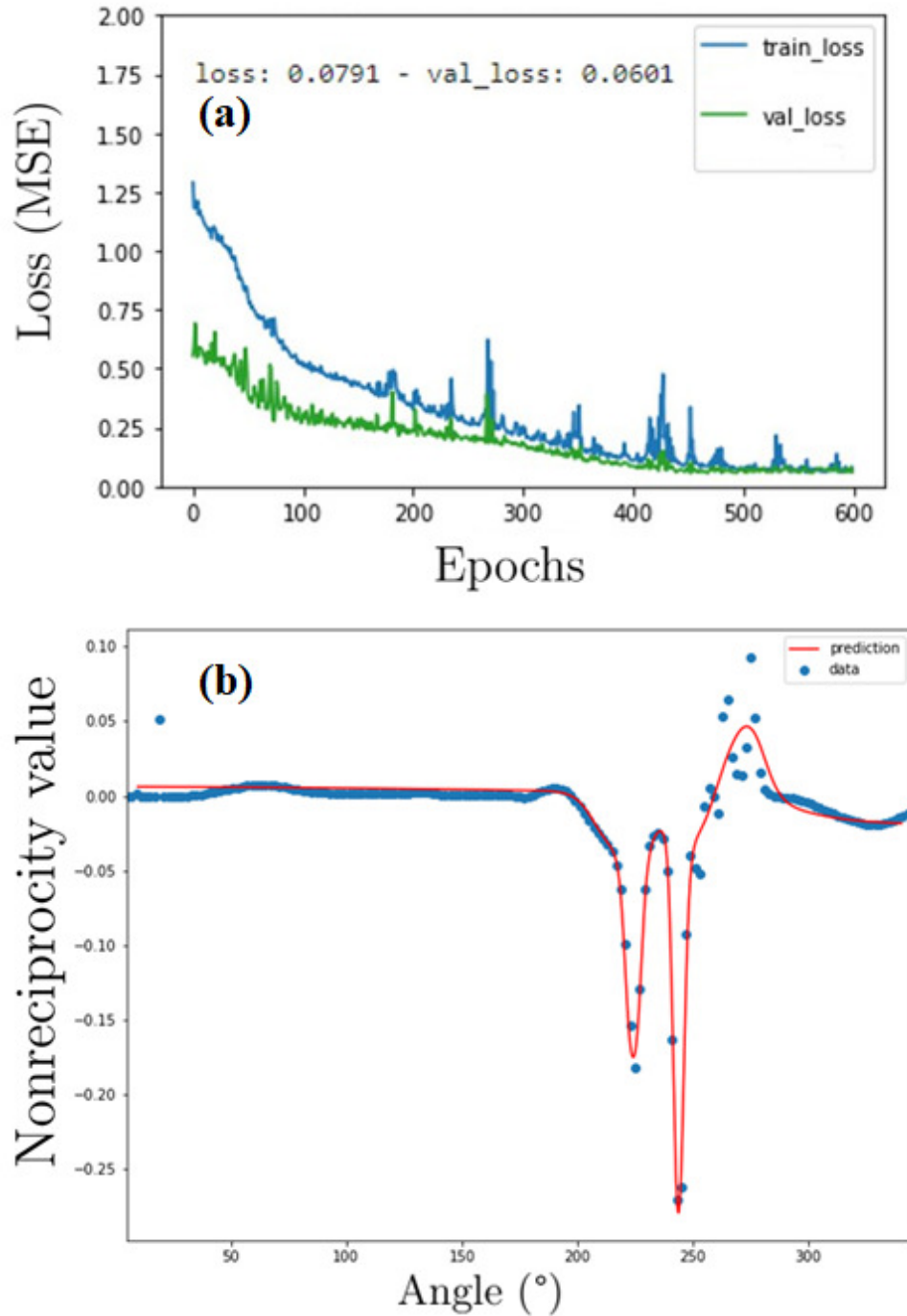


FIGURE 3.5. (a) Loss (mean squared error) as a function of the number of epochs for the  $NR$  optimization model. (b) Original data points and predictions made with a DNN model for the optimization of  $NR$ .

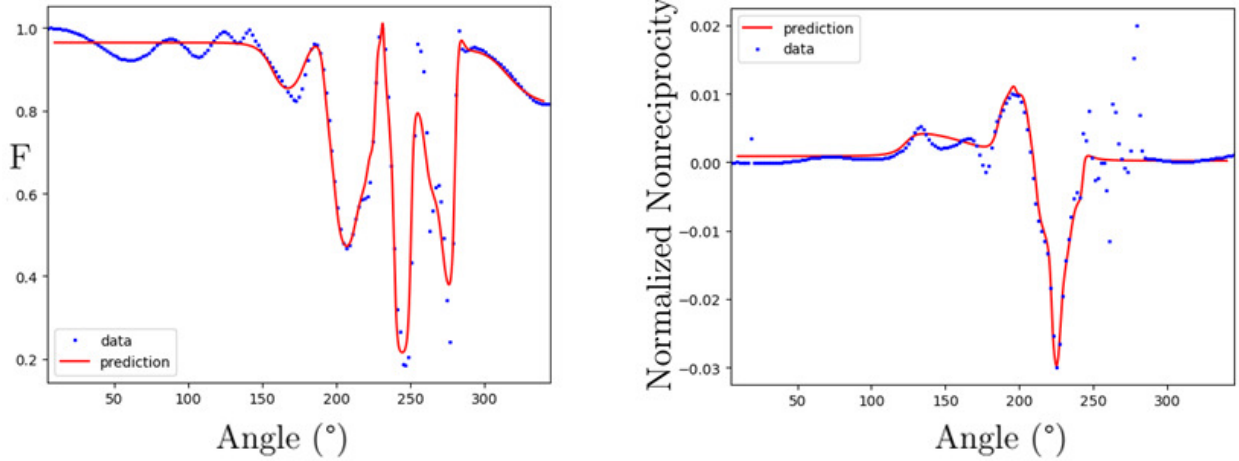


FIGURE 3.6. Original data points and predictions made with a DNN model.

Left pannel: Optimization for  $F$ . Right pannel: Optimization for  $NNR$ .

For the values of  $NNR$  and  $F$ , optimal predictions from the model may not be better than the best values obtained from the original dataset. However, the angles at which these models predict to have optimal values do indeed exhibit better values than those from the original dataset, and COMSOL calculations validate the correctness of these models, see Table 3.2.

Method	NR (a.u.)	Angle (deg)	NNR (%)	Angle (deg)	F (%)	Angle (deg)
Dataset	0.27	243	2.99	225	18.5	247
Prediction	0.279	243.7165	2.97	225.1017	21.2	245.5978
COMSOL Validation	0.382	243.7165	3.01	225.1017	18.4	245.5978

TABLE 3.2. The best nonreciprocity  $NR$  (maximizing), normalized nonreciprocity  $NNR$  (maximizing), and diode efficiency  $F$  (minimizing) from the dataset with model predictions and COMSOL validated values for the optimized parameters.

To analyze the effectiveness of the acoustic diode represented by a  $5 \times 5$  sample with the parameters corresponding to the best  $F$ -value, the transmission spectra in viscous water as well as the band structure for the corresponding infinite crystal with inviscid water are calculated. The results for the region of frequencies near 100 kHz are represented by Fig.

3.7.

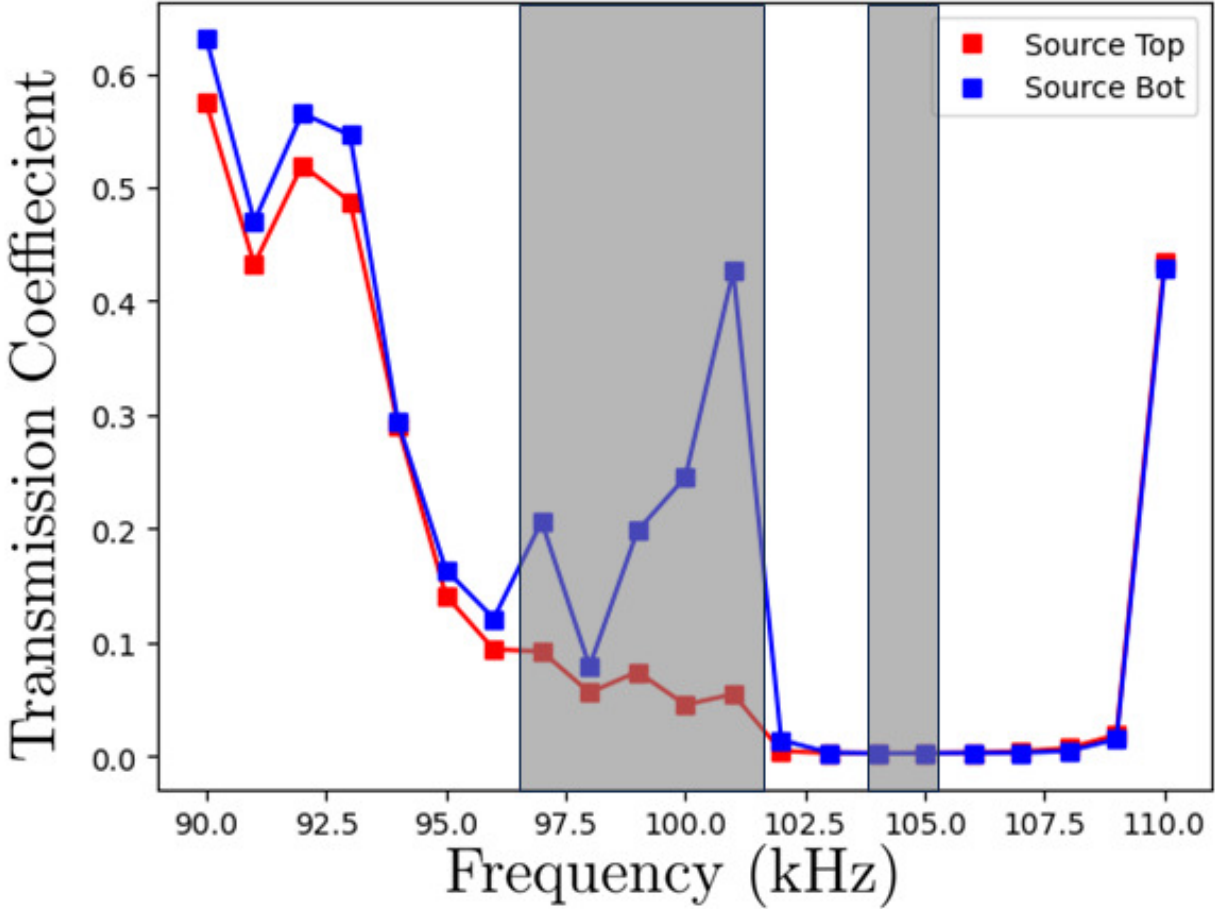


FIGURE 3.7. Transmission spectra for the  $5 \times 5$  phonic crystal sample in viscous water with the parameters corresponding to the best  $F$ -value. Downward propagation ("Source Top") is shown with red color, while upward propagation ("Source Bot") is depicted with blue color. The top/bottom positions of the source are indicated in Fig. 2.1. The shaded areas are the regions of the band gaps in the infinite phonic crystal with inviscid water. Note that the narrow transmission region between the gaps is not resolved for the finite-size sample.

Since the 100 kHz frequency lies within the band gap, the transmission in the infinite crystal is zero in both directions. Moreover, it was shown in Ref. [31] that the dispersion relation, being a complex function in a viscous environment, remains an even function  $\omega(\mathbf{k}) =$

$\omega(-\mathbf{k})$ , i.e., the dissipation-induced nonreciprocity is a finite-size effect which gradually disappears with sample length. Due to the finite size of the crystal, viscosity of water, and sound hard boundaries on the left and right boundaries of the finite crystal, the asymmetry in the transmission is clearly manifested. For one direction (downward, when source is above the crystal) of the wave propagation, the transmission coefficient is high enough to detect it. For the other direction (upward, when source is below the crystal), there is a good suppression of the sound intensity, which indicates blocking a signal. Moreover, an even better value for  $F$  can be achieved at 101 kHz where  $F = 12.7\%$  and the transmission coefficient of the acoustic diode in the forward direction exceeds 40%.

### 3.5. Multiple Parameters Optimization

The next step in the generalization of a prototype is to consider asymmetric scatterers composed of several sectors of  $60^\circ$  each with variable radius  $r$  and variable orientation of the sector characterized by angle  $\beta$ . Ten different geometries shown in Fig. 3.8 were analyzed. The angle  $\beta$  characterizes orientation of the scatterer as a whole. In Fig. 3.8 the rotation by angle  $\beta$  is shown for the cross-sections (1) and (10). All other scatterers are displaced for  $\beta = 0$ .

Geometry #	1	2	3	4	5	6	7	8	9	10
$\beta$										
$0^\circ$										
$60^\circ$										

FIGURE 3.8. Ten different asymmetric cross-sections of scatterers.

The original dataset is created calculating transmissions for each type of geometry with a radius in the range of 1 mm and 7 mm with a step of 1 mm and with a rotational angle in the range of  $0^\circ$  and  $180^\circ$  with a step of  $10^\circ$ . The limitation for the radius is due to the size of the unit cell ( $a = 15\text{mm}$ ). The geometries with angles  $180^\circ < \beta < 360^\circ$  do not provide any new information about the transmission coefficient and are, therefore, not numerically

calculated in COMSOL. More than 5000 transmission values are calculated including those for viscous and inviscid water in the upward and downward directions. For visualization and predictions, a polar representation is chosen which accounts for the periodic behavior of the data (Fig. 3.9). In this approach,  $\cos \beta$  and  $\sin \beta$  are considered as features along with the radius  $r$  for  $NR$  and  $NNR$  models. Since the  $F$ -value function has a period of  $\pi$  (Eq. 3.24), double angled trigonometric functions are used.

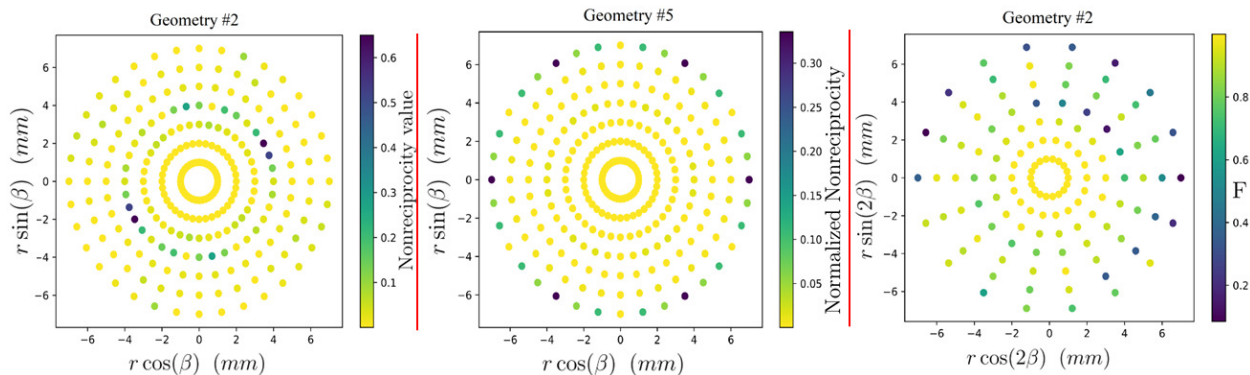


FIGURE 3.9. Original data for the geometry types with the highest  $NR$  (left),  $NNR$  (center) and the lowest  $F$  (right).

	NR (a.u)	NNR (%)	F (%)	F (%) Extended
Dataset	0.65	33.5	8.48	5.52
$\beta$ ( $^\circ$ )	30	0	0	180
$r$ (mm)	4	7	7	7.2
Geometry Type				

TABLE 3.3. The highest (lowest for  $F$ ) nonreciprocity, normalized nonreciprocity and diode efficiency from the dataset.

Examining Fig. 3.9 (right), it is evident that even lower  $F$ -values for higher radii of the scatter can be expected. Additional data was calculated for  $r = 7.2$  mm and  $r = 7.4$

mm using COMSOL and included in the extended dataset (Table 3.3).

Using a similar approach as in Section 3.4, the values for  $NR$ ,  $NNR$ , and  $F$  are predicted for all possible  $r$  and  $\beta$  values in the range between 1 mm and 7 mm (7.4 mm for  $F$ ) for the radius and  $0^\circ$  and  $180^\circ$  for the angle (Fig. 3.10). DNN models for  $NNR$  were either underfitted (provide poor predictions with training data) or overfitted (cannot be used for new predictions). In other words, because the highest  $NNR$  value (33.5%) is much greater than the remaining data, all tested machine learning models either considered it an outlier or fitted too closely to it to the point at which the model performed poorly on validation and testing data (unseen by the model). The 3-fold rotational symmetry in Fig. 3.9 (center) is due to the corresponding symmetry of the scatterer, where all maxima correspond to technically the same geometry.


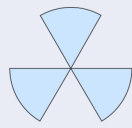
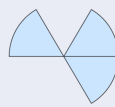
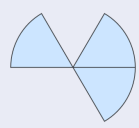
	NR (a.u)	NNR (%)	F (%)	F (%) Extended
Dataset	0.65	<b>33.5</b>	<b>8.48</b>	5.52
Prediction	0.71	8.91	-	5.88
COMSOL Validation	<b>0.70</b>	13.3	-	<b>5.30</b>
$\beta$ ( $^\circ$ )	27.7444	0	0	0
r (mm)	3.9657	7	7	7.1966
Geometry Type				

TABLE 3.4. The highest (lowest for F) nonreciprocity, normalized nonreciprocity and diode efficiency from the dataset and predictions as well as COMSOL validated values for the optimized parameters. The best values are highlighted and the corresponding radius and rotation angle are provided.

The model for nonreciprocity has relatively small final loss and is not overfitted. Predictions have two regions with high values that are located around 4 mm and 30 (210) degrees, which correlates to the original data. The highest nonreciprocity prediction, which is 9% higher than the one from the dataset, is validated with COMSOL. Direct calculations



prove the correctness of the model (Table 3.4).

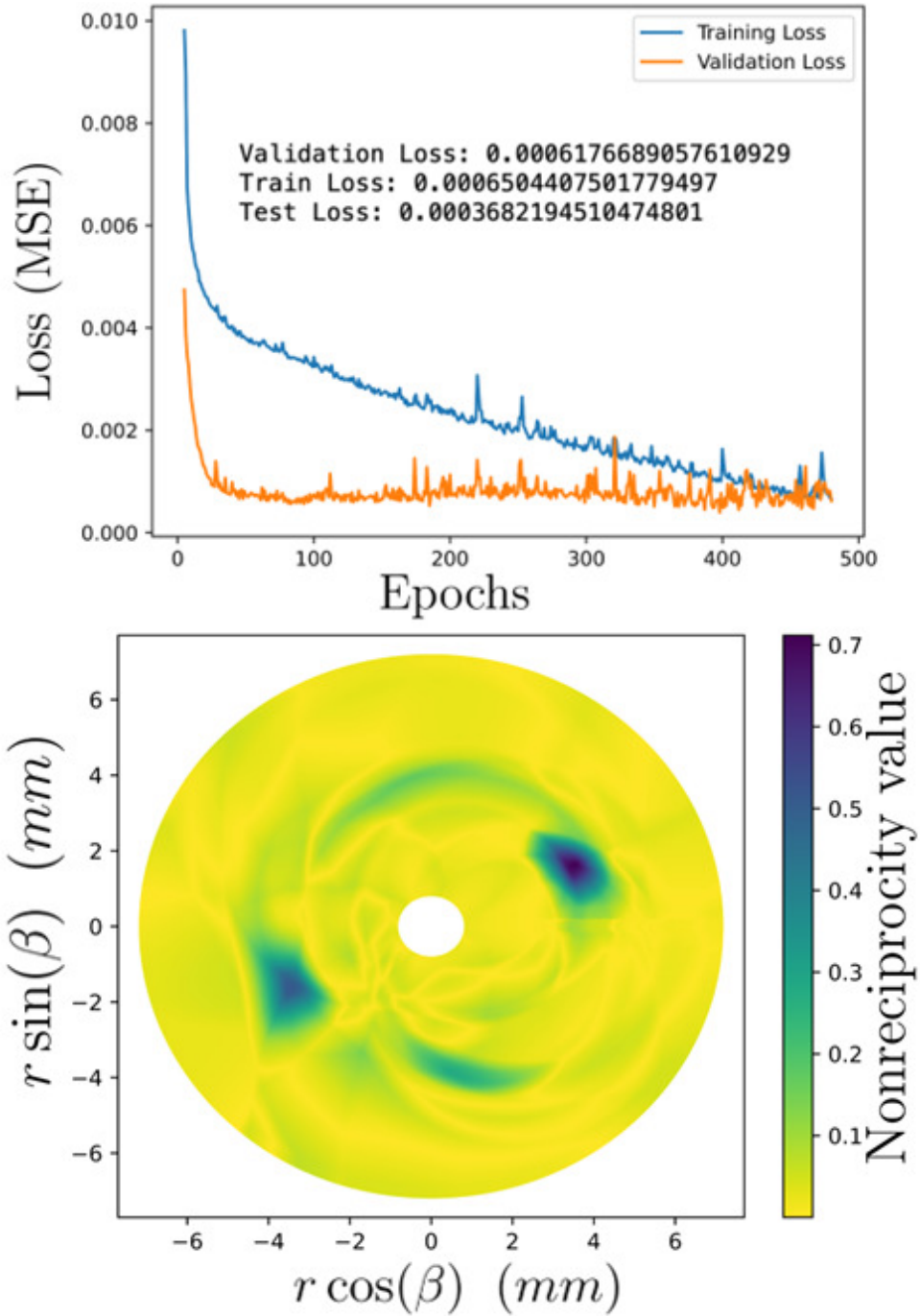


FIGURE 3.10. Nonreciprocity optimization. Loss (mean squared error) as a function of a number of epoch (top) and predictions of the DNN models of NR (bottom). The model consists of 4 hidden layers with 17 nodes each.

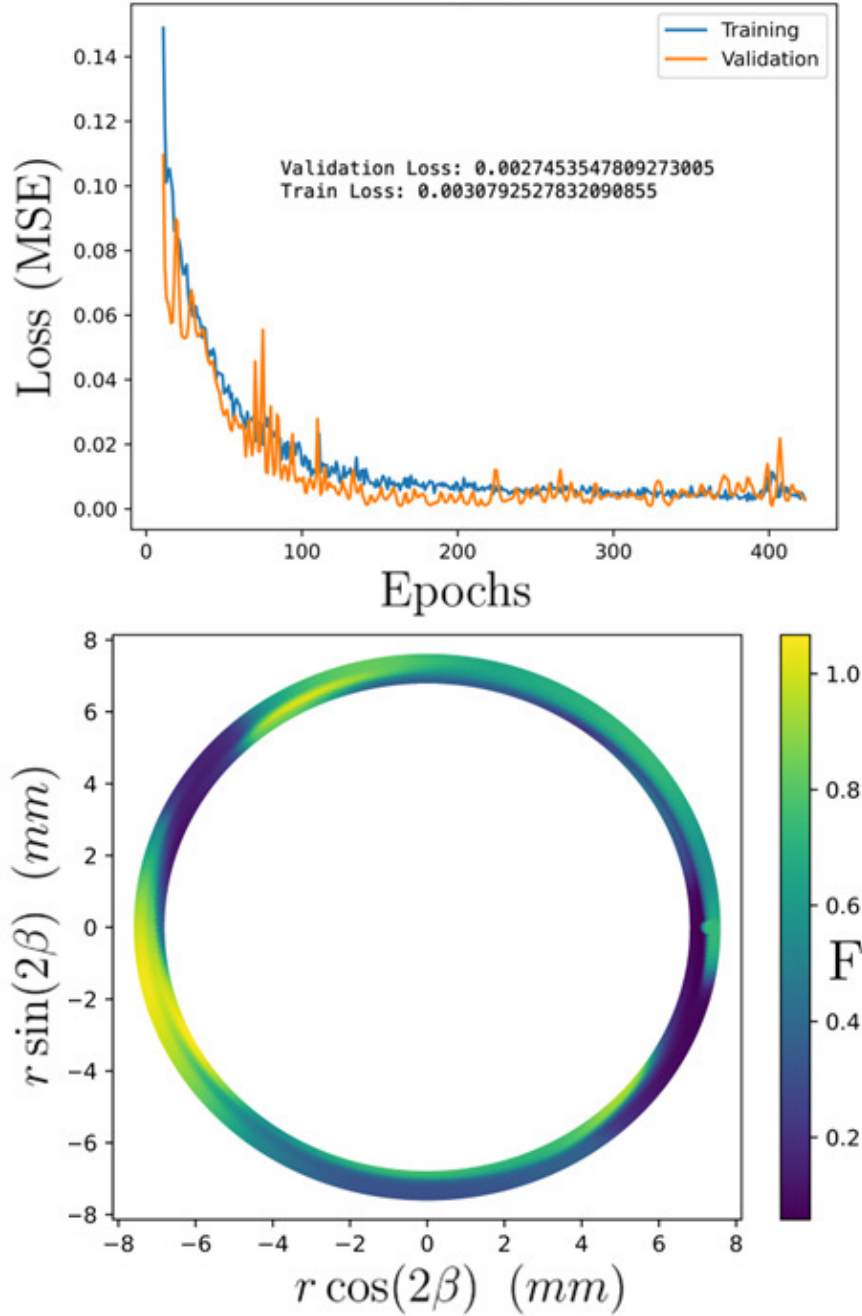


FIGURE 3.11. Diode efficiency optimization. Loss (mean squared error) as a function of a number of epoch (top) and predictions of the DNN models of  $F$  (bottom). The model consists of 5 hidden layers with 1000 nodes and a 15% dropout rate in each layer.

After optimization of the diode (Fig. 3.11), it is found that the lowest  $F$ -value is 5.3%, which means that the ratio of the transmissions in the forward and reverse direction is almost 20. The calculated transmission spectra for the optimized  $5 \times 5$  sample are shown in Fig. 3.12. Just like the spectra in Fig. 3.7, the best contrast between the forward and reverse transmission lies within the bandgap calculated for the corresponding infinite crystal.

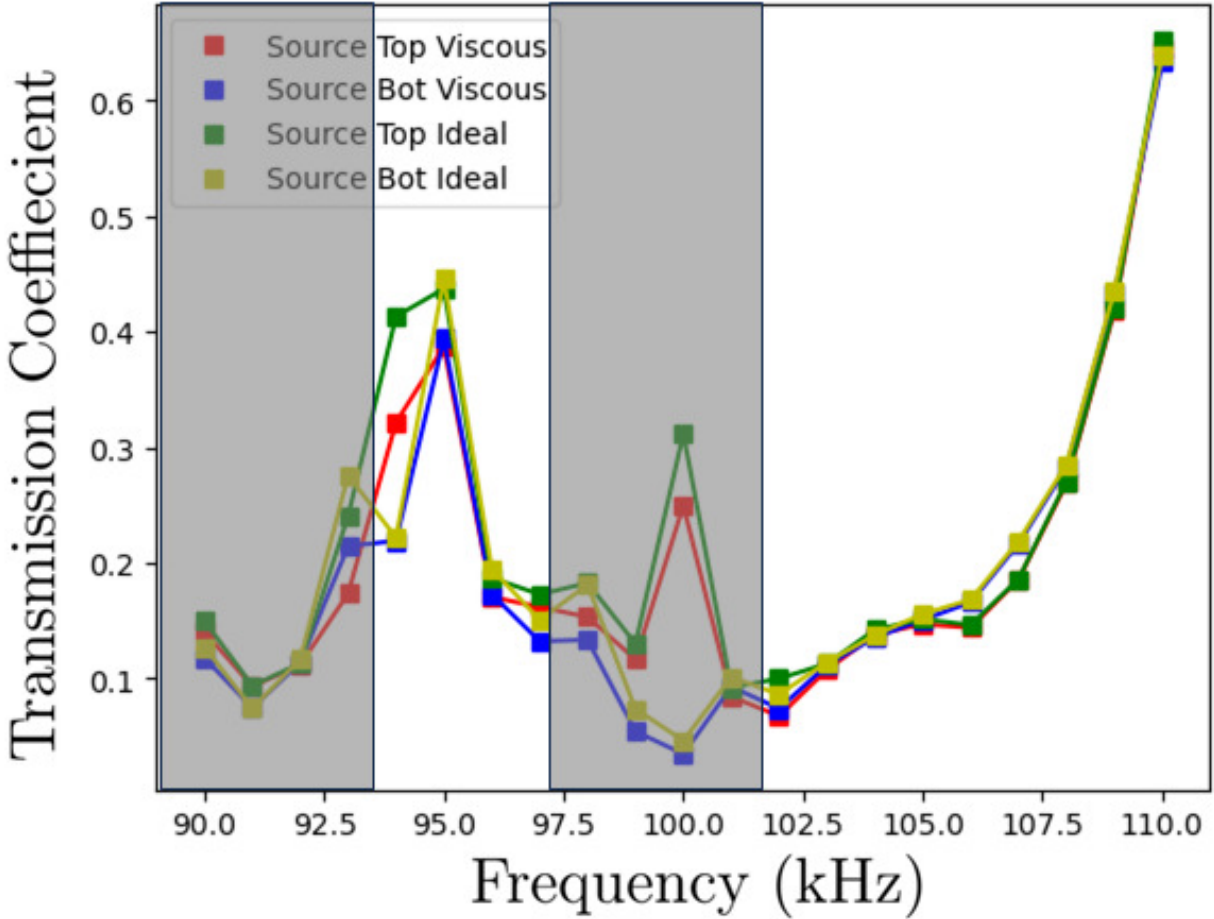


FIGURE 3.12. Transmission spectra through the  $5 \times 5$  sample with the parameters providing the highest value of nonreciprocity  $NR$ . The parameters of the scatterer are given in Table 3.4. Note that the narrow transmission band lying between two bandgaps (marked as shaded areas) is well-resolved, unlike similar transmission band in Fig.3.8.

This is one more manifestation of asymmetry, which means that the destructive in-

terference leading to the formation of a bandgap in an infinite crystal is sensitive to the direction of wave propagation (forward or reverse). Of course, the asymmetry vanishes with the size of the sample, but for the finite-length samples it may be explored for the rectification of acoustic signals. In particular, the phononic crystal with the parameters given in the last column of Table 3.4 can be used as an acoustic diode at 100 kHz.

### 3.6. Summary

In conclusion, I calculated the transmission for a  $5 \times 5$  phononic crystal with different shapes of scatterers placed in a waveguide and optimized the scatter geometry to achieve the highest nonreciprocity, normalized nonreciprocity and diode efficiency. It is shown that viscosity-induced nonreciprocity strongly depends on the shape of scatterers. Its contribution to the transmission difference between the forward and backward wave propagation is comparable to the reciprocal contribution due to asymmetry, which exists in an ideal fluid background. The asymmetric and nonreciprocal contributions to the transmission may mutually enhance or weaken each other. The geometry of the scatterers when these contributions enhance each other along one direction and weaken along the opposite direction is obtained at a given frequency of 100 kHz and validated with COMSOL software. This geometry is optimal for the sample to serve as a linear non-resonant passive acoustic diode. Although the highest transmission coefficient is essentially lower than 1, it is sufficient for secure signal transmission in the forward direction and strongly suppressed signal transmission in the reverse direction. A passive acoustic diode with higher transmission in the forward direction at a resonant frequency was proposed in Ref. [97]. The high asymmetry in transmission is achieved due to different symmetry (even/odd) of the eigenmodes propagating on the left and right wings of the proposed elastic waveguide. For active acoustic diode the transmission in the forward direction may be close to 1 due to the presence of external sources of energy [68]. In a passive nonlinear acoustic diode, the transmission may be close to one since the samples are relatively short and the rectification is due to the nonlinearity of the material [18]. With a machine learning approach of optimization it was possible to slightly adjust scatterer's geometry to predict and achieve parameters for better values of  $NR$ ,  $NNR$ , and

$F$ . When the best values from the original dataset are outliers (a big difference between its closest neighbors), models exhibit underfitting or overfitting. However, if the data distribution is relatively even, I get an improvement in the corresponding quantities. The final data shows that the best values of  $NR$ ,  $NNR$  and  $F$  are achieved, when the corresponding frequency is close to the edge of the band gap calculated for the corresponding infinite crystal and inviscid environment. The proposed structure may be used as a passive acoustic diode, serving without an external source of energy.

## CHAPTER 4

### RESULTS AND CONCLUSIONS

In this dissertation I study influence of the dissipation over sound propagation through phononic crystals with viscous components. Firstly, I developed a microscopic theory of sound propagation through a periodic layered structure containing viscous fluid constituents based on Navier - Stokes equation. Using boundary conditions approach, I obtained analytically dispersion relation for acoustic waves propagating in such media. Simplified dispersion equations were obtained when the other component of the unit cell is either elastic solid, viscous fluid, or ideal fluid. I analyzed dependence of the decay coefficient on the relevant parameters - wave frequency, viscosity coefficients etc. Another part of my dissertation is devoted to the nonreciprocal wave propagation in phononic crystals induced by viscosity. Using Fourier-transformed wave equation, I proved analytically that for an infinite phononic crystal dispersion relation remains the same switching the direction of the wave propagation, while Fourier components of velocity are nonreciprocal. Then, I considered a two-dimensional finite phononic crystal and optimized shape of the scatterer to reach the highest value of the nonreciprocity. Sound propagation through crystals with different unit cells was numerically simulated to create a dataset of transmission values. I introduced three parameters to describe nonreciprocal response of the system. For each quantity I obtained the optimized scatterer's geometry utilizing machine learning techniques. I found parameters of the crystal, which may work as a linear non-resonant passive acoustic diode.

In the first problem, I considered a superlattice - a one-dimensional phononic crystal with a unit cell comprising two layers of different materials, where at least one of the components is a viscous fluid. I started with an acoustic wave equation for sound propagating in an infinite viscous fluid and showed the existence of two modes with different polarization. Then, I examined refraction at the boundary between two fluids and derived generalized Snell's law for an inhomogeneous wave. Utilizing periodicity of the superlattice as well as continuity of velocity and stress tensor components, I obtained the general dispersion rela-

tion. Since it contains an enormous amount of terms, I simplified it in the approximation of low viscosity for three different cases - viscous fluid - solid, viscous fluid - viscous fluid and viscous fluid- ideal fluid structures. The limit of low frequencies when periodic structure homogenizes and the frequencies close to the band edge when propagating Bloch wave becomes a standing wave were considered and enhanced viscous dissipation was calculated. Angular dependence of the attenuation coefficient was analyzed. I showed that transition from dissipation in the bulk to dissipation in a narrow boundary layer occurs in the region of angles close to normal incidence. Enormously high dissipation was predicted for solid-fluid structure in the region of angles where transmission practically vanishes. For the case when the unit cell contains a narrow layer of high viscosity fluid, the anomaly related to acoustic manifestation of Borrmann effect was explained.

In the other problem, I considered an infinite phononic crystal to study reciprocal/nonreciprocal sound wave propagation. From the Navier-Stokes equation I derived wave equations in Fourier representation for sound propagating in the forward and backward direction. A new criteria of reciprocity were introduced since common quantities as transmission can not be used for infinite systems. I proved analytically, that dispersion relation remains reciprocal in all possible cases - dissipationless media, dissipative media with either symmetrical or asymmetrical scatterers. Also, I showed that eigenfunctions, which correspond to the Fourier components of the velocity, are reciprocal for the wave propagating through the phononic crystal without dissipation and nonreciprocal if viscosity is included. Next, I considered a finite 5x5 phononic crystal with highly asymmetric aluminum rods in viscous water. The cross-section of the rods was selected to be asymmetric to provide very different transmission in opposite directions along a given crystallographic line. I calculated numerically sound intensity distributions for acoustic wave propagating in the upward and downward direction through the crystal with various scatterer's geometries placed. Simulations were performed with viscous and inviscid environment. Difference in transmission contains the reciprocal part, caused by asymmetry of the scatterers, and the truly nonreciprocal part, related to non-equal viscous losses for sound waves propagating in opposite

directions. The rectification ratio for different levels of asymmetry was evaluated and optimized over its value at a fixed frequency, with various machine learning models. The possibility of using asymmetric phononic crystals as acoustic diodes was discussed.

In summary, I presented results of various fundamental physical phenomena with significant implications for physical acoustics. These findings not only contribute to the theoretical understanding of acoustics but also offer practical value by providing insights into the design of acoustic passive diodes and layered periodic structures.



## REFERENCES

- [1] Clémence L. Bacquet, Hasan Al Ba'ba'a, Michael J. Frazier, Mostafa Nouh, and Mahmoud I. Hussein, *Chapter two - metadamping: Dissipation emergence in elastic metamaterials*, Advances in Crystals and Elastic Metamaterials, Part 1 (Mahmoud I. Hussein, ed.), Advances in Applied Mechanics, vol. 51, Elsevier, 2018, pp. 115–164.
- [2] Thomas Becker and Frieder Mugele, *Nanofluidics: Viscous dissipation in layered liquid films*, Phys. Rev. Lett. 91 (2003), 166104.
- [3] Jacob Biamonte, Peter Wittek, Nicola Pancotti, Patrick Rebentrost, Nathan Wiebe, and Seth Lloyd, *Quantum machine learning*, Nature 549 (2017), no. 7671, 195–202.
- [4] M. V. Bogdanova, Yu. E. Lozovik, and S. L. Eiderman, *An optical analog of the Borrmann effect in photonic crystals*, Soviet Journal of Experimental and Theoretical Physics 110 (2010), no. 4, 604–612.
- [5] G. Borrmann, *Über extinktionsdiagramme der röntgenstrahlen von quarz*, Phys. Z 42 (1941), 157–162.
- [6] L.M. Brekhovskikh, *Waves in layered media*, Academic Press Inc., New York, 1960.
- [7] Giuseppe Carleo, Ignacio Cirac, Kyle Cranmer, Laurent Daudet, Maria Schuld, Naftali Tishby, Leslie Vogt-Maranto, and Lenka Zdeborová, *Machine learning and the physical sciences*, Rev. Mod. Phys. 91 (2019), 045002.
- [8] Giuseppe Carleo and Matthias Troyer, *Solving the quantum many-body problem with artificial neural networks*, Science 355 (2017), no. 6325, 602–606.
- [9] Juan Carrasquilla and Roger G Melko, *Machine learning phases of matter*, Nature Physics 13 (2017), no. 5, 431–434.
- [10] A. Cebrecos, R. Picó, V. Romero-García, A. M. Yasser, L. Maigyte, R. Herrero, M. Botey, V. J. Sánchez-Morcillo, and K. Staliunas, *Enhanced transmission band in periodic media with loss modulation*, Applied Physics Letters 105 (2014), no. 20, 204104.
- [11] Tom Charnock, Guilhem Lavaux, and Benjamin D. Wandelt, *Automatic physical inference with information maximizing neural networks*, Phys. Rev. D 97 (2018), 083004.

- [12] A. K. Chopra, *Dynamics of structures, 2nd ed*, Prentice-Hall, New Jersey, 2001.
- [13] Alfonso Climente, Daniel Torrent, and José Sánchez-Dehesa, *Omnidirectional broadband acoustic absorber based on metamaterials*, Applied Physics Letters 100 (2012), no. 14, 144103.
- [14] Jr. Cooper, Henry F., *Reflection and Transmission of Oblique Plane Waves at a Plane Interface between Viscoelastic Media*, The Journal of the Acoustical Society of America 42 (1967), no. 5, 1064–1069.
- [15] Antonin Coutant, Yves Aurégan, and Vincent Pagneux, *Anomalous transmission through periodic resistive sheets*, The Journal of the Acoustical Society of America 147 (2020), no. 5, 3124–3135.
- [16] Vincent S. J. Craig, Chiara Neto, and David R. M. Williams, *Shear-dependent boundary slip in an aqueous newtonian liquid*, Phys. Rev. Lett. 87 (2001), 054504.
- [17] Richard V. Craster and Sébastien Guenneau, *Acoustic metamaterials: Negative refraction, imaging, lensing and cloaking*, Acoustic Metamaterials (2013).
- [18] Amir Darabi, Lezheng Fang, Alireza Mojahed, Matthew D. Fronk, Alexander F. Vakakis, and Michael J. Leamy, *Broadband passive nonlinear acoustic diode*, Phys. Rev. B 99 (2019), 214305.
- [19] Sander Dieleman, Kyle W. Willett, and Joni Dambre, *Rotation-invariant convolutional neural networks for galaxy morphology prediction*, Monthly Notices of the Royal Astronomical Society 450 (2015), no. 2, 1441–1459.
- [20] Yujiang Ding, Yugui Peng, Yifan Zhu, Xudong Fan, Jing Yang, Bin Liang, Xuefeng Zhu, Xiangang Wan, and Jianchun Cheng, *Experimental demonstration of acoustic chern insulators*, Phys. Rev. Lett. 122 (2019), 014302.
- [21] B. Djafari-Rouhani and Leonard Dobrzynski, *Vibrational contribution to the surface specific heat of a fluid*, Journal de Physique I 43 (1982), 523–529.
- [22] Y. El Hassouani, E. H. El Boudouti, B. Djafari-Rouhani, and H. Aynaou, *Sagittal acoustic waves in finite solid-fluid superlattices: Band-gap structure, surface and con-*

- fined modes, and omnidirectional reflection and selective transmission*, Phys. Rev. B 78 (2008), 174306.
- [23] Xinsheng Fang, Nikhil Gerard, Zhiling Zhou, Hua Ding, Nengyin Wang, Bin Jia, Yuanchen Deng, Xu Wang, Yun Jing, and Yong Li, *Observation of higher-order exceptional points in a non-local acoustic metagrating*, Communications Physics 4 (2021).
- [24] Romain Fleury, Dimitrios Sounas, Michael R. Haberman, and Andrea Alù, *Nonreciprocal acoustics*, Acoustics Today 11 (2015), 14–21.
- [25] Romain Fleury, Dimitrios Sounas, Caleb Sieck, Michael Haberman, and Andrea Alù, *Sound isolation and giant linear nonreciprocity in a compact acoustic circulator*, Science (New York, N.Y.) 343 (2014), 516–519.
- [26] Michael J. Frazier and Mahmoud I. Hussein, *Viscous-to-viscoelastic transition in phononic crystal and metamaterial band structures*, The Journal of the Acoustical Society of America 138 (2015), no. 5, 3169–3180.
- [27] Matthew Guild, Victor Garcia-Chocano, Weiwei Kan, and Jose Sanchez-Dehesa, *Enhanced inertia from lossy effective fluids using multi-scale sonic crystals*, AIP Advances 4 (2014).
- [28] Matthew D. Guild, Victor M. García-Chocano, Weiwei Kan, and José Sánchez-Dehesa, *Acoustic metamaterial absorbers based on multilayered sonic crystals*, Journal of Applied Physics 117 (2015), no. 11, 114902.
- [29] Cheng He, Xu Ni, Hao Ge, Xiao-Chen Sun, Yan-Bin Chen, Ming-Hui Lu, Xiao-Ping Liu, Liang Feng, and Yan-Feng Chen, *Acoustic topological insulator and robust one-way sound transport*, Nature Physics 12 (2016), 1124–1129.
- [30] Vicente Cutanda Henríquez, Victor M. García-Chocano, and José Sánchez-Dehesa, *Viscothermal losses in double-negative acoustic metamaterials*, Phys. Rev. Appl. 8 (2017), 014029.
- [31] Hyeonu Heo, E. Walker, Yurii Zubov, Dmitrii Shymkiv, Dylan Wages, Arkadii Krokhin, Tae-Youl Choi, and Arup Neogi, *Non-reciprocal acoustics in a viscous environment*,

- Proceedings of the Royal Society A: Mathematical, Physical and Engineering Sciences 476 (2020), 20200657.
- [32] Tyler W. Hughes, Momchil Minkov, Yu Shi, and Shanhui Fan, *Training of photonic neural networks through in situ backpropagation and gradient measurement*, *Optica* 5 (2018), no. 7, 864–871.
- [33] Mahmoud I. Hussein, *Theory of damped bloch waves in elastic media*, *Phys. Rev. B* 80 (2009), 212301.
- [34] Mahmoud I Hussein and Michael J Frazier, *Damped phononic crystals and acoustic metamaterials*, *Acoustic metamaterials and phononic crystals*, Springer, 2012, pp. 201–215.
- [35] M. Ibarias, Yu. Zubov, J. Arriaga, and A. A. Krokhin, *Phononic crystal as a homogeneous viscous metamaterial*, *Phys. Rev. Res.* 2 (2020), 022053.
- [36] Martin Ibarias, J. Doporto, A. Krokhin, and Jesus Arriaga, *Tuning the decay of sound in a viscous metamaterial*, *Philosophical Transactions of the Royal Society A: Mathematical, Physical and Engineering Sciences* 380 (2022).
- [37] J. D. Jackson, *Classical electrodynamics, 3rd ed.*, Wiley, New York, 1998.
- [38] Xue Jiang, Yong Li, and Likun Zhang, *Thermoviscous effects on sound transmission through a metasurface of hybrid resonances*, *The Journal of the Acoustical Society of America* 141 (2017), no. 4, EL363–EL368.
- [39] Sajeev John, *Strong localization of photons in certain disordered dielectric superlattices*, *Phys. Rev. Lett.* 58 (1987), 2486–2489.
- [40] C. Kittel, *Interaction of spin waves and ultrasonic waves in ferromagnetic crystals*, *Phys. Rev.* 110 (1958), 836–841.
- [41] B.P. Konstantinov, *On the absorption of acoustic waves reflected from a solid boundary*, *Zh. Tekh. Fiz* 9 (1939), 226.
- [42] Zhaxylyk A. Kudyshev, Alexander V. Kildishev, Vladimir M. Shalaev, and Alexandra Boltasseva, *Machine-learning-assisted metasurface design for high-efficiency thermal emitter optimization*, *Applied Physics Reviews* 7 (2020), no. 2, 021407.

- [43] M. S. Kushwaha, P. Halevi, L. Dobrzynski, and B. Djafari-Rouhani, *Acoustic band structure of periodic elastic composites*, Phys. Rev. Lett. 71 (1993), 2022–2025.
- [44] Sir Horace Lamb, *Hydrodynamics, 6th ed*, New York, 1945.
- [45] L.D. Landau and E.M. Lifshitz, *Fluid mechanics 2nd ed.*, Elsevier, Oxford, 1984.
- [46] Vincent Laude, Jose Maria Escalante, and Alejandro Martínez, *Effect of loss on the dispersion relation of photonic and phononic crystals*, Phys. Rev. B 88 (2013), 224302.
- [47] B. Lax and K.J. Button, *Microwave ferrites and ferrimagnetics*, McGraw-Hill, New York, 1962.
- [48] Xiang Li, Shaowu Ning, Zhanli Liu, Ziming Yan, Chengcheng Luo, and Zhuo Zhuang, *Designing phononic crystal with anticipated band gap through a deep learning based data-driven method*, Computer Methods in Applied Mechanics and Engineering 361 (2020), 112737.
- [49] Xinwei Li, Miao Zhao, Xiang Yu, Jun Wei Chua, Yong Yang, Kian Lim, and Wei Zhai, *Multifunctional and customizable lattice structures for simultaneous sound insulation and structural applications*, Materials & Design 234 (2023), 112354.
- [50] Bin Liang, Xiasheng Guo, Juan Tu, D Zhang, and J Cheng, *An acoustic rectifier*, Nature materials 9 (2010), 989–92.
- [51] Bin Liang, Bo Yuan, and Jian-chun Cheng, *Acoustic diode: Rectification of acoustic energy flux in one-dimensional systems*, Phys. Rev. Lett. 103 (2009), 104301.
- [52] Wen H. Lin and A. C. Raptis, *Acoustic scattering by elastic solid cylinders and spheres in viscous fluids*, The Journal of the Acoustical Society of America 73 (1983), no. 3, 736–748.
- [53] Guancong Ma and Ping Sheng, *Acoustic metamaterials: From local resonances to broad horizons*, Science advances 2 (2016), no. 2, e1501595.
- [54] Itzik Malkiel, Michael Mrejen, Achiya Nagler, Uri Arieli, Lior Wolf, and Haim Suchowski, *Plasmonic nanostructure design and characterization via deep learning*, Light: Science & Applications 7 (2018).

- [55] A.A. Maznev, A.G. Every, and O.B. Wright, *Reciprocity in reflection and transmission: What is a ‘phonon diode’?*, Wave Motion 50 (2013), no. 4, 776–784.
- [56] Rayisa P. Moiseyenko and Vincent Laude, *Material loss influence on the complex band structure and group velocity in phononic crystals*, Phys. Rev. B 83 (2011), 064301.
- [57] Miguel Molerón, Marc Serra-Garcia, and Chiara Daraio, *Visco-thermal effects in acoustic metamaterials: from total transmission to total reflection and high absorption*, New Journal of Physics 18 (2016), no. 3, 033003.
- [58] R. Moussa, S. Foteinopoulou, Lei Zhang, G. Tuttle, K. Guven, E. Ozbay, and C. M. Soukoulis, *Negative refraction and superlens behavior in a two-dimensional photonic crystal*, Phys. Rev. B 71 (2005), 085106.
- [59] H. Nassar, H. Chen, A. N. Norris, and G. L. Huang, *Quantization of band tilting in modulated phononic crystals*, Phys. Rev. B 97 (2018), 014305.
- [60] Hussein Nassar, Behrooz Yousefzadeh, Romain Fleury, Massimo Ruzzene, Andrea Alù, Chiara Daraio, Andrew Norris, Guoliang Huang, and Michael Haberman, *Nonreciprocity in acoustic and elastic materials*, Nature Reviews Materials 5 (2020), 1–19.
- [61] Andrew N. Norris, *An inequality for longitudinal and transverse wave attenuation coefficients*, The Journal of the Acoustical Society of America 141 (2017), no. 1, 475–479.
- [62] V. B. Novikov and T. V. Murzina, *Borrmann effect in photonic crystals*, Opt. Lett. 42 (2017), no. 7, 1389–1392.
- [63] Juhyuk Park and Young Seok Song, *Assembling hydrodynamic cloaks to conceal complex objects from drag*, Journal of Fluids and Structures 98 (2020), 103136.
- [64] J. B. Pendry, *Negative refraction makes a perfect lens*, Phys. Rev. Lett. 85 (2000), 3966–3969.
- [65] Y. Pennec, B. Djafari-Rouhani, Hocine Larabi, Jérôme Vasseur, and Anne-Christine Hladky-Hennion, *Phononic crystals and manipulation of sound*, physica status solidi (c) 6 (2009), 2080 – 2085.
- [66] Allan Pierce, *Acoustics: An introduction to its physical principles and applications*, vol. 34, 06 1989.

- [67] A. B. Pippard, *The surface impedance of superconductors and normal metals at high frequencies ii. the anomalous skin effect in normal metals*, Proc. R. Soc. Lond. A 191 (1947), 385–399.
- [68] Bogdan-Ioan Popa and Steven Cummer, *Non-reciprocal and highly nonlinear active acoustic metamaterials*, Nature communications 5 (2014), 3398.
- [69] I. E. Psarobas, *Viscoelastic response of sonic band-gap materials*, Phys. Rev. B 64 (2001), 012303.
- [70] Ting Qu, Bo Wang, and Hequn Min, *Lightweight composite partitions with high sound insulation in hotel interior spaces: Design and application*, Buildings 12 (2022), no. 12.
- [71] Ilyasse Quotane, El Houssaine El Boudouti, and Bahram Djafari-Rouhani, *Trapped-mode-induced fano resonance and acoustical transparency in a one-dimensional solid-fluid phononic crystal*, Phys. Rev. B 97 (2018), 024304.
- [72] J.W.S. Rayleigh, *The theory of sound, 2nd ed*, Macmillan and Co., New York, 1896.
- [73] Lord Rayleigh, *On the application of the principle of reciprocity to acoustics*, Proceedings of the Royal Society of London 25 (1876), 118–122.
- [74] G. E. H. Reuter and E. H. Sondheimer, *The theory of the anomalous skin effect in metals*, Proc. R. Soc. Lond. A 195 (1948), 336–364.
- [75] Edgar Reyes-Ayona, Daniel Torrent, and José Sánchez-Dehesa, *Homogenization theory for periodic distributions of elastic cylinders embedded in a viscous fluid*, The Journal of the Acoustical Society of America 132 (2012), no. 4, 2896–2908.
- [76] S.M. Rytov, *Acoustical properties of a thinly laminated medium*, Soviet Phys. Acous. 2 (1956).
- [77] R. P. Shaw and P. Bugl, *Transmission of Plane Waves through Layered Linear Viscoelastic Media*, The Journal of the Acoustical Society of America 46 (1969), no. 3B, 649–654.
- [78] Dmitrii Shymkiv and Arkadii Krokhin, *Effects of viscous dissipation in propagation of sound in periodic layered structures*, The Journal of the Acoustical Society of America 155 (2024), no. 2, 990–1004.

- [79] Dmitrii Shymkiv, Arnav Mazumder, Jesús Arriaga, and Arkadii Krokhin, *Optimization of nonreciprocal transmission through dissipative phononic crystals with machine learning techniques*, IEEE Open Journal of Ultrasonics, Ferroelectrics, and Frequency Control PP (2023), 1–1.
- [80] Rudolf Sprik and Gerard H. Wegdam, *Acoustic band gaps in composites of solids and viscous liquids*, Solid State Communications 106 (1998), no. 2, 77–81.
- [81] Sewell C. J. T., *The extinction of sound in a viscous atmosphere by small obstacles of cylindrical and spherical form*, Proc. R. Soc. Lond. A 83 (1910), 547–548.
- [82] Yukihiro Tanaka, Yukito Shimomura, and Norihiko Nishiguchi, *Acoustic wave rectification in viscoelastic materials*, Japanese Journal of Applied Physics 57 (2018), no. 3, 034101.
- [83] G Theocharis, O Richoux, V Romero García, A Merkel, and V Tournat, *Limits of slow sound propagation and transparency in lossy, locally resonant periodic structures*, New Journal of Physics 16 (2014), no. 9, 093017.
- [84] Françoise Tisseur and Karl Meerbergen, *The quadratic eigenvalue problem*, SIAM Review 43 (2001), no. 2, 235–286.
- [85] Nicholas W Tschoegl, *The phenomenological theory of linear viscoelastic behavior: an introduction*, Springer Science & Business Media, 2012.
- [86] E. Walker, A. Neogi, A. Bozhko, Yu. Zubov, J. Arriaga, H. Heo, J. Ju, and A. A. Krokhin, *Nonreciprocal linear transmission of sound in a viscous environment with broken  $p$  symmetry*, Phys. Rev. Lett. 120 (2018), 204501.
- [87] Yifan Wang, Behrooz Yousefzadeh, Hui Chen, Hussein Nassar, Guoliang Huang, and Chiara Daraio, *Observation of nonreciprocal wave propagation in a dynamic phononic lattice*, Phys. Rev. Lett. 121 (2018), 194301.
- [88] G. P. Ward, R. K. Lovelock, A. R. J. Murray, A. P. Hibbins, J. R. Sambles, and J. D. Smith, *Boundary-layer effects on acoustic transmission through narrow slit cavities*, Phys. Rev. Lett. 115 (2015), 044302.



- [89] W.S. Jardetzky W.M. Ewing and F. Press, *Elastic waves in layered media*, McGraw-Hill Book Co., New York, 1957.
- [90] Haoran Xue, Yihao Yang, and Baile Zhang, *Topological acoustics*, Nature Reviews Materials 7 (2022), no. 12, 974–990.
- [91] Eli Yablonovitch, *Inhibited spontaneous emission in solid-state physics and electronics*, Phys. Rev. Lett. 58 (1987), 2059–2062.
- [92] Suxia Yang, John Page, Zhengyou Liu, Michael Cowan, Che Chan, and Ping Sheng, *Ultrasound tunneling through 3d phononic crystals*, Physical review letters 88 (2002), 104301.
- [93] Zhaoju Yang, Fei Gao, Xihang Shi, Xiao Lin, Zhen Gao, Yidong Chong, and Baile Zhang, *Topological acoustics*, Phys. Rev. Lett. 114 (2015), 114301.
- [94] Jia Ying and Chen Yiling, *Application of elastic layered system in the design of road*, Int. Journal of Engineering Research and Applications 5 (2015), 82–85.
- [95] Xin Zhang, Zhengyou Liu, Jun Mei, and Youyan Liu, *Acoustic band gaps for a two-dimensional periodic array of solid cylinders in viscous liquid*, Journal of Physics: Condensed Matter 15 (2003), no. 49, 8207.
- [96] Jie Zhu, Johan Christensen, Jesper Jung, Luis Martin-Moreno, X Yin, Lee Fok, Xiang Zhang, and FJ Garcia-Vidal, *A holey-structured metamaterial for acoustic deep-subwavelength imaging*, Nature physics 7 (2011), no. 1, 52–55.
- [97] Jie Zhu, Xuefeng Zhu, Xiaobo Yin, Yuan Wang, and Xiang Zhang, *Unidirectional extraordinary sound transmission with mode-selective resonant materials*, Phys. Rev. Appl. 13 (2020), 041001.
- [98] Xuefeng Zhu, Xinye Zou, Bin Liang, and Jianchun Cheng, *One-way mode transmission in one-dimensional phononic crystal plates*, Journal of Applied Physics 108 (2010), no. 12, 124909.
- [99] Yi-Fan Zhu, Xin-Ye Zou, Bin Liang, and Jian-Chun Cheng, *Acoustic one-way open tunnel by using metasurface*, Applied Physics Letters 107 (2015), no. 11, 113501.

- [100] Yingxi Zhu and Steve Granick, *Viscosity of interfacial water*, Phys. Rev. Lett. 87 (2001), 096104.
- [101] Yurii Zubov, B. Djafari-Rouhani, Yuqi Jin, Mathew Sofield, E. Walker, Arup Neogi, and Arkadii Krokhin, *Long-range nonspreading propagation of sound beam through periodic layered structure*, Communications Physics 3 (2020), 155.